ABSTRACT

Title of Document: MINIMIZING THE ACOUSTIC COUPLING OF FLUID LOADED PLATES USING TOPOLOGY OPTIMIZATION

Khalid H. Almitani, Doctor of Phelosophy, 2009

Directed By: Professor Amr Baz, Department of Mechanical Engineering, A. James Clark School of Engineering

Optimization of the topology of a plate coupled with an acoustic cavity is investigated in an attempt to minimize the fluid-structure interactions at different structural frequencies. A mathematical model is developed to simulate such fluid-structure interactions based on the theory of finite elements. The model is integrated with a topology optimization approach which utilizes the Moving Asymptotes Method. The obtained results demonstrate the effectiveness of the proposed approach in simultaneously attenuating the structural vibration and the sound pressure inside the acoustic domain at several structural frequencies by proper redistribution of the plate material.

Prototypes of plates with optimized topologies are manufactured at tested to validate the developed theoretical model. The performance characteristics of plates optimized for different frequency ranges are determined and compared with the theoretical predictions

of the developed mathematical model. A close agreement is observed between theory and experiments.

The presented topology optimization approach can be an invaluable tool in the design of a wide variety of critical structures which must operate quietly when subjected to fluid loading.

MINIMIZING THE ACOUSTIC COUPLING OF FLUID LOADED PLATES USING TOPOLOGY OPTIMIZATION

By

Khalid H. Almitani

Dissertation submitted to the Faculty of the Graduate School of the
University of Maryland, College Park in partial fulfillment
of the requirements for the degree of
Doctor of Philosophy
2009

Advisory Committee:

Professor A. Baz, Chair/Advisor

Professor A. Flatau

Professor B. Balachandran

Professor M. Yu

Professor N. Chopra

DEDICATION

To my family.

ACNOWLEDGEMENT

Obtaining a Ph.D. is a long and difficult process. At the end, I want to remember only the good things and to thank those who made it possible.

First, Dr. Amr Baz, who I was, and forever will be, proud to call him “My advisor”. I would like to thank him for his invaluable assistance, encouragement and helpful guidance during the development of this work. His help has been tremendous. As far as I am concerned, one cannot find a better advisor. He is great not only as a researcher but also as a person. All I can say about him is that he inspired me to be a better man.

I am indebted to my committee members: Dr. Alison Flatau, Dr. Balakumar Balachandran, Dr. Miao Yu, Dr. Nikhil Chopra and Dr. Norman Wereley who served on my original committee. They have provided, with kindness, their insight and suggestions, which are precious to me.

I would like to thank all my colleagues at University of Maryland. Specifically, I would like to thank Dr. Wael Akl, Dr. Adel El-Sabbagh and Dr. Moustafa El-Bassyionni for their help and support. Also, special thanks go to Dr. Zheng Gu, Chang, and Daniel, current members of the center for small smart systems for their help with the experimental work.

Family is extremely important to me in all likelihood because I am blessed to have such a wonderful one. It is a pity my mother passed away in 2001 and did not see this day. At least I am sure if she lived long enough, she would be proud of her son. My ALLAH have mercy on her and grant her with paradise.

My special thanks go to my family; my father, brother, sisters, mother-in-law and father-in-law. And that includes, in a very special way, my wife and my two young daughters. I would like to thank them all for being a constant source of love, concern, support and strength all these years. This dissertation is dedicated to all of them.

Above all, I am eternally grateful to ALMIGHTY ALLAH and bow my head before him by the grace of whom I was able to achieve my ambition. He is the reason I can be at this stage today.

TABLE OF CONTENTS

LIST OF TABELS

LIST OF FIGURES

NOMENCLTURE

V	volume of fluid
$P.E.$	Potential Energy
$K.E.$	Kinetic Energy
W_P	Work done on the acoustic cavity by the plate elements
ρ_A	Equilibrium density of the acoustic medium
ρ	Density of the structure medium
c	Sonic speed in the acoustic medium
u_A	Particle displacement in the acoustic medium
$\dot{u}_A$	Particle velocity in the acoustic medium
p	Acoustic pressure
w	Transverse displacement of the plate
θ_x	Rotation of the node about the y-axis
θ_y	Rotation of the node about the x-axis
N_φ	Shape function for the velocity potential
N_w	Shape function for the plate transverse displacement
A	Fluid-Structure boundary area
$\{\boldsymbol{\delta}\}$	Degrees of freedom for the structure element
$\{\mathbf{p}\}$	Nodal pressure values in the acoustic domain
$[M_A]$	Mass matrix of the acoustic domain
$[K_A]$	Stiffness matrix of the acoustic domain
$[\Omega]$	Fluid-Structure coupling matrix
$[M_{st}]$	Mass matrix of the structure domain
$[K_{st}]$	Stiffness matrix of the structure domain
f_{st}	Externally applied mechanical force on the structure
v_f	Volume fraction
A^e	Surface area for structure finite element
h_{max}	Maximum permissible plate thickness

h_{min}	Minimum permissible plate thickness
h^e	Plate finite element thickness
N^e	Number of elements in the plate structure
ω	Angular velocity

CHAPTER 1

BACKGROUND

1.1 Basic Concepts of Topology Optimization

Topology optimization is often referred to as “layout optimaization” or “generalized shape optimization” in the literature [1]. The importance of this type of problem lies in the fact that the choice of the appropriate topology of a structure is generally decisive for the cost efficiency of the structure. Moreover, the optimization of the geometry and topology of structural layouts has great impact on the performance of structures [2].

The traditional optimization problems aim at optimizing the size, shape, or topology of an elastic body and its material properties under specific loading conditions as shown in Figure 1.1.

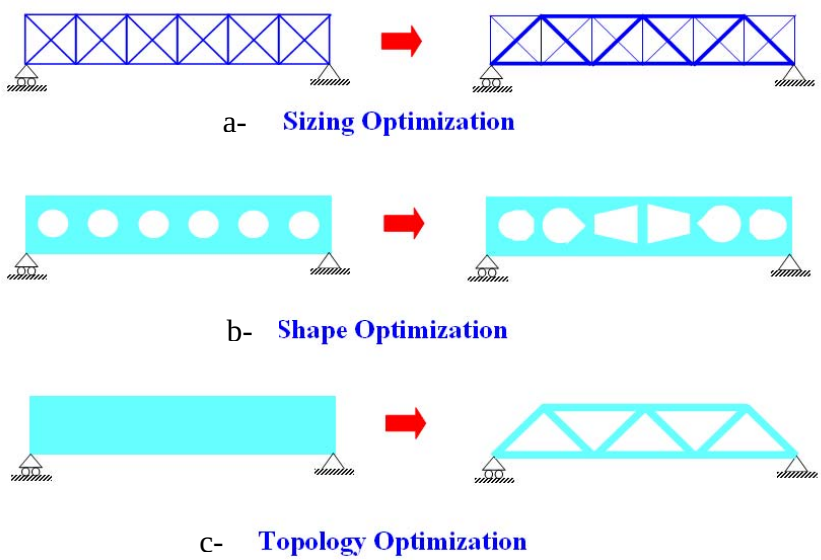

Figure 1.1: Different types of optimization objectives

In the sizing and shape optimization problems, the structural material is distributed in such a way in order to satisfy the imposed stress constraints while maintaining the same topology

of the base structure (Figures (1.1a) and (1.1b)). In the case of topology optimization, the topology of the original and the optimized structures are completely different as the optimization algorithms carves the unnecessary material from the original structure in order to minimize the weight of the structure while satisfying constraints imposed on the structural performance (Figure (1.1c).

In topology optimization, the geometry of the body is usually modeled using a raster representation realizing the material distribution of the work piece and the classical performance objective is to maximize the stiffness of load elastic body subject to a volume constrain. But quickly the method was extended to other objectives like minimizing the weight or maximizing the fundamental eigenvalue while being subjected to numerous design constraints like buckling constraints, displacement constraints, design dependent loads (e.g. pressure loads) and stress constraints.

The significant development of topology optimization was supported by the interest of engineers and industry. The design process followed during typical industrial development process can be broken into the following distinct phases: Conceptual design, preliminary design, detailed design, and finally, testing. Ideally, the feedback of the simulations indicates only changes in the detailed design and repeated testing. These loops are rather cheap in comparison to the situation if changes in the conceptual design are enforced. Then it could happen that the whole development process is relocated to its conceptual stage, which is usually expansive in both, time and costs. Due to the fundamental role of the conceptual design phase topology optimization became a valuable computational tool for the basic layout [3].

In recent years, extensive applications of topology optimization of continuum structures have been reported, as it has been verified that using such an approach would yield structures

with optimal dynamic and static characteristics. For these reasons, topology optimization has found its ways in aeronautical, civil and mechanical engineering implementations, and even started to become a standard part of commercial finite element analysis software such as ANSYS.

1.2 Literature Review

Literature on structural topology optimization is quite extensive and research activities in these fields were focused on large diversity of applications. The optimization problem was treated as a material distribution problem to minimize / maximize a certain objective function. In other words the material in a structure is redistributed to achieve the optimization goal bounded by various constraints, among which is the volume fraction of the material. The efficiency of this method was clearly demonstrated by Bendsoe and Kikuchi [4] and Bendsoe [5] for the minimum compliance problem.

Later on, structural dynamics started to gain interest of researchers working in topology optimization. Maximization of the dynamic properties of structures such as the eigen-frequencies, either the fundamental or higher order ones, as well as maximizing the band gap between two consecutive eigen-frequencies, was tackled by Bendsoe and Diaz [6], Krog and Olhoff [7], Pederson [8], Olhoff and Du [9] and Jensen and Pedersen [10]. Minimizing the dynamical response of a structure for a given driving frequency or frequency range was studied by Jog [11]. The problem of maximization of the fundamental buckling load of structures was investigated by Bendsoe and Sigmund [3].

1.3 Topology Optimization of Fluid-Structure Interaction Problem

When a flexible structure vibrates, it produces vibrational disturbances to the fluid with which it is in contact. The resulting fluid-structure interactions are governed by the coupling between the dynamics of the structures as well as the fluid. According to Crocker [12], the disturbances generate sound pressure levels which are uniquely determined by:

(1) The properties of the fluid.

(2) The geometry of the vibrating structure.

(3) The acoustics properties and geometric distribution of any other passive structures bounding the fluid.

(4) The spatial distribution of the component of vibrational acceleration normal to the vibrating surface.

The fluid is coupled to the structure by its pressure at the interface and the structure is coupled to the fluid by the acceleration of the vibrating surface. In the general case, the action of a fluid on a structure has several effects such as radiation damping and modification of the eigen-frequencies [13].

In the literature, only a few investigators have considered using topology optimization for optimizing fluid-structure interaction problems. For example, Yoon, Jensen and Ole [14] used the (u, p) mixed finite element model to represent a fluid-structure coupled domain, where the structure was placed inside an acoustic medium. Using this approach, the authors were able to formulate the problem without explicit boundary interface representation. The objective of the optimization scheme was to minimize the sound pressure inside the acoustic medium, when exciting the structure by fixed excitation frequency.

Du and Olhoff [15] tried to minimize the sound power radiated from a structure surface placed inside an acoustic cavity. They claimed to have taken the fluid-structure coupling into consideration. Nevertheless, they stated later that since air was the acoustic medium, a feedback coupling between the acoustic medium and the structure can be neglected. In addition, they assumed weak coupling and ignored the acoustic pressure in the structural equation. Also, during their study the excitation frequency was maintained fixed at certain value regardless of the effect of the material redistribution on the stiffness of the structure domain, and hence on the modal frequencies.

Wang and Lee [16] presented a sizing optimization using the design sensitivity analysis through chain-ruled derivatives from the finite and boundary element methods. However, their study was limited only to closed structures because they used Helmholtz integral equation. If the structures have holes, their acoustic optimization approach fails to yield reliable solutions.

In 2004, Lee *et al*. [17] applied topology optimization which is integrated with genetic algorithms to fluid–structure interaction problems in order to minimize the noise pressure levels. Using a simple hexahedral box model, they proposed a topology optimization technique to design holes for the radiation and scattering from thin-body structures using the normal gradient integral equation. The formulation which was proposed by Wu and Wan [18], was used for the acoustic analysis of thin-bodies and the genetic algorithm was adopted as an optimization algorithm.

Hence, topology optimization of fluid-structure interaction problems, where true coupling is considered and the external excitation being locked to the modal frequencies has yet to be studied in a comprehensive manner. It is therefore the objective of the current work to model a

fluid-structure interaction problem, where a flexible plate is coupled to a closed acoustic cavity and subject to external mechanical excitation.

1.4 Solid Isotropic Material with Penalization (SIMP)

It is also known as the power-law approach, in which the material properties can be expressed in terms of the design variable material density using a simple “power-law” interpolation as an explicit means to suppress intermediate values of the bulk density. This method has been presented by Bendsoe [5]. In the traditional SIMP material model, material properties are assumed constant within each finite element used to discretize the design domain with the design variables being the element “densities”. In each point of the design domain, the material properties are modeled as the relative material density raised to some power times the material properties of solid material. For instance, in SIMP model, Young’s modulus of elasticity is given by equation (1.1)

$$E(x) = \rho^p E_o(x) \tag{1.1}$$

where E and E_o are the Young’s modulus of the homogenized and basic material that will be distributed in the domain, respectively. Also, ρ denotes the density describing the amount of material in each point of the domain which can assume values between 0 and 1, and p is a penalization factor to recover the discrete nature of the design. For $\rho = 0$, the material is equal to void, and for $\rho = 0$, the material is equal to solid material. The effect of the exponent p is to penalize intermediate densities. Since intermediate densities are allowed in this method, a penalization of these densities is necessary to prevent the so called "grey" designs from appearing as they are not manufacturable from a two-constituent, i.e. material or void, model. In Figure (1.2), we can see that as the exponent increases, fewer and fewer intermediate density values are possible.

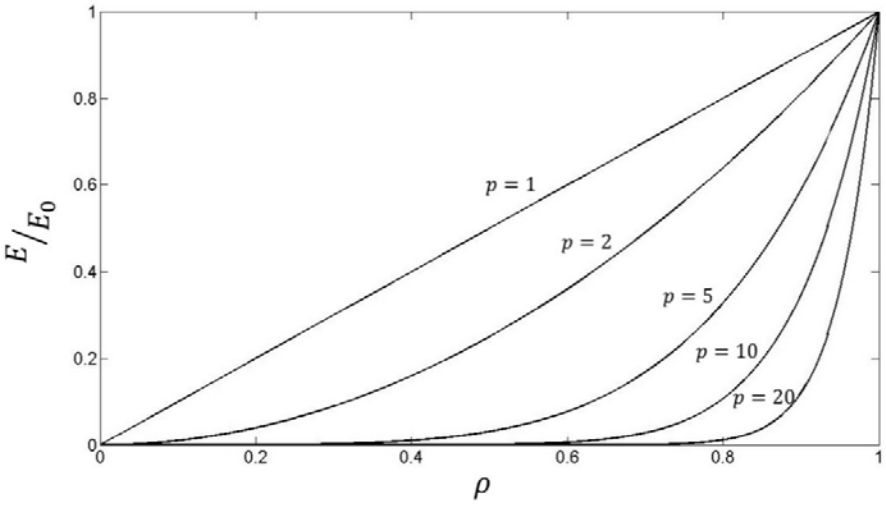

Figure 1.2: Effect of SIMP penalty parameter

According to Sigmund [19], this approach has been criticized since it was argued that no physical material exists with properties described by the power-law interpolation. However, the work done by Bendsoe and Sigmund [20] proved that the power-law approach is physically permissible as long as simple conditions on the power are satisfied (e.g. $p = 3$ for a material with Poisson's ratio equals to $\frac{1}{3}$).

Moreover, like most of the other topology optimization methods, the SIMP method does not directly resolve the problem of non-existence of solutions (ill-posedness) and thus numerical instabilities may occur. One of the most serious numerical instabilities is the occurrence of checkerboard patterns in the final solutions as shown in Figure (1.3). This occurs when, around a single node, there are just two solid elements diagonally connected, as a checkerboard. Another numerical problem is the fact that different solutions can be obtained just by choosing different number of elements. This is the mesh-dependence problem. There are many solutions to a topology optimization problem, one global and many local minima. Different solutions to the same problem with the same discretization by using different starting solutions are often

obtained. This is known as non-convergence problem. Various approaches have been proposed to relieve these problems.

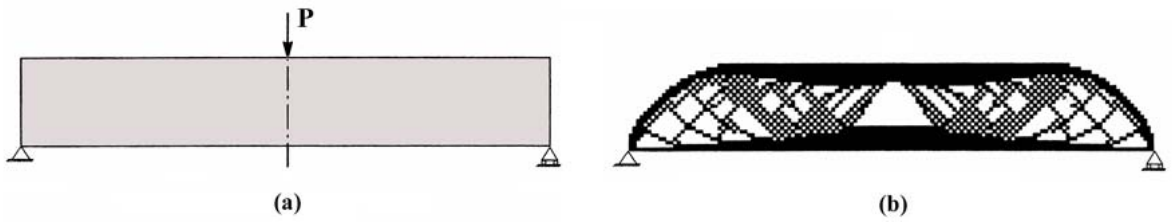

Figure 1.3: Checkerboard pattern in layout optimization. (a) Design domain of a beam under loading, (b) final design with checkerboard patterns.

The problem of non-existence was considered by Petersson and Sigmund [21] and Zhou *et al*. [22]. They used an upper bound to constrain the maximum density slope. This extra constraint makes the problem well-posed in the sense that existence of solutions is guaranteed, and the solutions obtained by a finite element method will converge uniformly to the set of exact solutions as the mesh is refined.

Cardoso and Fonseca [23] proposed a general mesh independent filter as a mean to control the complexity of topology optimization designed structures. They used a sequential linear programming algorithm as an optimizer and applied the filter over the move-limits. In their work, they showed that the new filter can prevent the checkerboard instability and also controls the complexity of the topology. To alleviate the influence of the finite element solution on the final topology, they suggested using a non-regular meshes for the design domain together with the proposed filter. Figure (1.4) shows the output topology configuration after applying the proposed filter which resulted in a well-posed problem.

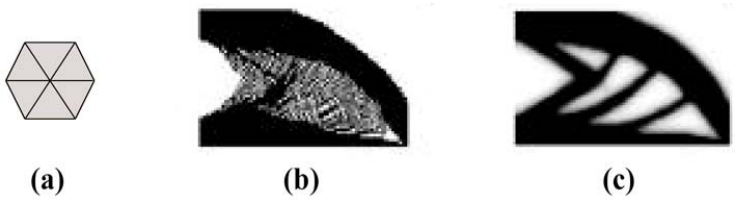

Figure 1.4: Influence of the mesh pattern. (a) Mesh pattern, (b) final design without filtering, (c) final design with filtering [23].

Jang *et al*. [24] showed that the checkerboard problem in topology optimization can be overcome by the use of the non-conforming finite elements since the convergence of the non-conforming finite element is independent of the Lame parameters. Solving three typical design problems, they were able to show that a non-conforming element is capable of predicting correctly behaving stiffness of the checkerboard patch. As it can be seen in Figure (1.5), the checkerboard pattern was has been successfully removed in the final design using a non-conforming element rather than a conforming one.

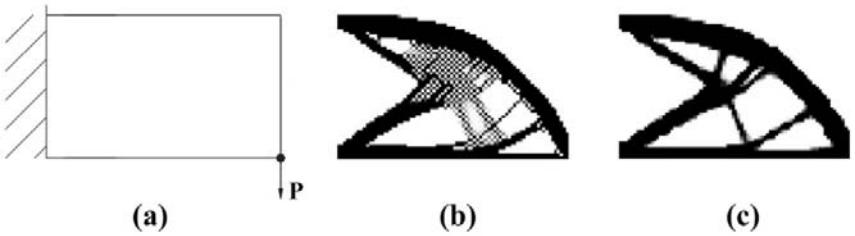

Figure 1.5: Effect of using non-conforming elements. (a) Design domain under investigation, (b) final design using conforming elements in the compliance minimization, (c) final design using non-conforming elements [24].

1.5 Method of Moving Asymptotes (MMA)

The method of moving asymptotes belongs to a group of optimization methods which represent a family of convex approximation methods suitable for structural optimization

problems. These methods involve solving successive convex approximations to the optimization problem. In MMA, the efficiency of solving a problem depends strongly on asymptote and move limit locations [25]. A well established general approach for solving a structural problem using MMA is to generate and solve a sequence of explicit subproblems according to the following iterative scheme:

Step (0): Choose a starting point $x^{(0)}$, and let the iteration index $k = 0$.

Step (I): Given an iteration point $x^{(k)}$, calculate $f_i(x^{(k)})$ and the gradients $\nabla f_i(x^{(k)})$ for $i = 0,1, \dots, m$.

Step (II): Generate a subproblem $P^{(k)}$ by replacing, in the original optimization problem, the usually implicit functions f_i by approximating explicit functions $f_i^{(k)}$ based on the calculations in step I.

Step (III): Solve $P^{(k)}$ and let the optimal solution of the subproblem be the next iteration point $x^{(k+1)}$. Let $k = k + 1$ and go to step I.

The generalized topology optimization problem has the following form:

$$\begin{cases} \min\limits_{x} f(x) \\ \text{Subject to:} \\ g_i(x) \le 0 \qquad i = 1, \dots, m \\ 0 \le x_{min} \le x_j \le 1 \qquad j = 1, \dots, n \end{cases} \tag{1.2}$$

where, $x = (x_1, \dots, x_n)^T$ is the vector of design variables, $f(x)$ is the objective function, $g_i(x)$ are behavior constraints such as limitations on stresses or displacements and x_{min} is a given lower bound on the design variables.

Using the method of moving asymptotes, the above general formulation will be reformulated as follows:

$$\begin{cases} \min\limits_{x} \; f(x) + \sum\limits_{i=1}^{m} (c_i y_i + \frac{1}{2}\, d_i y_i^2) + z \\ \text{Subject to:} \\ g_i(x) - a_i z - y_i \le 0 \qquad i = 1, \dots, m \\ x_{min} \le x_j \le x_{max} \qquad j = 1, \dots, n \\ y_i \ge 0 \\ z \ge 0 \end{cases} \tag{1.3}$$

where, $y \in R^m$ and $z \in R$ are additional "artificial variables" and a_i, c_i and d_i are non-negative, real valued constants such that $c_i + d_i > 0$ for each i.

The above formulation has two main advantages [28]:

i. The optimization will proceeds even when the problem becomes "infeasible", i.e. when the original constraints are violated, in which case the variable values are pushed back toward the acceptable region of the design space.

ii. It can be used to solve special classes of optimization problems, such as the min-max problems, by adding some minor adjustments.

The convex subproblem corresponding to the above problem (1.3) is written as follows:

$$\begin{cases} \min\limits_{x} \; \tilde{f}^{(k)}(x) + \sum\limits_{i=1}^{m} (d_i y_i + \frac{1}{2}\, d_i y_i^2) + z \\ \text{Subject to:} \\ \tilde{g_\iota}^{(k)}(x) - a_i z - y_i \le 0 \qquad i = 1, \dots, m \\ \propto_j{}^{(k)} \le x_j \le \beta_j{}^{(k)} \qquad j = 1, \dots, n \\ y_i \ge 0 \\ z \ge 0 \end{cases} \tag{1.4}$$

The approximation functions $\tilde{f}^{(k)}$ and $\tilde{g}_i^{(k)}$ are recalculated for each iteration (k) of the main problem and have the following asymptotic form:

$$\tilde{f}^{(k)}(x) = \sum_{j=1}^{n}\left(\frac{p_{0j}^{(k)}}{U_j^{(k)} - x_j} + \frac{q_{0j}^{(k)}}{x_j - L_j^{(k)}}\right) + r_0^{(k)} \qquad i = 0, \dots, m \tag{1.5}$$

$$\tilde{g}_i{}^{(k)}(x) = \sum_{j=1}^{n}\left(\frac{p_{ij}^{(k)}}{U_j^{(k)} - x_j} + \frac{q_{ij}^{(k)}}{x_j - L_j^{(k)}}\right) + r_i^{(k)} \qquad i = 0, \dots, m \tag{1.6}$$

where:

- $$p_{ij}^{(k)} = \begin{cases} \left(U_j^{(k)} - x_j^{(k)}\right)^2 \frac{\partial g_i}{\partial x_j}\left(x^{(k)}\right) & if \ \frac{\partial g_i}{\partial x_j}\left(x^{(k)}\right) > 0 \\ 0 & if \ \frac{\partial g_i}{\partial x_j}\left(x^{(k)}\right) \le 0 \end{cases} \tag{1.7.1}$$

- $$q_{ij}^{(k)} = \begin{cases} 0 & if \ \frac{\partial g_i}{\partial x_j}\left(x^{(k)}\right) \ge 0 \\ \left(x_j^{(k)} - L_j^{(k)}\right)^2 \frac{\partial g_i}{\partial x_j}\left(x^{(k)}\right) & if \ \frac{\partial g_i}{\partial x_j}\left(x^{(k)}\right) < 0 \end{cases} \tag{1.7.2}$$

- $$r_i^{(k)} = g_i\left(x^{(k)}\right) - \sum_{j=1}^{n}\left(\frac{p_{ij}^{(k)}}{U_j^{(k)} - x_j} + \frac{q_{ij}^{(k)}}{x_j - L_j^{(k)}}\right) \tag{1.7.3}$$

- $$\propto_j{}^{(k)} = max\left\{x_j^{min}, 0.9L_j^{(k)} + 0.1x_j^{(k)}\right\} \tag{1.7.4}$$

- $$\beta_j{}^{(k)} = max\left\{x_j^{min}, 0.9U_j^{(k)} + 0.1x_j^{(k)}\right\} \tag{1.7.5}$$

Thus each $\tilde{g}_i{}^{(k)}$ is obtained by a linearization of g_i in variables of the type $1/(x_j - L_j)$ or $1/(U_j - x_j)$ dependent on the signs of the derivatives of g_i at $x^{(k)}$.

The parameters L_i and U_i are normally changed between the iterations and referred to as "moving asymptotes". These parameters provide a means of controlling the speed of algorithm convergence. A heuristic method is used to update the locations of the upper and lower asymptotes U_i and L_i based on the absolute limits on the design variables as well as the design variable values from previous iteration.

The subproblem $P^{(k)}$ is solved by forming the Lagrangian and satisfying Kuhn-Tucker optimality conditions of stationarity ($\partial L/\partial x = 0$); primal feasibility, which means that the

values $(x_1, x_2, \dots, x_n)$ should correspond to a feasible point; dual feasibility, meaning the Lagrange multipliers must be non-negative; and complementary slackness, which means that the Lagrange multipliers associated with inactive constraints should be equal to zero.

The convexity of the subproblem causes the method to converge quit rapidly using Newton's method to determine the direction of each optimization step. This method is highly robust and has been used successfully in a variety of structural optimization problems. For this reason, it is among primary choices in optimization methods used in structural optimization and particularly in topology optimization [28].

The method of moving asymptotes (MMA) was firstly presented in (Svanberg, 1987). In that work, an empirical technique that gradually modifys the asymptote values depending upon results obtained after each iteration during the optimization process was proposed. Afterwards the method was further studied and developed.

In (Zillober 1993), an efficient global convergent sequential convex programming method was developed by combining MMA with a line search performed afterwards.

Bletzinger (1993) presented a simple extension with respect to strict convex approximation of the objective function, deterministic asymptote adaption, and consistent treatment of equality constraints. His approximation was based on second-order information estimated by forward finite differences. In his work, he showed that if the upper and lower asymptotes were set to positive and negative infinity, then the method is identical with diagonal quasi Newton sequential quadratic programming.

In (Ni, 2003), a globally convergent method of moving asymptotes with trust region technique was proposed. In the modified method, the choice of asymptotes is controlled by the

trust region radius and a convex separable subproblem is being solved in each iteration such that global convergence of the algorithm is obtained.

Fleury (1989) suggested a rational scheme based on second order derivatives. Although this method gives suitable values for asymptotes, its efficiency in practical applications is not obvious because of high cost of second order derivatives calculations.

1.6 Scope of the dissertation

In this dissertation, topology optimization will be used to minimize the fluid-structure interactions between a flexible plate coupled with an acoustic cavity at different structural modal frequencies. A finite element model will be developed, in Chapter 2, to model the fluid-structure interactions. The theoretical predictions of the vibration and sound radiation of a topology optimized plate/acoustic cavity system will be presented in Chapter 3 along with comparisons of the characteristics of plain plate/cavity system. Experimental verification of the predictions of the developed finite element model will be carried out in Chapter 4. Chapter 5 will present a summary of the conclusions and the recommendations for future work.

CHAPTER 2

FINITE ELEMENT MODELING

2.1 Basic Model and Main Assumptions

Consider the plate-cavity system shown schematically in Figure (2.1). In this system, a rectangular flexible plate is coupled with an acoustic cavity that has five rigid walls. The plate is subjected to external excitation and a finite element model will be developed to predict the interaction between the plate vibration and the associated sound radiation into the acoustic cavity.

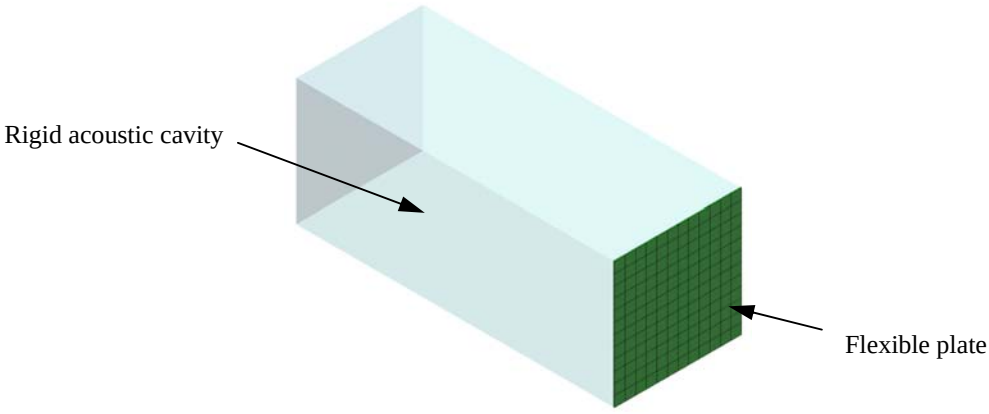

Figure 2.1: Coupled plate-cavity system

Finite element modeling is used to predict the plate displacements as well as the sound pressure inside the acoustic cavity for the coupled fluid-structure system. The finite element model consists of two different types of elements. The first one is 4-node quad elements with 3 degrees of freedom per node (w, θ_x, θ_y) representing the transverse displacement of the node, the rotation about the y-axis and that about the x-axis respectively. The second type of elements

is a cubic 8-node element for the acoustic domain with the acoustic pressure (p) as the sole degree of freedom per node. The element shapes are as presented in Figures (2.1) and (2.2).

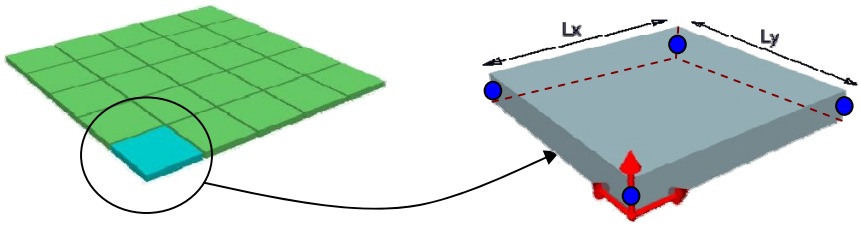

Figure 2.2: Plate 4-node quad element

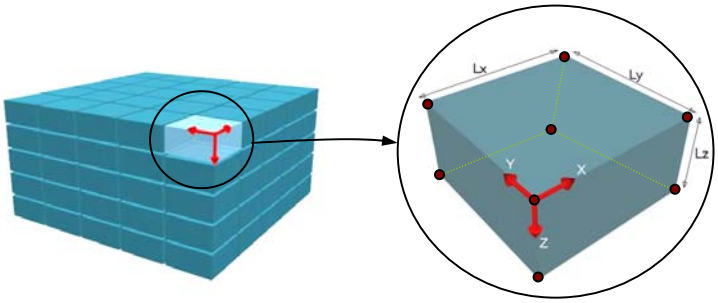

Figure 2.3:Acoustic 8-node brick element.

The plate finite element model is based on the first order shear deformation theory, which is efficiently used for relatively thick as well as thin plates. In this model it is assumed that planes normal to the mid-surface of the plate in the un-deformed state remain plane but not necessarily normal to the mid-surface in the deformed state. Hence the rotation degrees of freedom θ_x and θ_y are considered as independent degrees of freedom and not derivatives of the mid-surface out of plane displacements. This approach was adopted, since it a general way in modeling plates and is capable for the special case of thin plates by considering reduced order Gaussian numerical integration for the terms that tend to approach zero, when the thickness gets smaller.

2.2 System Energies and Work

Considering a fluid volume "V", then the Kinetic Energy (K.E.) can be written as

$$K.E. = \frac{1}{2}\,\rho_A \int_V (\dot{u}_A)^2\, dV \tag{2.1}$$

and the Potential Energy (P.E.) can be expressed as

$$P.E. = \frac{1}{2}\,\rho_A c^2 \int_V (div\, u_A)^2\, dV \tag{2.2}$$

The work done on the acoustic cavity by the plate (W_P) element is given by,

$$W_P = \int_{\substack{Boundary \\ Area}} pw\, dA \tag{2.3}$$

where:

- ρ_A is the equilibrium density of the acoustic medium
- u_A is the particle displacement in the acoustic medium
- $\dot{u}_A$ is the particle velocity in the acoustic medium
- c is the sonic speed in the acoustic medium
- p is the acoustic pressure
- w is the transverse displacement of the plate

For the sake of simplifying the calculations, the velocity potential φ, which is a scalar quantity, can be used instead of the acoustic pressure p using the following identities:

- $p = -\rho_A \frac{\partial \varphi}{\partial t}$ (2.4.1)

- $\dot{u}_A = \nabla\varphi = \left[\frac{\partial\varphi}{\partial x}\,\vec{\imath} + \frac{\partial\varphi}{\partial y}\,\vec{\jmath} + \frac{\partial\varphi}{\partial z}\,\vec{k}\right]$ (2.4.2)

- $(\dot{u}_A)^2 = (\nabla\varphi)^2 = \left[\left(\frac{\partial\varphi}{\partial x}\right)^2 + \left(\frac{\partial\varphi}{\partial y}\right)^2 + \left(\frac{\partial\varphi}{\partial z}\right)^2\right]$ (2.4.3)

- $div\, u_A = -\frac{1}{c^2}\frac{\partial\varphi}{\partial t}$ (2.4.4)

Hence, the previous expressions for the Kinetic Energy, Potential Energy and Work can be rewritten as:

$$\text{K. E.} = \frac{1}{2}\,\rho_A \int_V (\nabla\varphi)^2\, dV \tag{2.5}$$

$$\text{P. E.} = \frac{1}{2}\,\frac{\rho_A}{c^2} \int_V (\dot{\varphi})^2\, dV \tag{2.6}$$

$$\text{W}_\text{P} = -\rho_A \int_{\substack{Bounday\\ Area}} \dot{\varphi}\, w\, dA \tag{2.7}$$

2.3 Equation of Motion

Hamilton's principle, as given in equation (2.7) is used to extract the differential equation of motion of the acoustic fluid, as influenced by the external forces applied on the exposed plate.

$$\int_{t_1}^{t_2} \delta(\mathbf{K.E} - \mathbf{P.E} + \mathbf{W_P})\; dt = 0 \tag{2.8}$$

Let $\varphi = \text{N}_\varphi\,\boldsymbol{\varphi}$ where N_φ denotes an appropriate shape function and $\boldsymbol{\varphi}$ represents the nodal velocity potential vector of the element. Similarly, let $w = N_w\{\boldsymbol{\delta}\}$ where N_w is an appropriate shape function is and $\{\boldsymbol{\delta}\}$ denotes the nodal deflection vector of the plate. Then,

The variation of the Kinetic Energy ($\delta K.E$) is written as:

$$\delta(\mathbf{K}.\mathbf{E}) = \rho_A \int_V \{\boldsymbol{\delta\varphi}\}^T \left[\left(\nabla N_\varphi\right)^T \left(\nabla N_\varphi\right)\right] \{\boldsymbol{\varphi}\}\, dV \tag{2.9}$$

And the variation of the Potential Energy $(\delta P.E)$ can be written as:

$$\delta(\mathbf{P}.\mathbf{E}) = \frac{\rho_A}{c^2} \int_V \{\boldsymbol{\delta\dot{\varphi}}\}^T \left[\left(\nabla N_\varphi\right)^T \left(\nabla N_\varphi\right)\right] \{\boldsymbol{\dot{\varphi}}\}\, dV \tag{2.10}$$

Using integration by parts to eliminate $\{\delta\dot{\varphi}\}$ yields:

$$\delta(\mathbf{P}.\mathbf{E}) = -\frac{\rho_A}{c^2} \int_V \{\boldsymbol{\delta\varphi}\}^T \left[\left(\nabla N_\varphi\right)^T \left(\nabla N_\varphi\right)\right] \{\boldsymbol{\ddot{\varphi}}\}\, dV + (B.C = 0) \tag{2.11}$$

Finally, the variation of the work done by the plate element (δW_P) is found to be

$$\delta(\mathbf{W_P}) = -\rho_A \int_A \{\boldsymbol{\delta\dot{\varphi}}\}^T \left[\left(N_\varphi\right)^T N_w\right] \{\boldsymbol{\delta}\}\, dA \tag{2.12}$$

Again, using integration by parts to eliminate $\{\boldsymbol{\delta\dot{\varphi}}\}$ yields:

$$\delta(\mathbf{W_P}) = -\rho_A \int_A \{\boldsymbol{\delta\varphi}\}^T \left[\left(N_\varphi\right)^T N_w\right] \{\boldsymbol{\dot{\delta}}\}\, dA + (B.C = 0) \tag{2.13}$$

Substituting with the variations of the system energies and work in equation (2.7) and summing up the terms of $\{\delta\varphi\}$ inside the time integral and equating them to zero results in the required equation of motion of the acoustic element:

$$\left[\frac{\rho_A}{c^2} \int_V \left(N_\varphi\right)^T N_\varphi\, dV\right] \{\boldsymbol{\ddot{\varphi}}\} + \left[\rho_A \int_V \left[\left(\nabla N_\varphi\right)^T \left(\nabla N_\varphi\right)\right] dV\right] \{\boldsymbol{\delta}\} = \left[\rho_A \int_A \left(N_\varphi\right)^T (N_w) dA\right] \{\boldsymbol{\dot{\delta}}\} \tag{2.14}$$

Differentiating the above equation with respect to time and utilizing the following identities:

- $\dot{\varphi} = -\frac{p}{\rho_A}$ (2.15.1)

- $\ddot{\varphi} = -\frac{\dot{p}}{\rho_A}$ (2.15.2)
- $\dddot{\varphi} = -\frac{\ddot{p}}{\rho_A}$ (2.15.3)

gives:

$$\left[\frac{1}{c^2}\int_V \left(N_\varphi\right)^T N_\varphi dV\right]\{\ddot{\mathbf{p}}\} + \left[\int_V \left(\nabla N_\varphi\right)^T \left(\nabla N_\varphi\right) dV\right]\{\mathbf{p}\} = \left[-\rho_A \int_A \left(N_\varphi\right)^T (N_w) dA\right]\{\ddot{\boldsymbol{\delta}}\} \quad (2.16)$$

where $\{p\}$ is the nodal pressure vector.

Equation (2.16) could also be written as

$$[\mathrm{M}_A]\{\ddot{\mathbf{p}}\} + [K_A]\{\mathbf{p}\} = -[\Omega]^T\{\ddot{\boldsymbol{\delta}}\} \quad (2.17)$$

where:

- $\{\boldsymbol{\delta}\}$ represents the degrees of freedom of the structure element,
- $[\mathrm{M}_A] = \frac{1}{c^2}\int_V \left(N_\varphi\right)^T N_\varphi dV$ is the mass matrix of the acoustic medium,
- $[K_A] = \int_V \left(\nabla N_\varphi\right)^T \left(\nabla N_\varphi\right) dV$ is the stiffness matrix of the acoustic medium,
- $[\Omega]^T = \rho_A \int_A \left(N_\varphi\right)^T (N_w) dA$ is the fluid-structure coupling matrix.

2.4 Coupling the Acoustic Cavity with the Plate Structure

The equation of motion of the plate is given as:

$$[\mathrm{M}_s]\{\ddot{\boldsymbol{\delta}}\} + [K_s]\{\boldsymbol{\delta}\} = F_S \quad (2.18)$$

where $\boldsymbol{F_S}$ represents the forces exerted by the acoustic fluid on the plate elements.

The forcing function "$\boldsymbol{F_S}$" can be calculated from the work done by the acoustic field on the structure. From equation (2.3), it follows that

$$\mathbf{W_P} = \int_A \{\boldsymbol{\delta}\}^T (N_w)^T \left(N_\varphi\right)\{\mathbf{p}\}\, dA \tag{2.19}$$

Hence,

$$(\boldsymbol{\delta}\mathbf{W_P}) = \int_A \{\delta\boldsymbol{\delta}\}^T (N_w)^T \left(N_\varphi\right)\{\mathbf{p}\}\, dA \tag{2.20}$$

Since the Work = Force × Displacement, then the forcing term on the plate can be calculated as:

$$F_S = \frac{[\Omega]\mathbf{p}}{\rho_A} \tag{2.21}$$

where $[\boldsymbol{\Omega}]$ is as defined previously.

Thus, the complete differential equation of the composite plate is given as:

$$[\mathrm{M}_s]\{\ddot{\boldsymbol{\delta}}\} + [K_s]\{\boldsymbol{\delta}\} = \frac{[\Omega]\mathbf{p}}{\rho_A} \tag{2.22}$$

The equation of motion of the coupled system is given in the following matrix form:

$$\begin{bmatrix} M_s & 0 \\ [\Omega]^T & M_A \end{bmatrix}\begin{Bmatrix} \ddot{\boldsymbol{\delta}} \\ \ddot{\mathbf{p}} \end{Bmatrix} + \begin{bmatrix} K_s & -\dfrac{[\Omega]}{\rho_A} \\ 0 & K_A \end{bmatrix}\begin{Bmatrix} \boldsymbol{\delta} \\ \mathbf{p} \end{Bmatrix} = \begin{Bmatrix} f_s \\ 0 \end{Bmatrix} \tag{2.23}$$

where "$\boldsymbol{f_s}$" is the externally applied force.

From equation (2.23), for harmonic excitation at angular frequency $\boldsymbol{\omega}$, we can write

$$\left[K_s - M_s\,\omega^2\right]\boldsymbol{\delta} - \frac{[\Omega]}{\rho_o}\mathbf{p} = \mathbf{f_s} \tag{2.24}$$

and

$$\omega^2[\Omega]^T\boldsymbol{\delta} = [K_A - M_A\omega^2]\mathbf{p} \tag{2.25}$$

Equation (2.25) can be rewritten as

$$\mathbf{p} = [K_A - M_A\omega^2]^{-1}\,\omega^2[\Omega]^T\boldsymbol{\delta} \tag{2.26}$$

Substituting for $\boldsymbol{p}$ from equation (2.26) into equation (2.24) results in:

$$\left[\left(K_s - M_s\,\omega^2\right) - \frac{[\Omega]}{\rho_o}\left(K_A - M_A\omega^2\right)^{-1}\,\omega^2[\Omega]^T\right]\boldsymbol{\delta} = \mathbf{f_s} \tag{2.27}$$

2.5 Formulation for the Optimization of the Fluid-Structure Interaction Problem

The topology optimization problem can be formulated as follows:

$$\begin{cases} \min\limits_{\rho} J = (\boldsymbol{\delta}^T C_w^T \mathbf{p}) \quad \text{defined at the boundary area} \\ \text{Subject to:} \\ \boldsymbol{\delta} = \begin{Bmatrix} w \\ \theta_x \\ \theta_y \end{Bmatrix} \\ \begin{bmatrix} M_s & 0 \\ [\Omega]^T & M_A \end{bmatrix}\begin{Bmatrix} \ddot{\boldsymbol{\delta}} \\ \ddot{\mathbf{p}} \end{Bmatrix} + \begin{bmatrix} K_s & -\dfrac{[\Omega]}{\rho_o} \\ 0 & K_A \end{bmatrix}\begin{Bmatrix} \boldsymbol{\delta} \\ \mathbf{p} \end{Bmatrix} = \begin{Bmatrix} \mathbf{f_s} \\ \mathbf{0} \end{Bmatrix} \\ \sum_{e=1}^{N_e} h^e\,A^e \le v_f \times h_{max} \times \sum_{e=1}^{N_e} A^e \\ 0 \le h_{min} \le h^e \le h_{max} \end{cases} \tag{2.28}$$

Note that $C_w\boldsymbol{\delta} = \mathbf{w}$ where C_w is a matrix that extracts the transverse deflection $\mathbf{w}$ from the nodal deflection vector $\boldsymbol{\delta}$. Also, the objective function can be explained literally as to minimize the coupling between the structure and the fluid domains. By doing this, minimum work or energy is transmitted between the structure and the fluid domains, resulting in minimization of the sound intensity and sound pressure levels, due to structure resonances inside the acoustic cavity. It is worth mentioning, that due to the formulated objective function, the cavity modes will not be affected as a result of the topology optimization of the flexible plate.

2.6 Sensitivity Analysis

Sensitivity analysis represents the crucial point of the entire optimization procedure. The main effort in order to determine these sensitivities is that for path-dependent problems, the

structural sensitivities are also path dependent. These sensitivities can be evaluated numerically by the finite difference method or analytically by the adjoint variable method or the direct differentiation method. In the current work, the direct differentiation method is being used to calculate the sensitivity of the objective function.

Sensitivity of the objective function, which is the fluid-structure coupling "*J*", with respect to the optimization variables, which are the densities of the plate elements "ρ", can be found firstly by differentiating the objective function given in problem (2.28) with respect to the optimization variables, which yields:

$$\frac{dJ}{d\rho} = \boldsymbol{\delta}^T C_w^T \frac{d\mathbf{p}}{d\rho} + \mathbf{p}^T C_w \frac{d\boldsymbol{\delta}}{d\rho} \tag{2.29}$$

To calculate $\frac{d\boldsymbol{\delta}}{d\rho}$, we differentiate equation (2.27) with respect to ρ:

$$\begin{aligned} &\frac{d}{d\rho}\left[(K_s - M_s\,\omega^2) - \frac{[\Omega]}{\rho_o}(K_A - M_A\omega^2)^{-1}\,\omega^2[\Omega]^T\right]\boldsymbol{\delta} \\ &\quad + \left[(K_s - M_s\,\omega^2) - \frac{[\Omega]}{\rho_o}(K_A - M_A\omega^2)^{-1}\,\omega^2[\Omega]^T\right]\frac{d\boldsymbol{\delta}}{d\rho} = 0 \end{aligned} \tag{2.30}$$

For simplification, the following identities will be defined:

- $K_{s\_D} = (K_s - M_s\,\omega^2)$ (2.31.1)
- $K_{fl\_D} = (K_A - M_A\,\omega^2)$ (2.31.2)
- $A = \frac{[\Omega]}{\rho_o}(K_A - M_A\,\omega^2)^{-1}\,\omega^2[\Omega]^T$ (2.31.3)

Substitution with equations (2.31.1-2.31.3) into equation (2.30) results in:

$$\frac{d}{d\rho}\left[K_{s\_D} - A\right]\boldsymbol{\delta} + \left[K_{s\_D} - A\right]\frac{d\boldsymbol{\delta}}{d\rho} = 0 \tag{2.32}$$

As $A = \frac{[\Omega]}{\rho_o}(K_A - M_A\,\omega^2)^{-1}\,\omega^2[\Omega]^T$ is independent of the optimization variable ρ, then

$$\frac{dK_{s\_D}}{d\rho}\boldsymbol{\delta} + \left[K_{s\_D} - A\right]\frac{d\boldsymbol{\delta}}{d\rho} = 0 \tag{2.33}$$

Again, define the following identities:

- $B = \left[K_{s\_D} - A\right]$ (2.34.1)
- $C = \frac{dK_{s\_D}}{d\rho}$ (2.34.2)

Substitution with equations (2.34.1) and (2.34.2) into equation (2.33) will result in:

$$\frac{d\boldsymbol{\delta}}{d\rho} = -B^{-1}C\boldsymbol{\delta} \tag{2.35}$$

To calculate $\frac{d\mathbf{p}}{d\rho}$, we differentiate equation (2.25) with respect to ρ. Hence,

$$\omega^2[\Omega]^T\frac{d\boldsymbol{\delta}}{d\rho} = [K_A - M_A\omega^2]\frac{d\mathbf{p}}{d\rho} \tag{2.36}$$

Define:

$$D = \omega^2[\Omega]^T \tag{2.37}$$

Then, substitution with equations (2.37) and (2.31.2) into equation (2.36) will result in:

$$\frac{d\mathbf{p}}{d\rho} = K_{fl\_D}^{-1}\,D\,\frac{d\boldsymbol{\delta}}{d\rho} \tag{2.38}$$

From equation (2.38), equation (2.29) will be rewritten as:

$$\frac{dJ}{d\rho} = \boldsymbol{\delta}^T C_w^T K_{fl\_D}^{-1}\,D\,\frac{d\boldsymbol{\delta}}{d\rho} + \mathbf{p}^T\frac{d\boldsymbol{\delta}}{d\rho} \tag{2.39}$$

Substituting $\frac{d\boldsymbol{\delta}}{d\rho}$ from equation (2.35) into equation (2.39) results in

$$\frac{dJ}{d\rho} = -\left[\boldsymbol{\delta}^T C_w^T\;K_{fl\_D}^{-1}\,D\,B^{-1}\,C\,\boldsymbol{\delta} + \mathbf{p}^T\,B^{-1}\,C\,\boldsymbol{\delta}\right] \tag{2.40}$$

Equation (2.40) represents the final form of the objective function sensitivity. During the topology optimization calculation, the effect of the density is substituted for by the effect of the thickness of the plate elements.

2.7 Summary

This chapter has presented the theoretical modeling of the fluid-structure interaction between the dynamics of a flexible flat plate and a rigid acoustic coupled with it. The developed model is integrated with a topology optimization algorithm which utilizes the Moving Asymptotes Method. The model is used to develop the sensitivity analysis necessary for the operation of the topology optimization algorithm.

The prediction of the performance of topology optimized plate/cavity systems will be presented in Chapter 3 and the experimental validation of the mathematical model is presented in Chapter 4.

CHAPTER 3

PERFORMANCE OF THE OPTIMIZED PLATE-CAVITY SYSTEM

3.1 Model Parameters

A finite element model for a closed acoustic cavity coupled with a flexible plate was developed. Two different sets of plates were analyzed for two different fluid domains. Air and water were used as fluid domains while aluminum and Fullcure-720 were used as structural materials of the plates. The physical and mechanical properties of the used materials are listed in table(3.1).

Table 3.1: Physical and mechanical properties for fluid and structural domains.

		Density (Kg/m^3)	Poisson's Ratio	Modulus of Elasticity (GPa)	Sonic Speed (m/s)
Structural Material	Aluminum	2700	0.3	71	N/A
	Fullcure-720	1193.4	0.25	2.87	N/A
Fluid domain	Air	1.2	N/A	N/A	343
	Water	1000	N/A	N/A	1482

One of the major concerns while developing the model was to force the excitation at the structural modal frequencies so that the optimization algorithm will redistribute the material of the plate in such a way to minimize the coupling at that specific modal frequency. The excitation force applied on the plate was selected to be symmetric, and the first 2 odd modes were studied. The initial thickness of the plate under consideration is 1⁄16". It was the objective to use 50% of the material of the plate and minimize the fluid-structure coupling. Therefore the initial guess will start with a plate with uniform thickness of 1⁄32" and while the optimization algorithm

evolves, the thickness should vary between 1⁄16" and 1⁄64", which represents the minimum permissible plate thickness. The plate is excited mechanically with external forces at frequencies locked at the modal frequencies of the coupled plate-cavity system. In specific, the 1st and 5th modes were considered since they represent the first 2 odd modes, which are known of their high acoustic coupling. At each optimization iteration, the structural modal frequencies are expected to change due to the effect of the material redistribution of the plate. Therefore at each iteration step the structural modal frequencies of the first two odd modes for the coupled system are calculated and the excitation frequency is locked on.

In the next sections, the resulted optimal configurations and predicted behaviors for different structural and fluid domains will be presented and discussed.

3.2 Excitation Frequency and Topology Optimization of Air-Aluminum Cavity

The characteristics of the coupled fluid-structure domain are as given in table (3.2).

Table 3.2: Coupled Air-Aluminum domain parameters

Cavity dimensions $(W \times H \times L)$	$12" \times 12" \times 30"$
Fluid domain	Air at 25° C and and 1 atm.
Flexible plate dimensions $(W \times H)$	$12" \times 12"$
Upper bound of flexible plate thickness (h_{max})	$1/16"$
Flexible plate material	Aluminum
Volume fraction (v_f)	0.5
Lower bound of flexible plate thickness (h_{min})	$0.25 \times h_{max}$

In the following two sections, the results of using these parameters in targeting the 1st and 2nd odd modes are being presented.

3.2.1 Excitation Frequency and Topology Optimization of the 1st Mode

The shape of material distribution and relative plate displacement field after 25 iterations are shown in Figure (3.1).

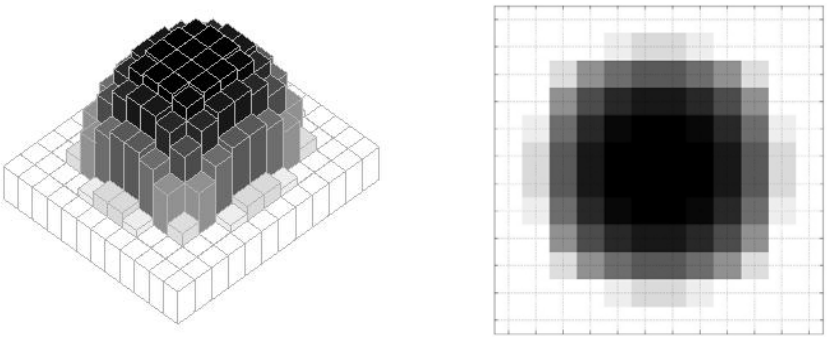

Figure 3.1: Material distribution for the 1st mode optimization of the Air-Aluminum cavity.

The optimization convergence of the objective function ($\boldsymbol{\delta}^T C_w^T \mathbf{p}$) which represents the coupling between the aluminum plate and the air inside the cavity during the optimization process is shown in Figure 3.2.

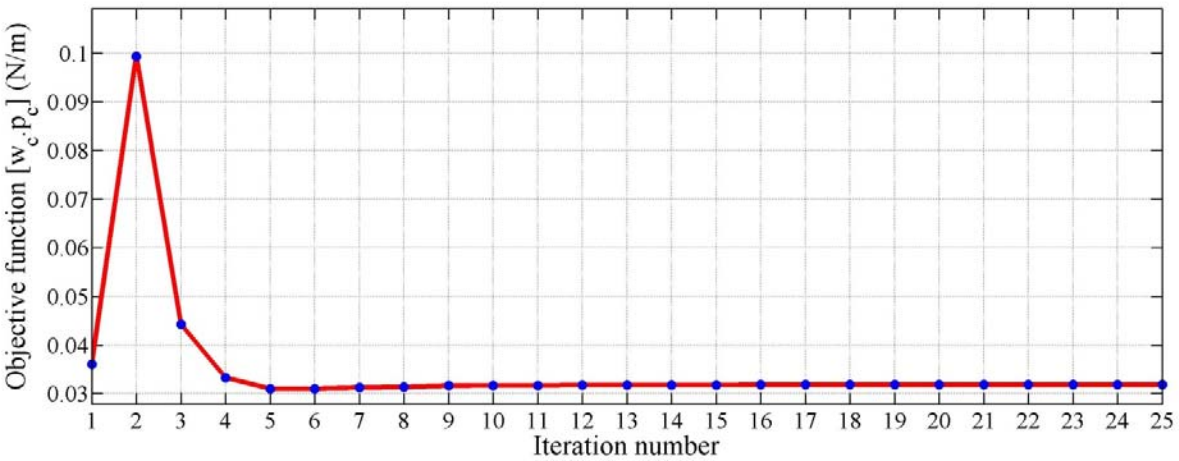

Figure 3.2: Optimization Convergence for 1st structural odd mode of the Air-Aluminum cavity

The frequency response for the plate displacement and the sound pressure level were also monitored. The plate displacement was monitored at the midpoint of the plate and the sound pressure was also calculated at a point 3" away from the midpoint of the plate inside the acoustic cavity.

The frequency responses for the plain and optimized cases are as shown in Figures 3.3 and 3.4.

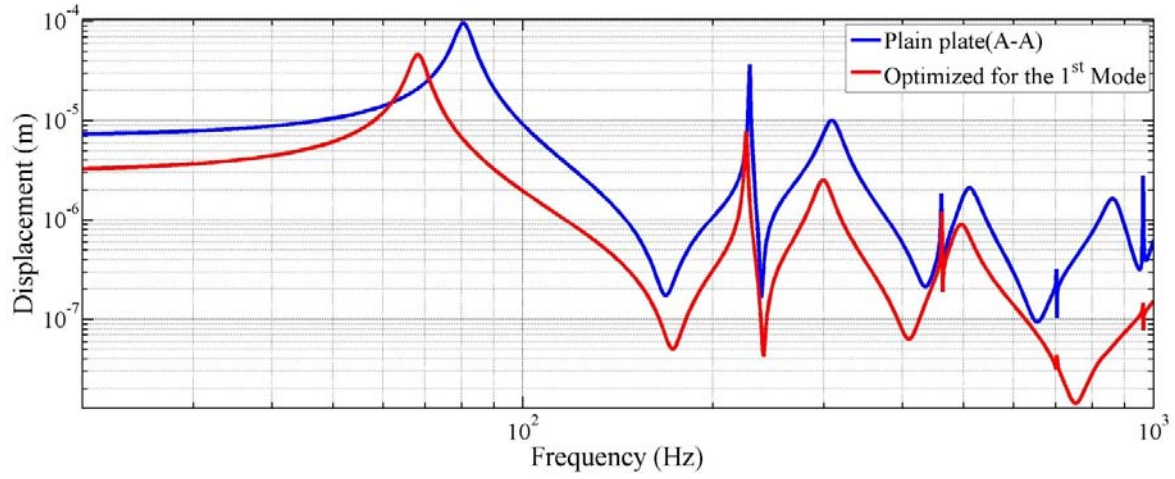

Figure 3.3: Displacements for plain and 1st mode optimized aluminum plates.

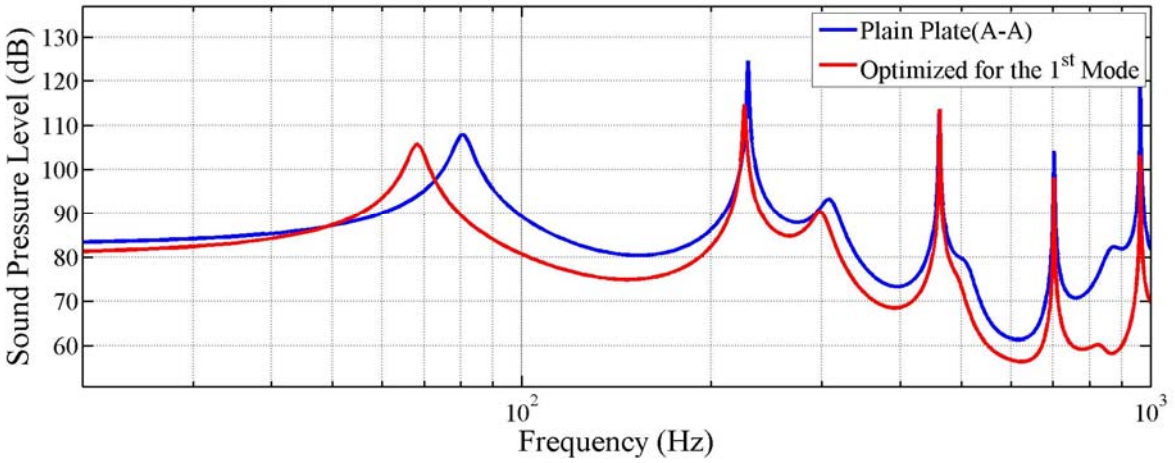

Figure 3.4: Average sound pressure levels inside Air-Aluminum cavity targeting the 1st structural mode

The results of the optimization targeting the 1st mode of the Air-Aluminum cavity are summarized in table (3.3).

Table 3.3: Results summary for Air-Aluminum cavity targeting 1st structural mode.

	Reduction at targeted mode (%)	Broadband reduction (%)
Plate displacement	92	65
Sound pressure level	37	49.5

It can be seen from the above table that by exciting the Aluminum plate at the 1st structural mode frequency, the plate displacement at the targeted mode was considerably reduced. Also, considerable reduction was obtained at other structural modes. The average sound pressure inside cavity was also reduced at the targeted mode and larger reduction can be noted within the selected broadband range.

3.2.2 Excitation Frequency and Topology Optimization of the 2nd Odd Mode

The shape of material distribution and relative plate displacement field after 25 iterations are shown in Figure 3.5.

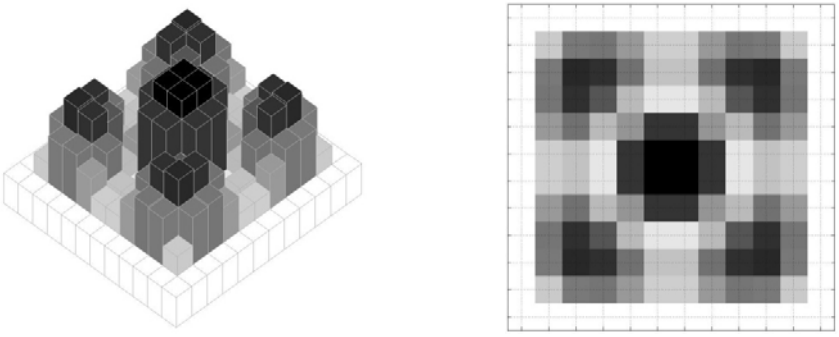

Figure 3.5: Material distribution for the 1st mode optimization of the Air-Aluminum cavity.

Again the solution convergence of the objective function during the optimization process is shown in Figure 3.6.

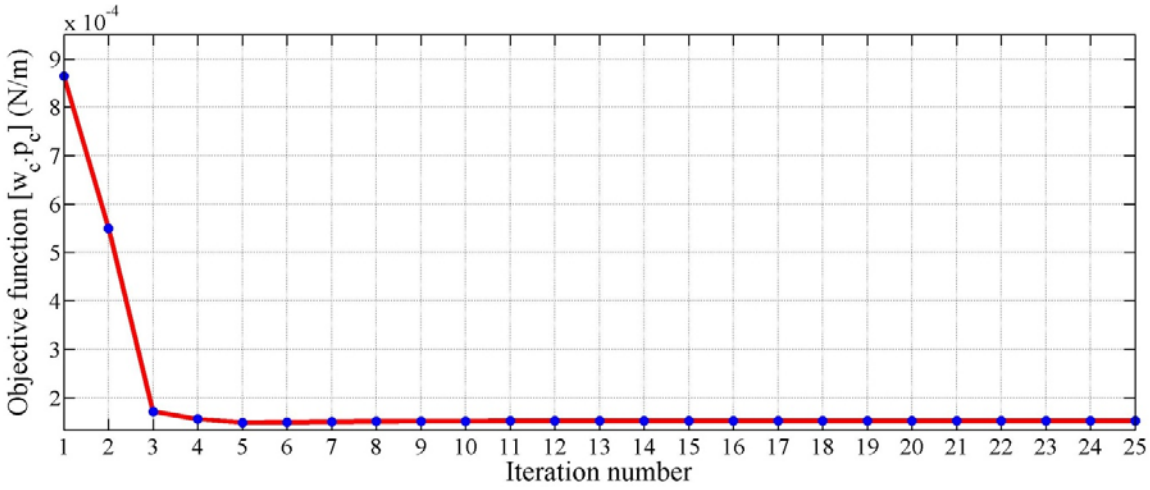

Figure 3.6: Optimization Convergence for 2nd structural odd mode (the 5th mode of vibration) of the Air-Aluminum cavity

The frequency response for the plate displacement, sound pressure level were also monitored for this mode. These responses are shown in Figures 3.7 and 3.8.

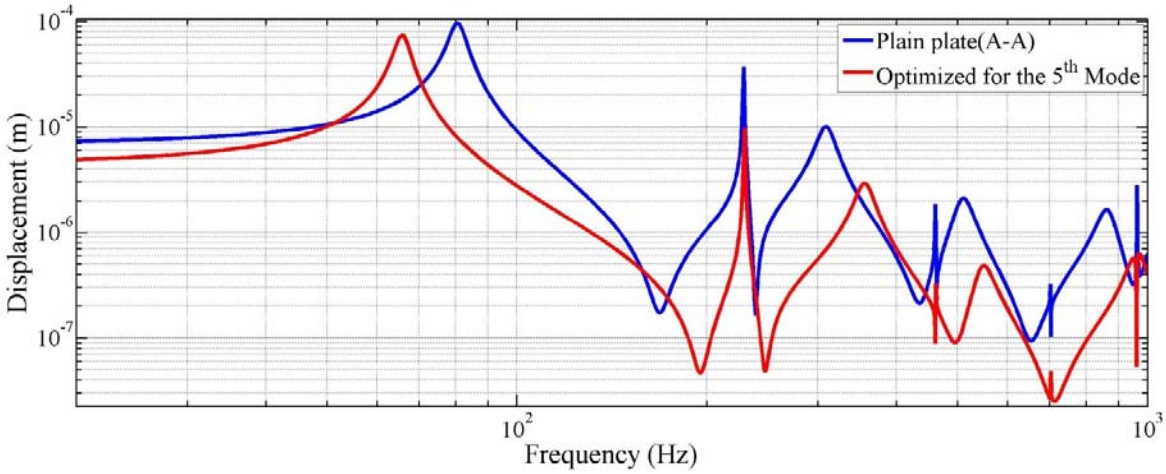

Figure 3.7: Displacements for plain and 2nd odd mode (the 5th mode of vibration) optimized aluminum plates.

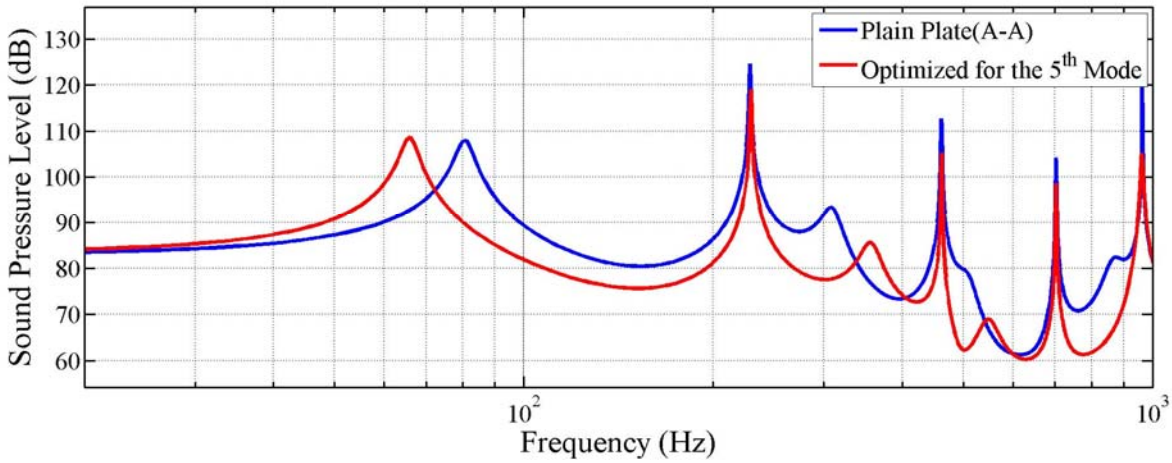

Figure 3.8: Average sound pressure levels inside Air-Aluminum cavity targeting the 5th structural mode

The results of the optimization targeting the 5th mode of the Air-Aluminum cavity are summarized in table (3.4).

Table 3.4: Results summary for Air-Aluminum cavity targeting 5th structural mode.

	Reduction at targeted mode (%)	Broadband reduction (%)
Plate displacement	71	49
Sound pressure level	83	35

Again, it can be seen from the above table that by exciting the Aluminum plate at the 5th structural mode frequency, the plate displacement at the targeted mode was considerably reduced. Also, considerable reduction was obtained at other structural modes. The average sound pressure inside cavity was dramatically reduced at the targeted mode, but lesser effect can be noted at other structural modes.

3.3 Excitation Frequency and Topology Optimization of Water-Aluminum Cavity

The characteristics of the coupled fluid-structure domain are as given in table (3.5).

Table 3.5: Coupled Water-Aluminum domain parameters

Cavity dimensions $(W \times H \times L)$	$12" \times 12" \times 30"$
Fluid domain	Water at 25° C and and 1 atm.
Flexible plate dimensions $(W \times H)$	$12" \times 12"$
Upper bound of flexible plate thickness (h_{max})	$1/16"$
Flexible plate material	Aluminum
Volume fraction (v_f)	0.5
Lower bound of flexible plate thickness (h_{min})	$0.25 \times h_{max}$

3.3.1 Excitation Frequency and Topology Optimization of the 1st Mode

The shape of material distribution and relative plate displacement field after 25 iterations are shown in Figure 3.9.

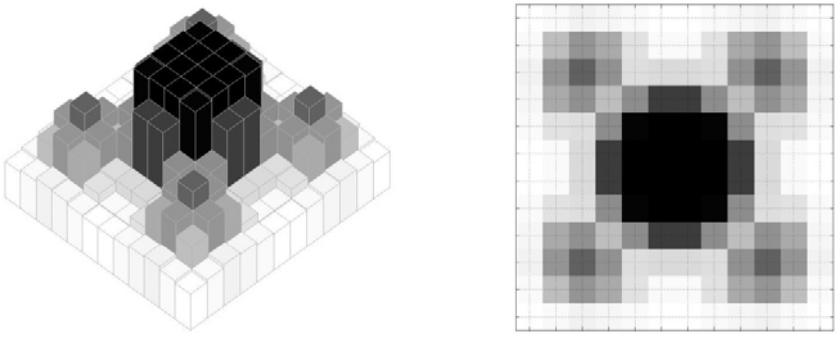

Figure 3.9: Material distribution for the 1st mode optimization of the Water-Aluminum cavity.

The solution convergence of the objective function during the optimization process is shown in Figure 3.10.

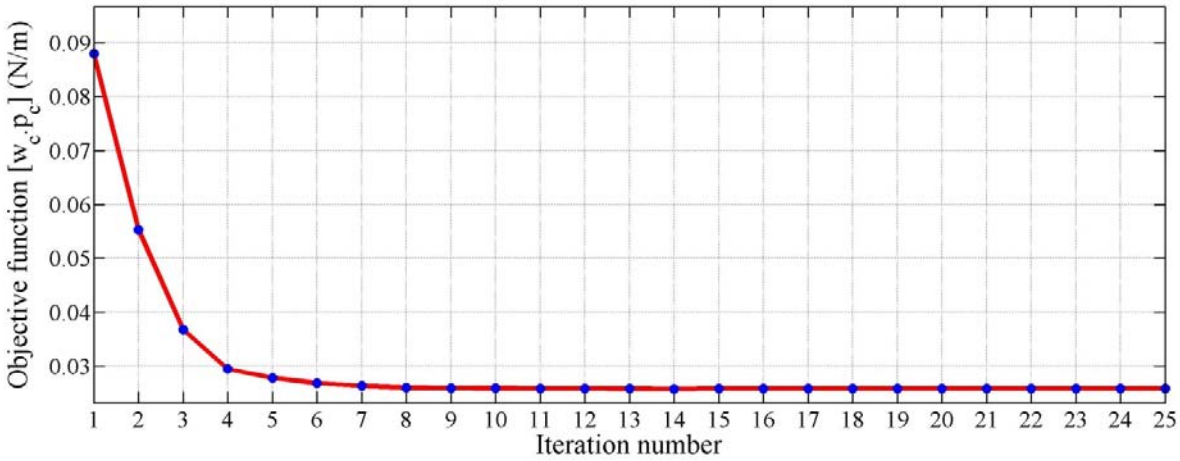

Figure 3.10: Optimization Convergence for 1st structural odd mode of the Water-Aluminum cavity

The frequency response for the plate displacement, sound pressure level and sound intensity are shown in Figures 3.11 and 3.12.

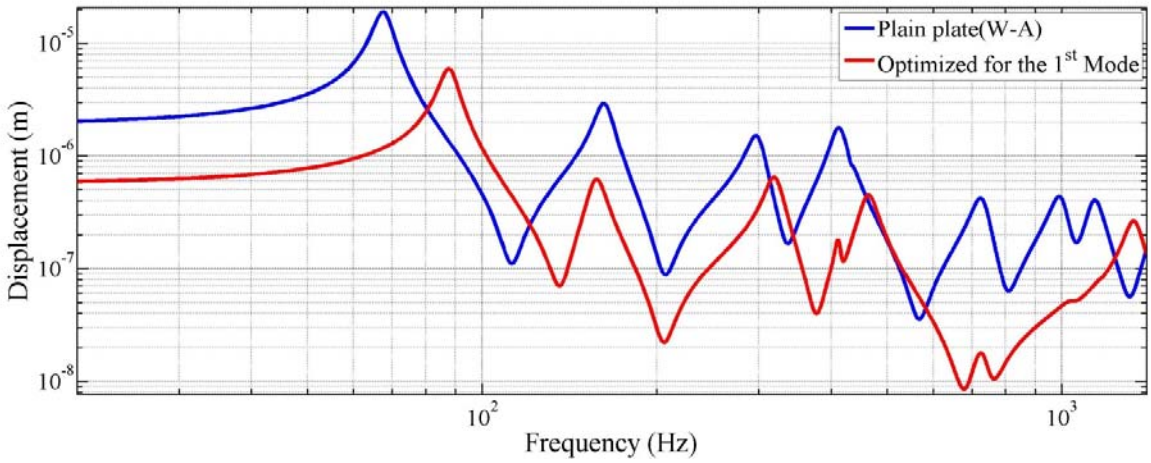

Figure 3.11: Displacements for plain and 1st odd mode optimized aluminum plates.

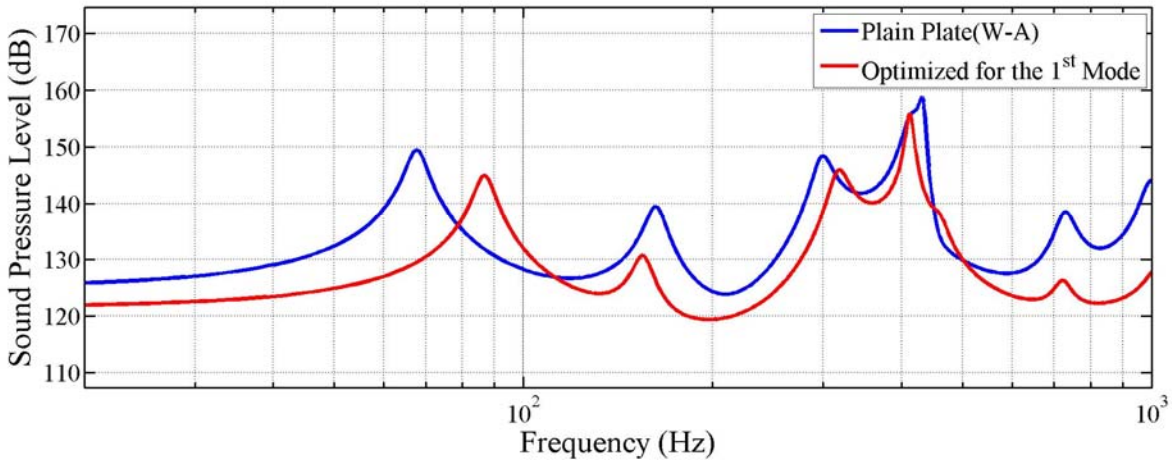

Figure 3.12: Average sound pressure levels inside Water-Aluminum cavity targeting 1st structural mode

The results of the optimization targeting the 1st mode of the Water-Aluminum cavity are summarized in table (3.6).

Table 3.6: Results summary for Water-Aluminum cavity targeting 1st structural mode.

	Reduction at targeted mode (%)	Broadband reduction (%)
Plate displacement	69	67
Sound pressure level	64	41

As it can be noticed, by exciting the Aluminum plate at the 1st structural mode frequency, the plate displacement was considerably reduced not only at the targeted mode but also at other structural modes. A considerable reduction was also obtained in the average sound pressure level at the 1st structural mode and the broadband range.

3.3.2 Excitation Frequency and Topology Optimization of the 2nd Odd Mode

The shape of material distribution and relative plate displacement field after 25 iterations are shown in Figure 3.13.

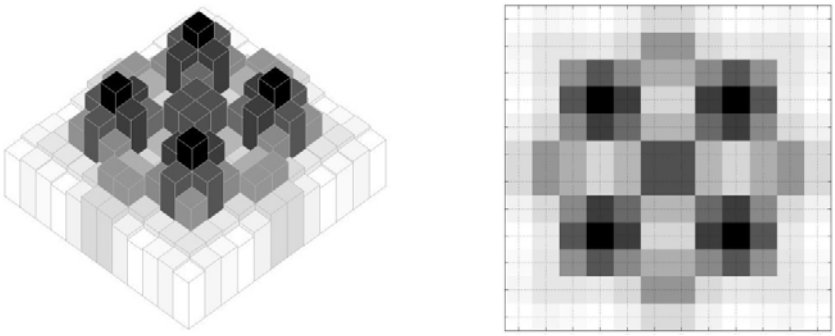

Figure 3.13: Material distribution for the 2nd odd mode optimization of the Water-Aluminum cavity

The solution convergence of the objective function during the optimization process is shown in Figure 3.14.

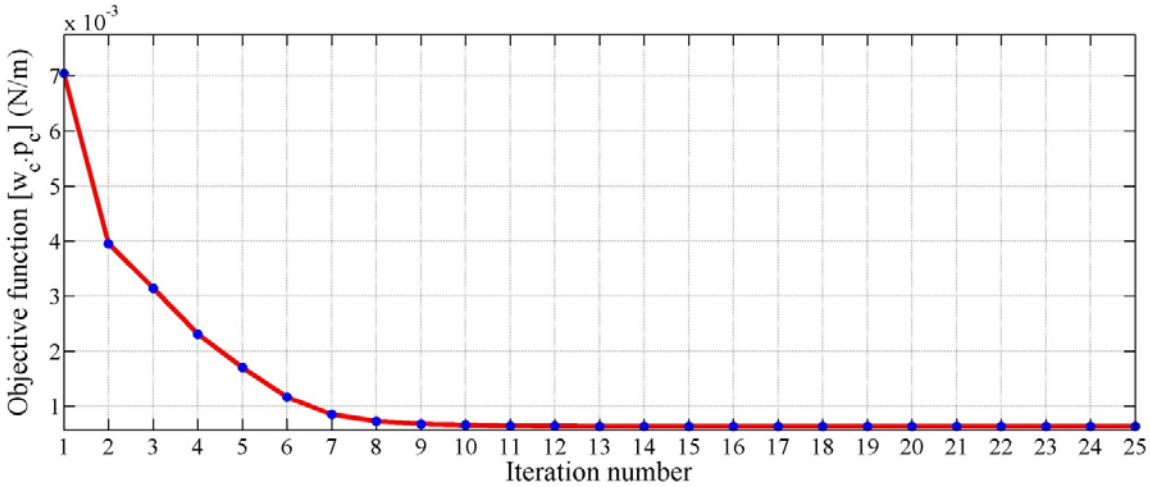

Figure 3.14: Optimization Convergence for 2nd structural odd mode of the Water-Aluminum cavity

The frequency response for the plate displacement, sound pressure level and sound intensity are shown in Figures 3.15 and 3.16.

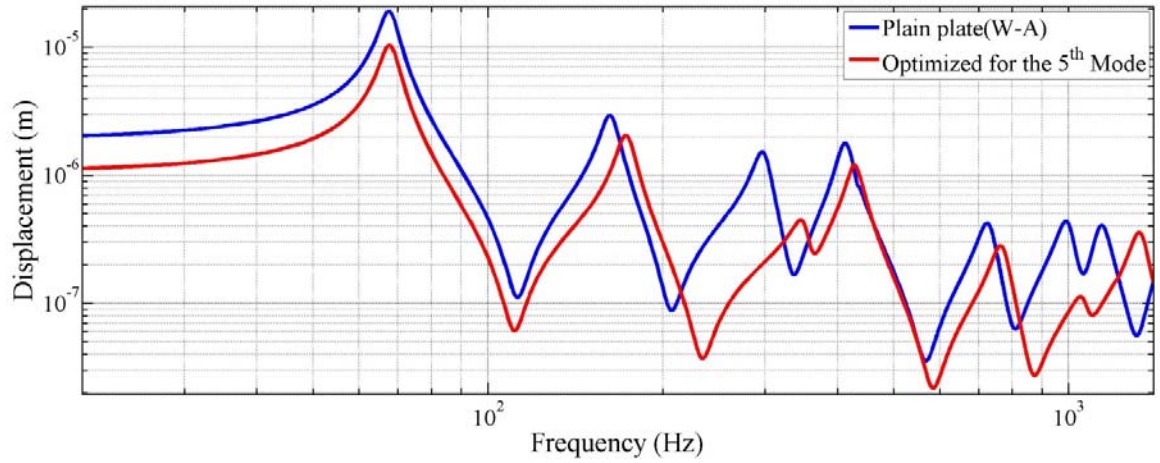

Figure 3.15: Displacements for plain and 2nd odd mode optimized aluminum plates.

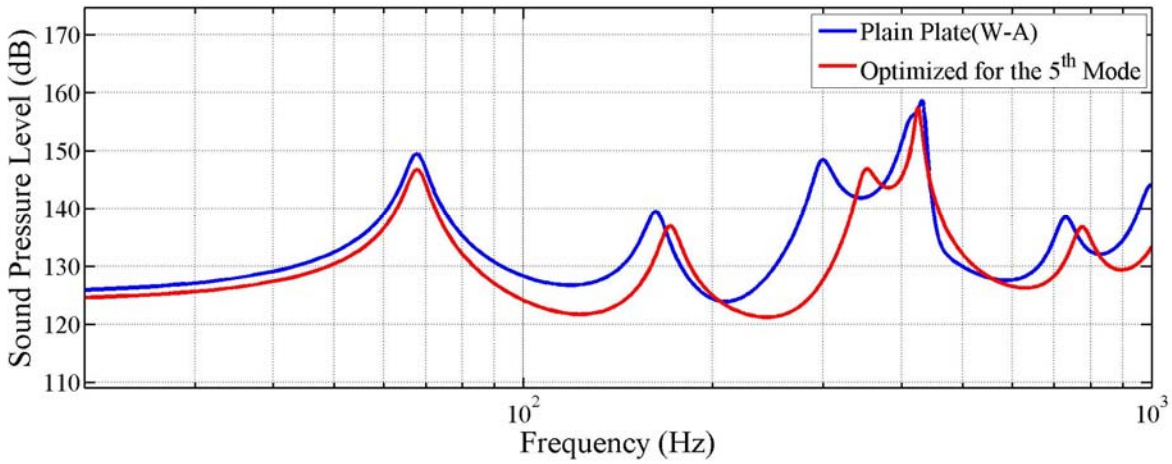

Figure 3.16: Average sound pressure levels inside Water-Aluminum cavity targeting the 5th structural mode

The results of the optimization targeting the 5th mode of the Water-Aluminum cavity are summarized in table (3.7).

Table 3.7: Results summary for Water-Aluminum cavity targeting 5th structural mode.

	Reduction at targeted mode (%)	Broadband reduction (%)
Plate displacement	71	44
Sound pressure level	31	25

As it can be noticed, by exciting the Aluminum plate at the 5th structural mode frequency, the plate displacement was considerably reduced at this mode but with lesser effect on other structural modes. The optimized plate has a reduced average sound pressure level at the 5th mode and through the broadband range.

3.4 Excitation Frequency and Topology Optimization of Air-Fullcure720 Cavity

The characteristics of the coupled fluid-structure domain are as given in table (3.8).

Table 3.8: Coupled Air-FullCure720 domain parameters

Cavity dimensions ($W \times H \times L$)	$12" \times 12" \times 30"$
Fluid domain	Air at 25° C and and 1 atm.
Flexible plate dimensions ($W \times H$)	$12" \times 12"$
Upper bound of flexible plate thickness (h_{max})	$1/16"$
Flexible plate material	Full Cure 720
Volume fraction (v_f)	0.5
Lower bound of flexible plate thickness (h_{min})	$0.25 \times h_{max}$

3.4.1 Excitation Frequency and Topology Optimization of the 1st Mode

The shape of material distribution and relative plate displacement field after 25 iterations are shown in Figure 3.17.

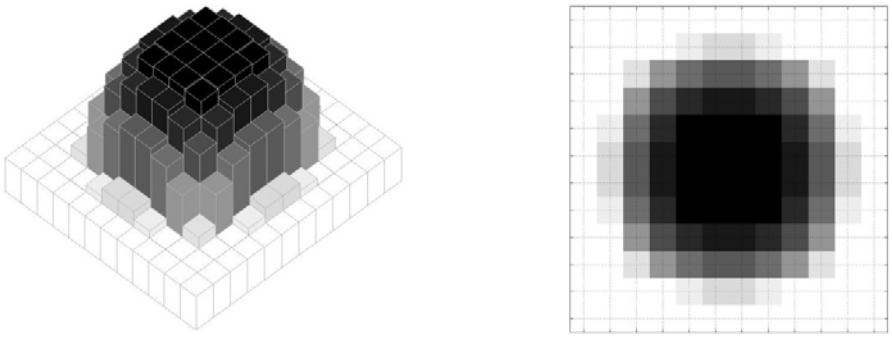

Figure 3.17: Material distribution for the 1st odd mode optimization of the Air-FullCure720 cavity

The solution convergence of the objective function during the optimization process is shown in Figure 3.18.

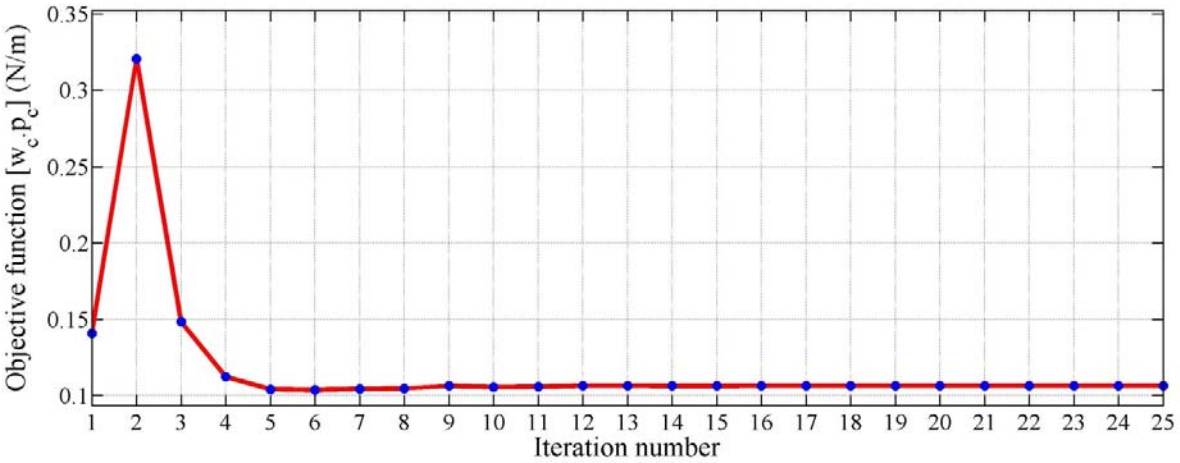

Figure 3.18: Optimization Convergence for 1st structural mode of the Air-FullCure720 cavity

The frequency response for the plate displacement, sound pressure level and sound intensity are shown in Figures 3.19 and 3.20.

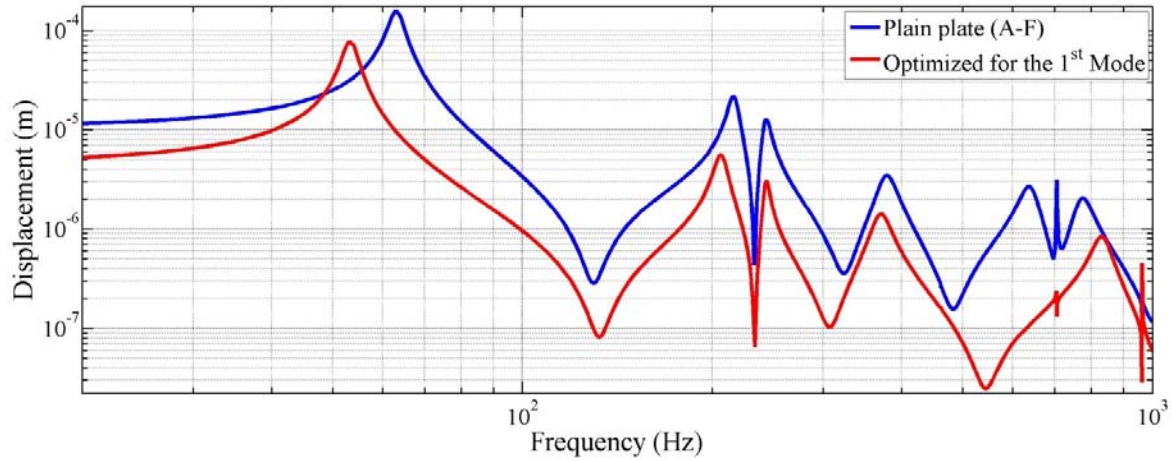

Figure 3.19: Displacements for plain and 1st mode optimized FullCure720 plates.

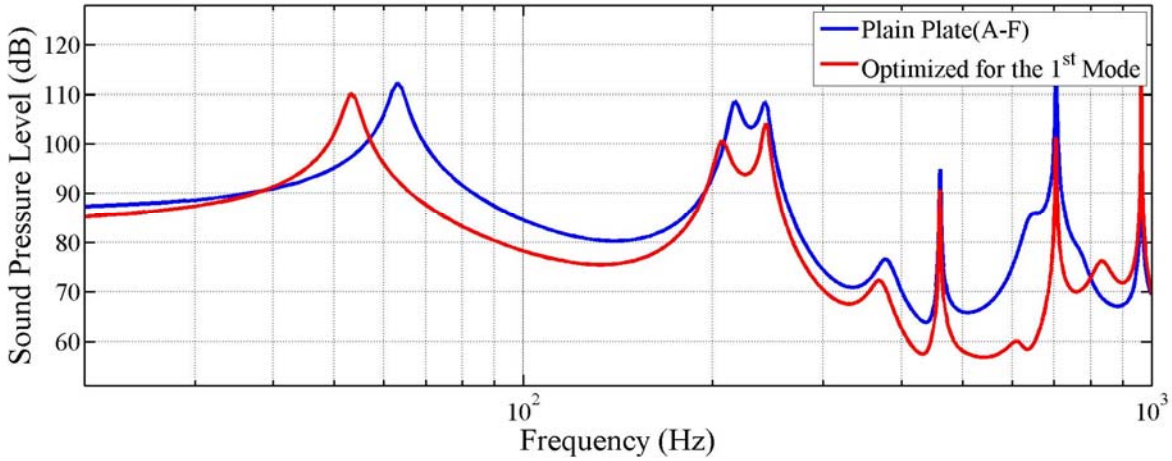

Figure 3.20: Average sound pressure levels inside Air-Fullcure720 cavity targeting 1st structural mode

The results of the optimization targeting the 1st mode of the Air-Fullcure720 cavity are summarized in table (3.9).

Table 3.9: Results summary for Air-FullCure720 cavity targeting 1st structural mode.

	Reduction at targeted mode %	Broadband reduction %
Plate displacement	51	65
Sound pressure level	39	38

It is clear that by exciting the Fullcure720 plate at the 1st structural mode frequency, the plate displacement was considerably reduced at the 1st mode and also at other structural modes. Good reduction was also achieved in the average sound pressure level at the targeted mode and through the broadband range.

3.4.2 Excitation Frequency and Topology Optimization of the 2nd Odd Mode

The shape of material distribution and relative plate displacement field after 25 iterations are shown in Figure 3.21.

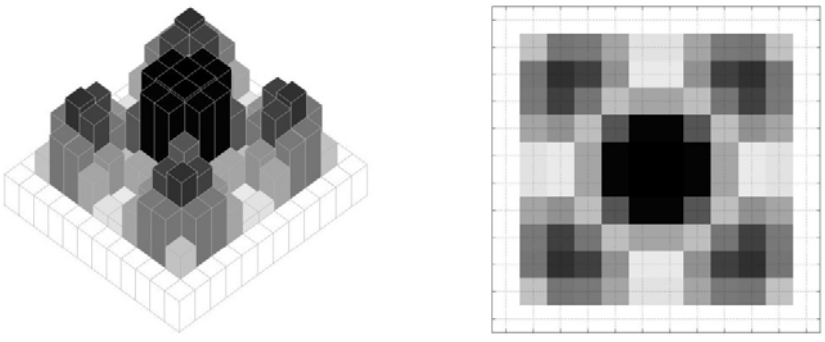

Figure 3.21: Material distribution for the 2nd odd mode optimization of the Air-FullCure720 cavity

The solution convergence of the objective function during the optimization process is shown in Figure 3.22.

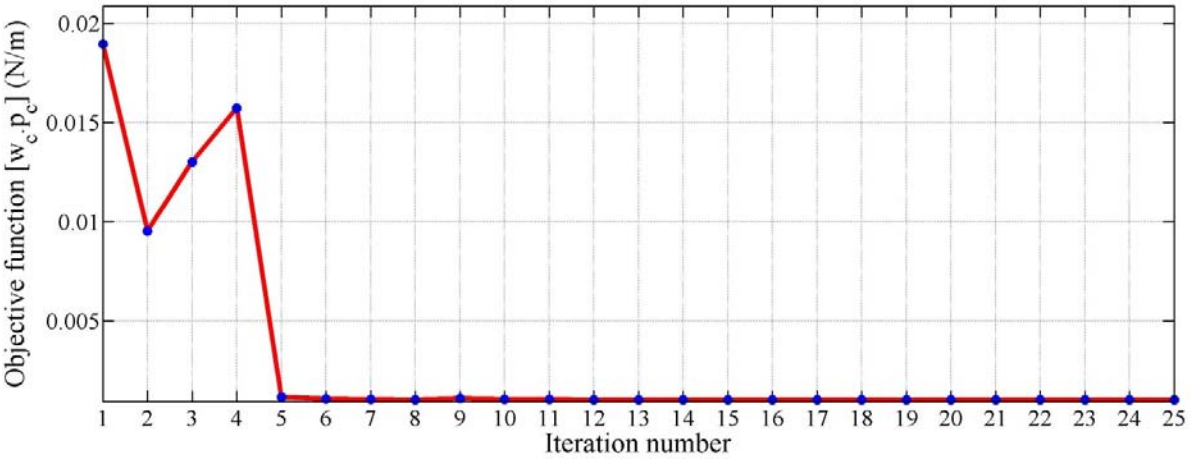

Figure 3.22: Optimization Convergence for 2nd structural odd mode of the Air-FullCure720 cavity

The frequency response for the plate displacement, sound pressure level and sound intensity are shown in Figures 3.23 and 3.24.

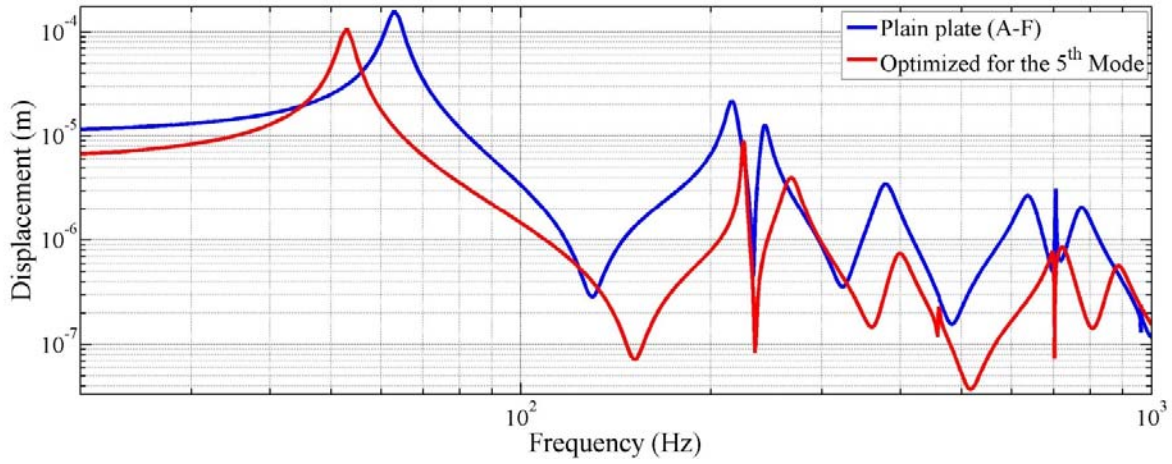

Figure 3.23: Displacements for plain and 2nd odd mode optimized FullCure720 plates.

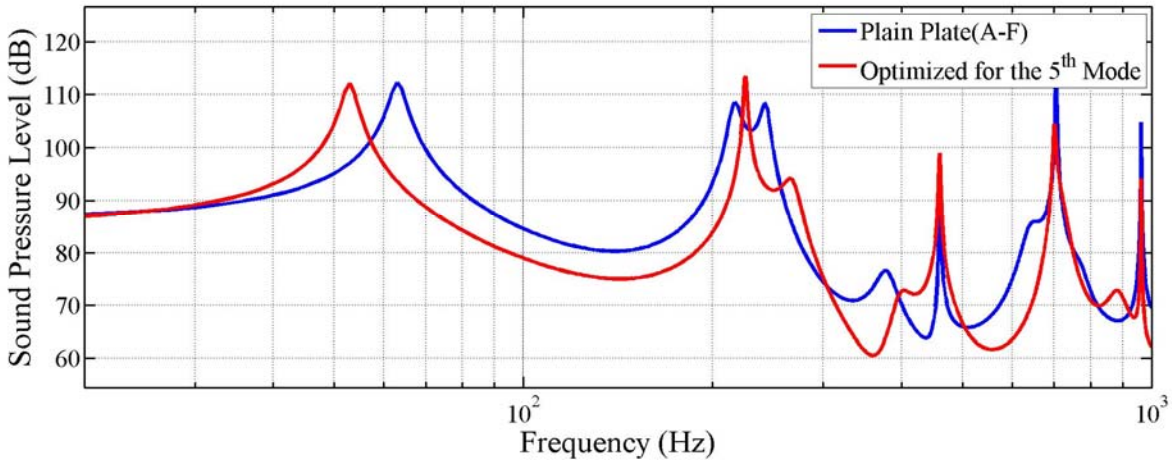

Figure 3.24: Average sound pressure levels inside Air-Fullcure720 cavity targeting the 5th structural mode

The results of the optimization targeting the 5th structural mode of the Air-Fullcure720 cavity are summarized in table (3.10).

Table 3.10: Results summary for Air-Fullcure720 cavity targeting 5th structural mode.

	Reduction at targeted mode %	Broadband reduction %
Plate displacement	69	56
Sound pressure level	96	22

It can be seen from the above table that by exciting the Fullcure720 plate at the 5th structural mode frequency, the plate displacement at the targeted mode was considerably reduced. Also, considerable reduction was obtained at other structural modes. The average sound pressure inside cavity was dramatically reduced at the targeted mode, but lesser effect can be noted through the broadband range.

3.5 Excitation Frequency and Topology Optimization of Water-Fullcure720 Cavity

The characteristics of the coupled fluid-structure domain are as given in table (3.11).

Table 3.11: Coupled Water-FullCure720 domain parameters

Cavity dimensions $(W \times H \times L)$	$12" \times 12" \times 30"$
Fluid domain	Water at 25° C and and 1 atm.
Flexible plate dimensions $(W \times H)$	$12" \times 12"$
Upper bound of flexible plate thickness (h_{max})	$1/16"$
Flexible plate material	Full Cure 720
Volume fraction (v_f)	0.5
Lower bound of flexible plate thickness (h_{min})	$0.25 \times h_{max}$

3.5.1 Excitation Frequency and Topology Optimization of the 1st Mode

The shape of material distribution and relative plate displacement field after 25 iterations are shown in Figure 3.25.

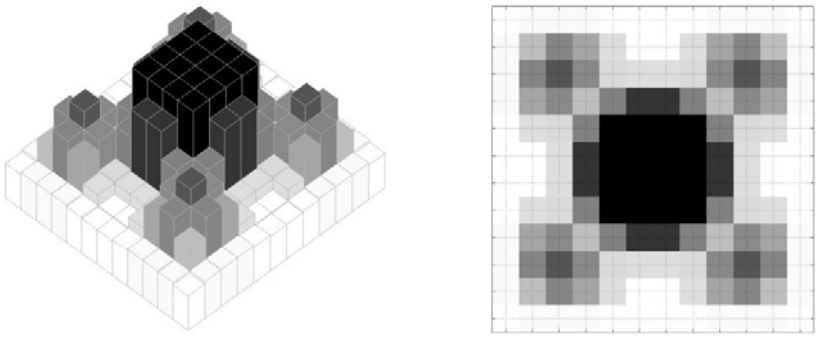

Figure 3.25: Material distribution for the 1st mode optimization of the Water-FullCure720 cavity

The solution convergence of the objective function during the optimization process is shown in Figure 3.26.

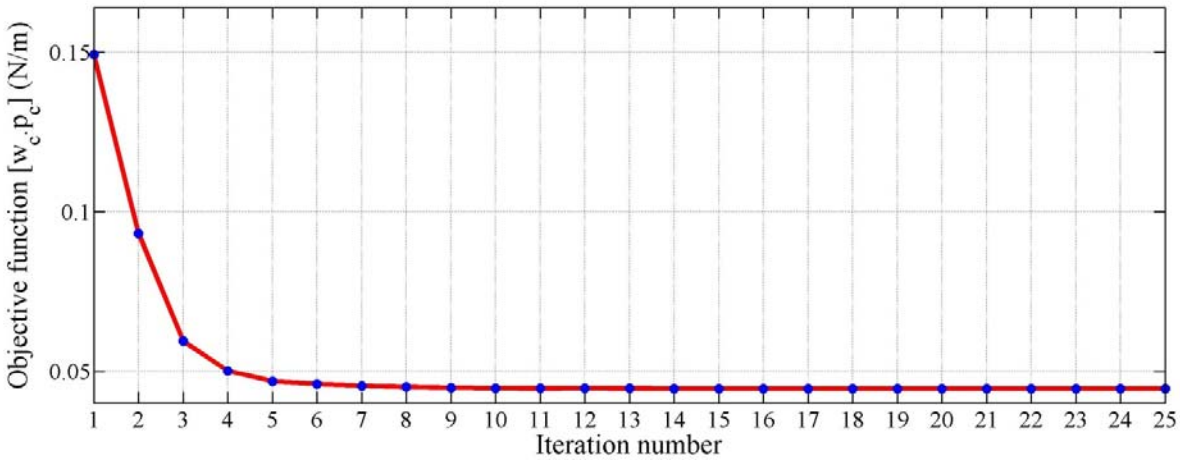

Figure 3.26: Optimization Convergence for 1st structural mode of the Water-FullCure720 cavity

The frequency response for the plate displacement, sound pressure level and sound intensity are shown in Figures 3.27 and 3.28.

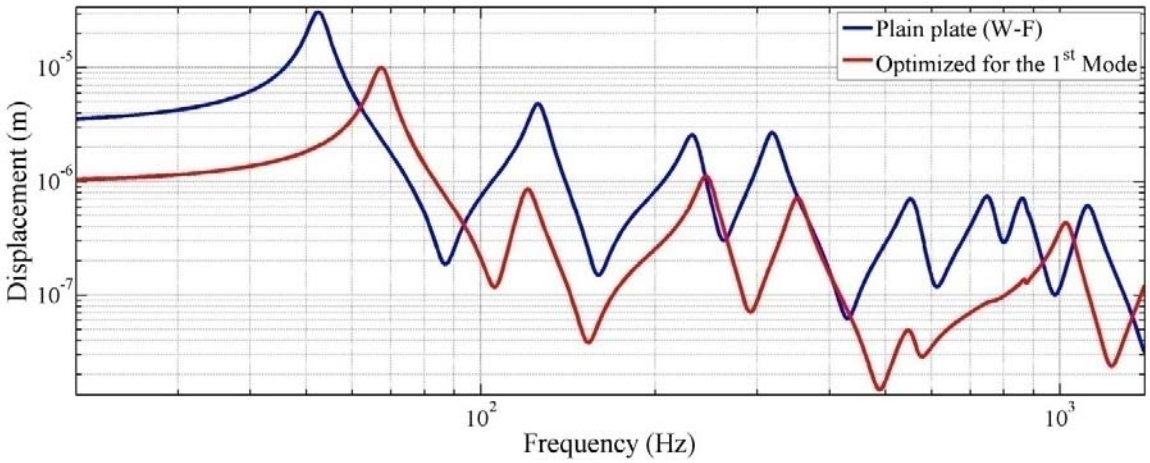

Figure 3.27: Displacements for plain and 1st mode optimized FullCure720 plates.

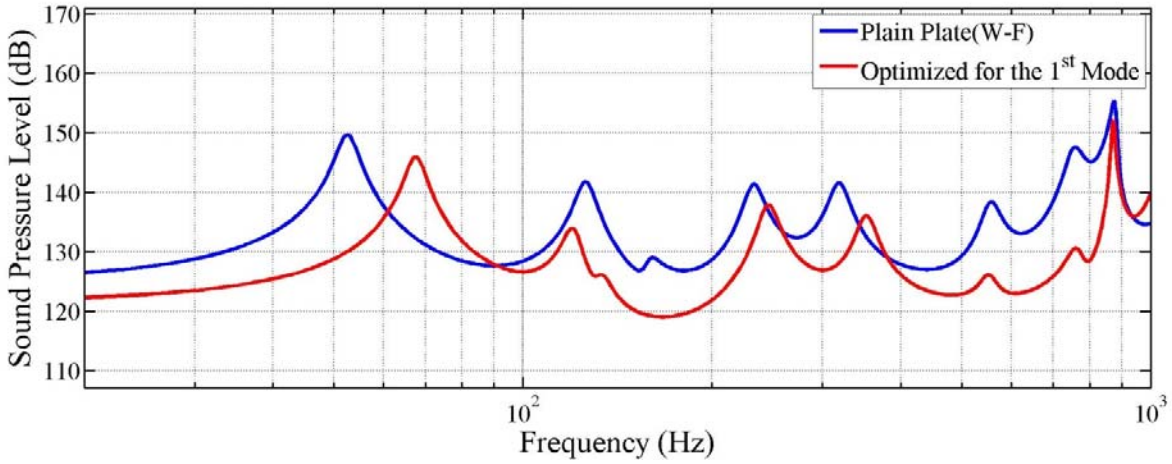

Figure 3.28: Average sound pressure levels inside Water-Fullcure720 cavity targeting the 1st structural mode

The results of the optimization targeting the 1st structural mode of the Air-Fullcure720 cavity are summarized in table (3.12).

Table 3.12: Results summary for Water-Fullcure720 cavity targeting 1st structural mode.

	Reduction at targeted mode %	Broadband reduction %
Plate displacement	67	66
Sound pressure level	47	43

As it can be noticed, by exciting the Fullcure720 plate at the 1st structural mode frequency, the plate displacement was considerably reduced not only at the targeted mode but also at other structural modes. A considerable reduction was also obtained in the average sound pressure level at the 1st structural mode and the broadband range.

3.5.2 Excitation Frequency and Topology Optimization of the 2nd odd Mode

The shape of material distribution and relative plate displacement field after 25 iterations are shown in Figure 3.29.

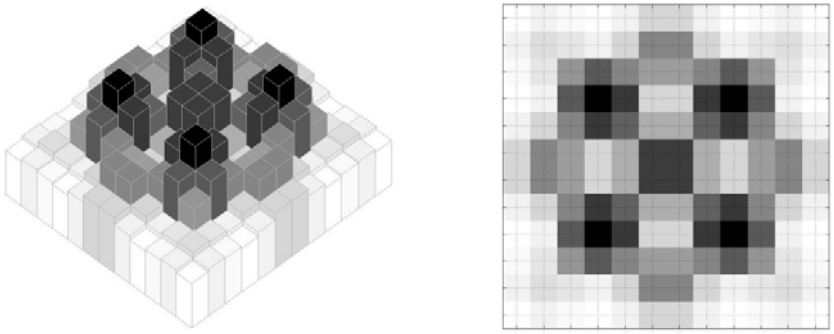

Figure 3.29: Material distribution for the 2nd odd mode optimization of the Water-FullCure720 cavity

The solution convergence of the objective function during the optimization process is shown in Figure 3.30.

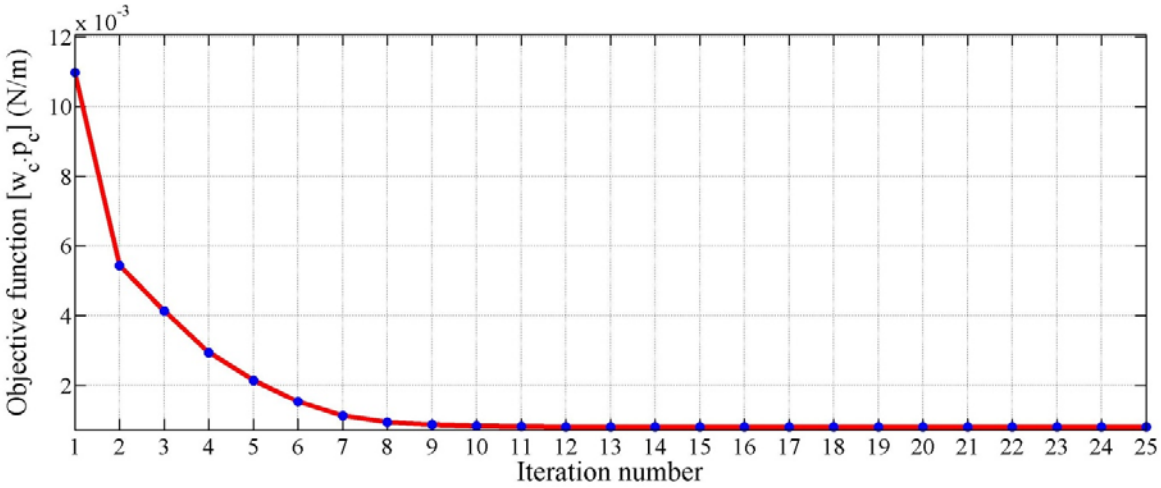

Figure 3.30: Optimization Convergence for 2nd odd structural mode of the Water-FullCure720 cavity

The frequency response for the plate displacement, sound pressure level and sound intensity are shown in Figures 3.31 and 3.32.

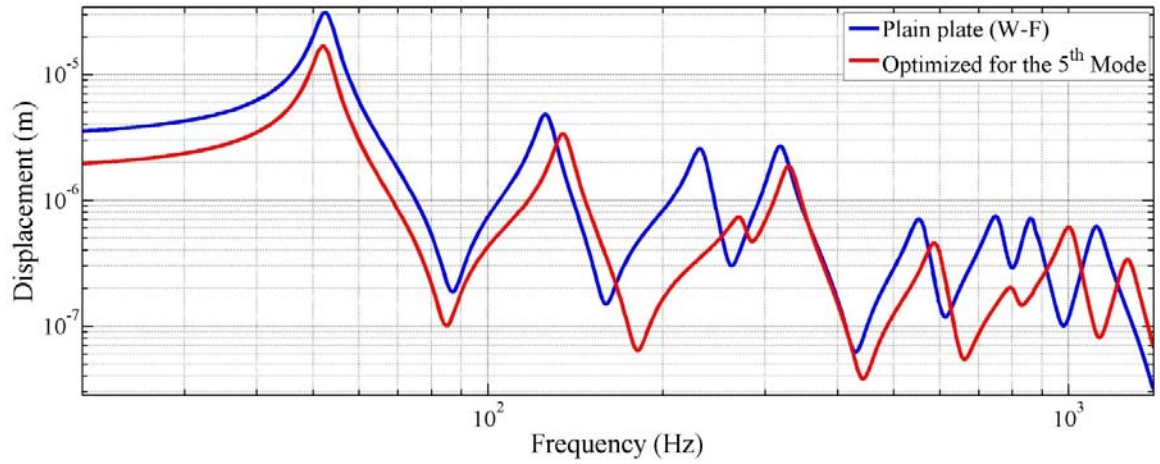

Figure 3.31: Displacements for plain and 2nd odd mode optimized FullCure720 plates.

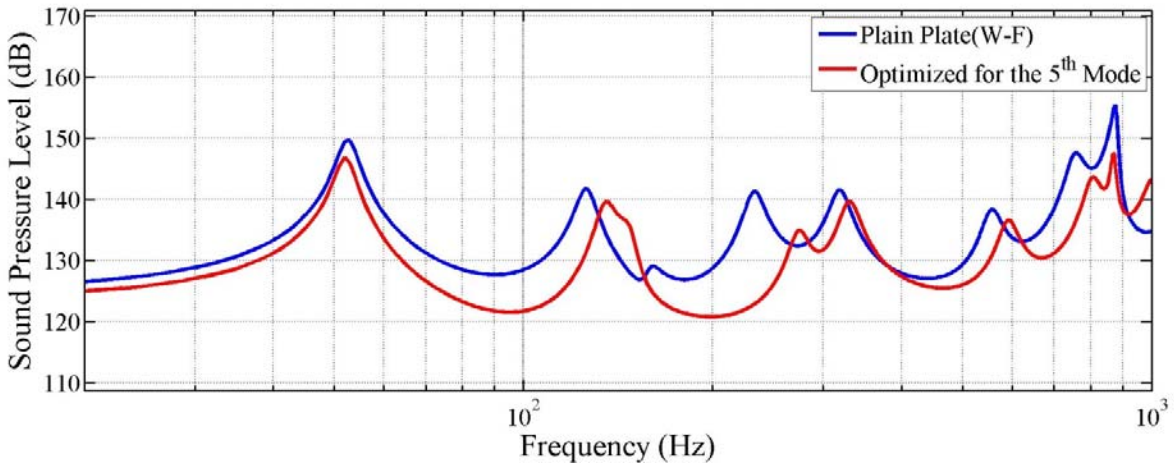

Figure 3.32: Average sound pressure levels inside Water-Fullcure720 cavity targeting the 5th structural mode

The results of the optimization targeting the 5th structural mode of the Water-Fullcure720 cavity are summarized in table (3.13).

Table 3.13: Results summary for Water-Fullcure720 cavity targeting 5th structural mode.

	Reduction at targeted mode %	Broadband reduction %
Plate displacement	72	42
Sound pressure level	75	25

It is clear that by exciting the Fullcure720 plate at the 5th structural mode frequency, the plate displacement and average sound pressure level inside cavity at targeted mode were dramatically reduced. Considerable reduction was also achieved in plate displacement through the broadband range. However, lesser effect was shown on the average sound pressure level at other structural modes.

3.4 Summary

This chapter has presented the theoretical performance characteristics of a plate coupled with an acoustic cavity when the plate topology is optimized to target the first or the second odd modes. The obtained results demonstrate the effectiveness of the developed approach in minimizing the coupling between the plate and the cavity, minimizing the structural vibration, and minimizing the sound radiation without the use of any passive or active damping means.

CHAPTER 4

EXPERIMENTAL VERIFICATION

4.1 Experimental setup

To verify the obtained results experimentally, a set of 3 different Aluminum plate configurations and a set of 3 different FullCure720 plate configurations were prepared. The first plate of each set has surface dimensions of 12"×12" and uniform thickness of 1/32". The 2nd and 3rd plates of each set have the optimal configurations resulted from the topology optimization processes when targeting the 1st and 2nd structural odd modes respectively, while maintaining the volume equal to the first plain case as shown in Figures 4.1 and 4.2.

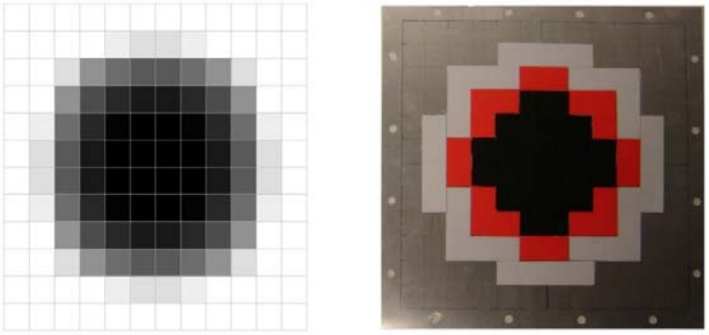

Figure 4.1 : Manufactured aluminum plate approximating the optimization results when targeting the 1st odd mode

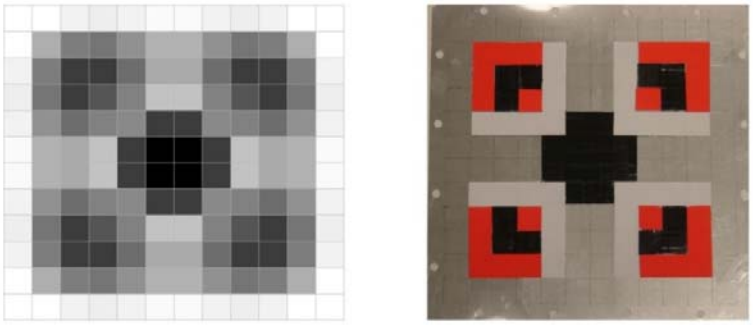

Figure 4.2: Manufactured aluminum plate approximating the optimization results when targeting the 2nd odd mode

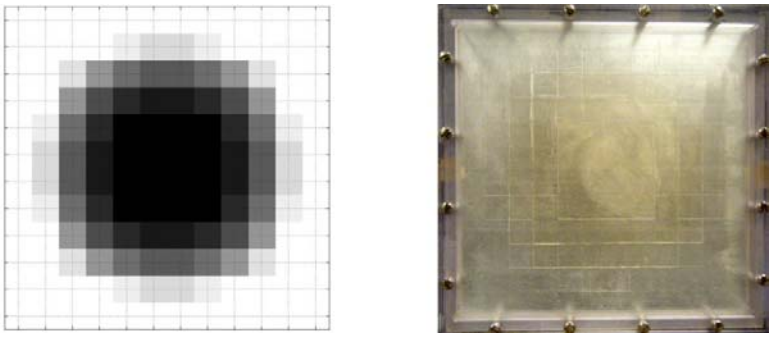

Figure 4.3: Manufactured FullCure720 plate with the exact optimization results when targeting the 1st odd mode

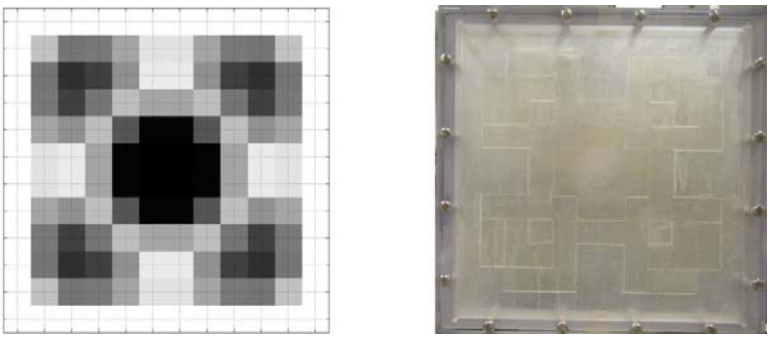

Figure 4.4: Manufactured FullCure720 plate with the exact optimization results when targeting the 2nd odd mode

In Figures 4.1 and 4.2, the plain uncovered metal has a thickness of 1/64", the white-covered parts have a thickness of 1/32", the red-covered parts have a thickness of 3/64" and finally the black-covered plate parts have a thickness of 1/16".

Also, a 12"×12"×30" closed acoustic cavity was prepared. The cavity has only one surface coupled to the flexible plate as shown in Figure 4.5. Each of the 3 different plates of each set was mounted and the plate acceleration as well as the sound pressure level inside the cavity was measured. The plate was mechanically excited with a speaker that is mounted in a position to cause the excitation to be symmetric.

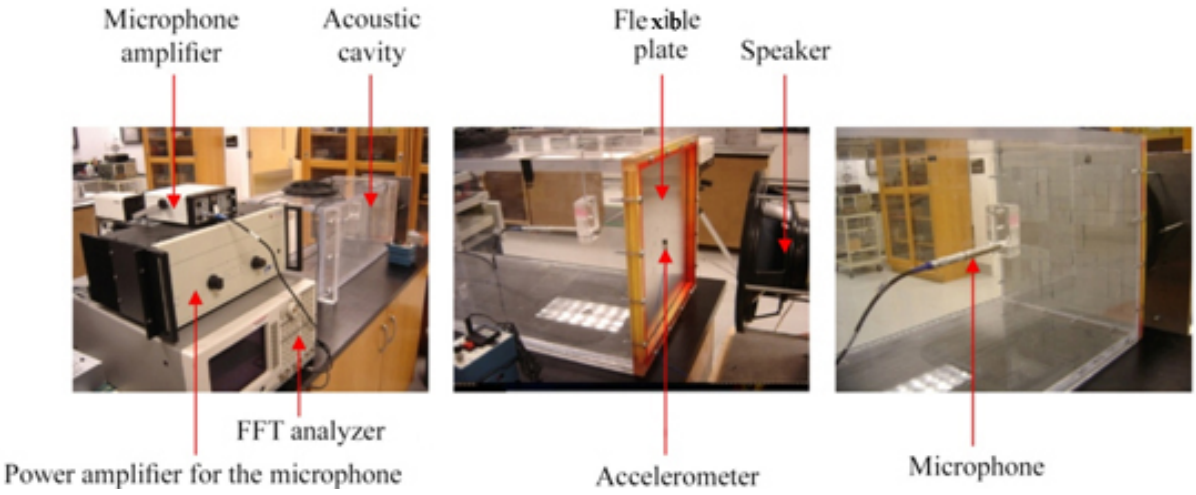

Figure 4.5 : Experimental setup

The speaker was excited with a function generator that sweeps a frequency range between 40 Hz and 1 kHz with a resolution of 0.5 Hz. The acceleration was measured at the midpoint of the plate and the sound pressure was measured at a point corresponding to the midpoint of the plate, only 3" away.

4.2 Experimental results for Air-Aluminum cavity

Frequency response for the aluminum plate acceleration as well as the sound pressure inside the acoustic cavity are shown in Figures 4.6 and 4.7 for the first case, where the optimization is tailored to the 1st structural odd mode. The same results for the optimization tailored to the 2nd odd mode are shown in Figures 4.8 and 4.9.

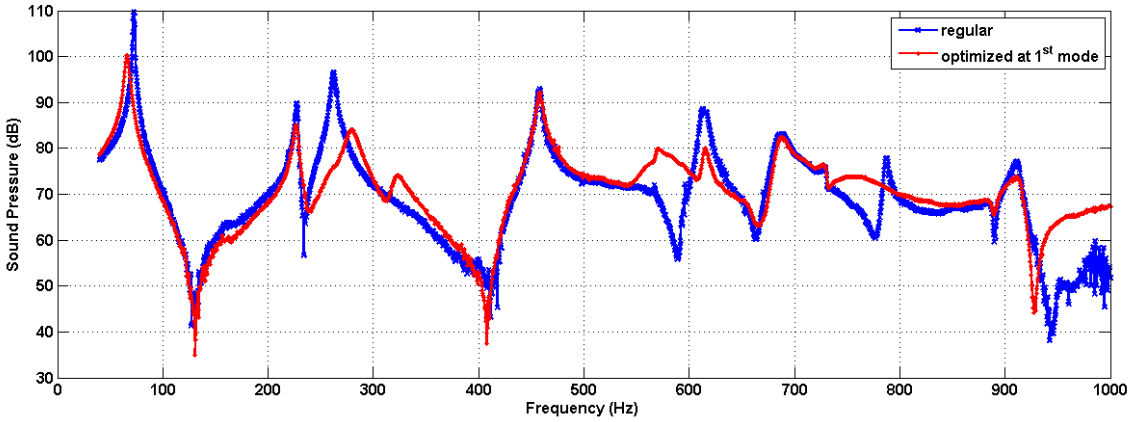

Figure 4.6 : Sound Pressure for regular and 1st mode optimized cases

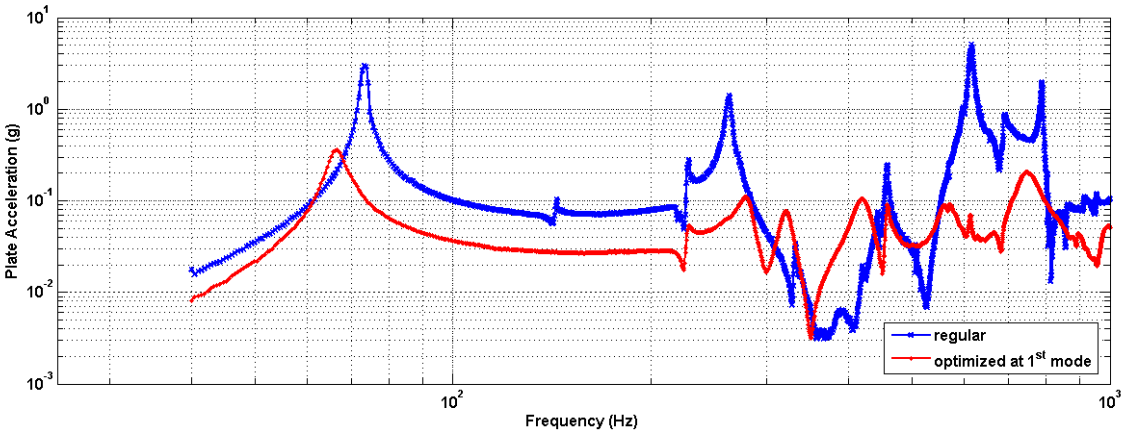

Figure 4.7: Plate acceleration for regular and 1st mode optimized cases

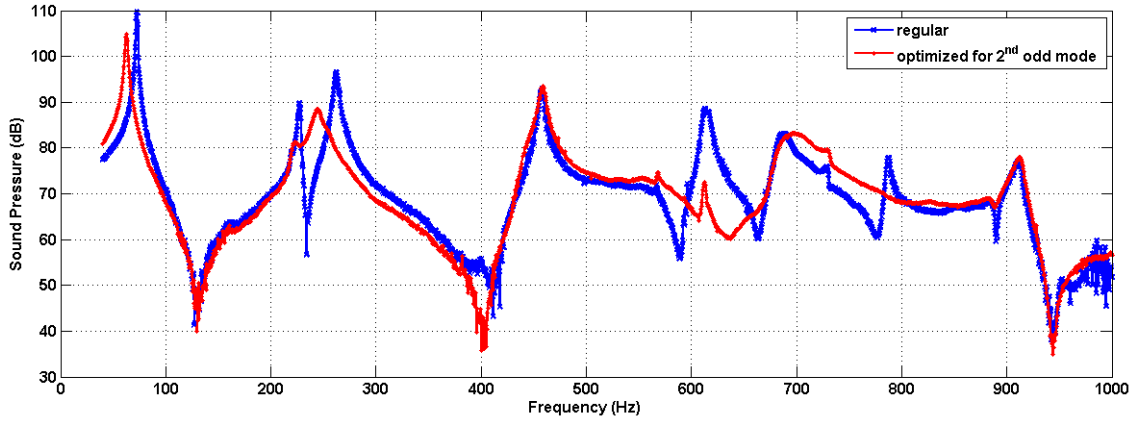

Figure 4.8: Sound Pressure for regular and 2nd odd mode optimized cases

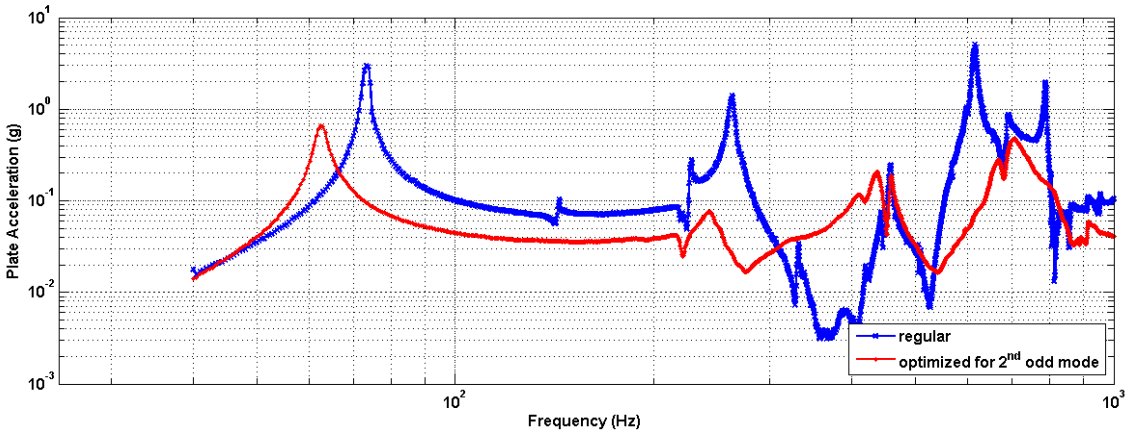

Figure 4.9: Plate acceleration for regular and 2nd odd mode optimized cases

In addition to the frequency response measurement for the plate vibration acceleration and sound pressure inside the acoustic cavity, the plate displacement field was measured using a laser vibrometer. The setup is shown in Figure 4.10.

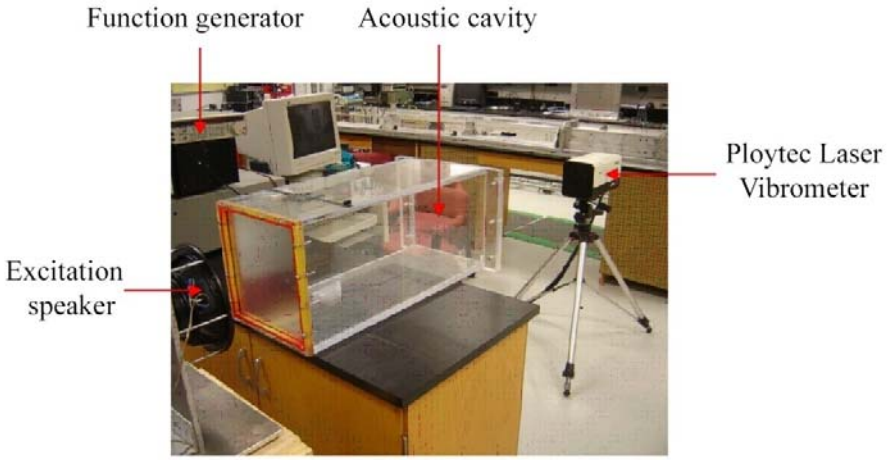

Figure 4.10: Laser vibrometer experimental setup

The 3 plate sets were excited at the 1st structural odd mode using a function generator and the excitation speaker. The laser vibrometer from the other hand was used to measure the displacement field of the different plates, while locked at the same excitation frequency. When attempting to apply the same for the 2nd structural odd mode, the plain plate was successful,

while the other optimized plates were not, due to the extremely low amplitude of the displacement at that mode due to the topology optimization. The displacement fields are shown in Figure 4.11 through Figure 4.14.

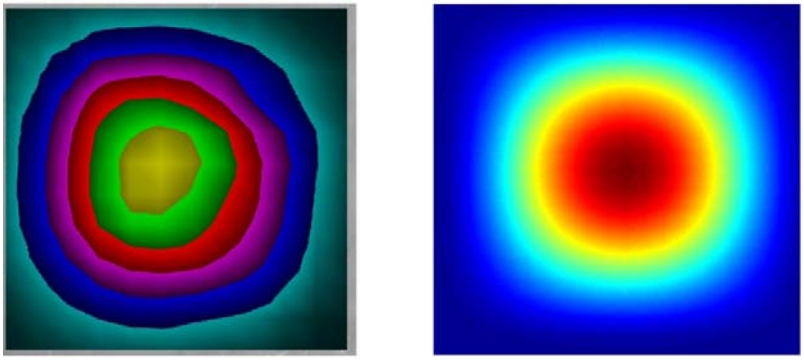

(a) (b)

Figure 4.11: Displacement field for the plain plate excited at the 1st structural odd mode. (a) Experimental, (b) Analytical.

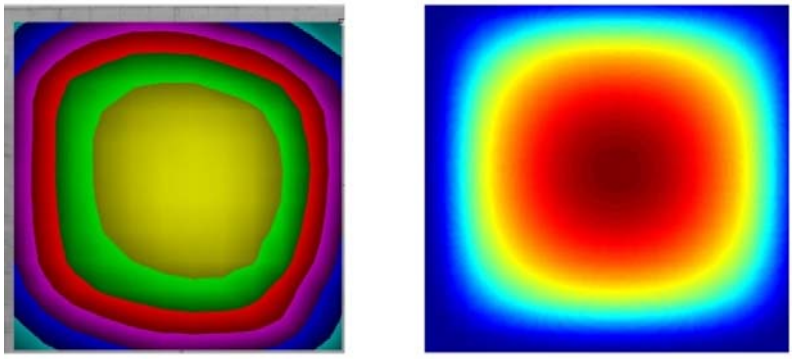

(a) (b)

Figure 4.12: Displacement field for the plate optimized for the 1st structural odd mode. (a) Experimental, (b) Analytical.

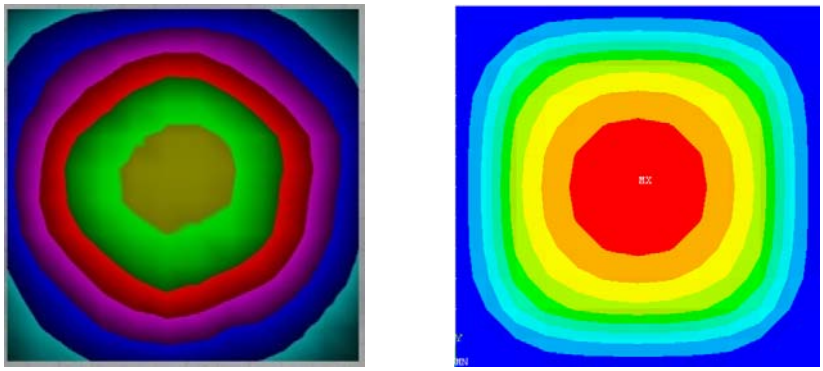

(a) (b)

Figure 4.13: displacement field for the plate optimized for the 2nd structural odd mode. (a) Experimental, (b) Analytical.

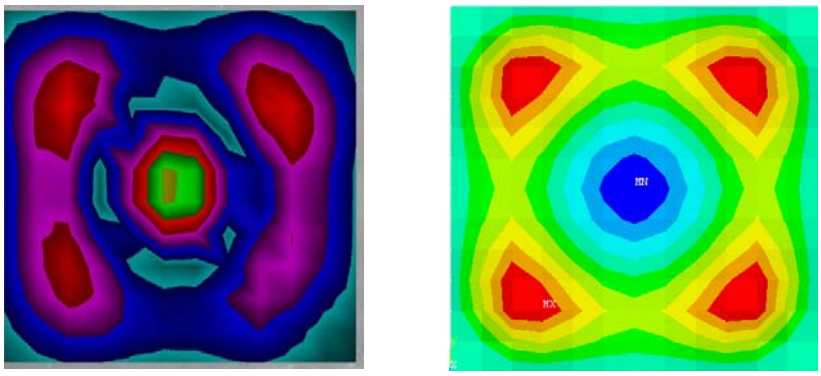

(a) (b)

Figure 4.14: displacement field for the plain plate excited at the 2nd structural odd mode. (a) Experimental, (b) Analytical.

4.2 Experimental results for Air-FullCure720 cavity

Frequency response for the FullCure720 plate acceleration as well as the sound pressure inside the acoustic cavity are shown in Figures 4.15 and 4.16 for the first case, where the optimization is tailored to the 1st structural odd mode. The same results for the optimization tailored to the 2nd odd mode are shown in Figures 4.17 and 4.18.

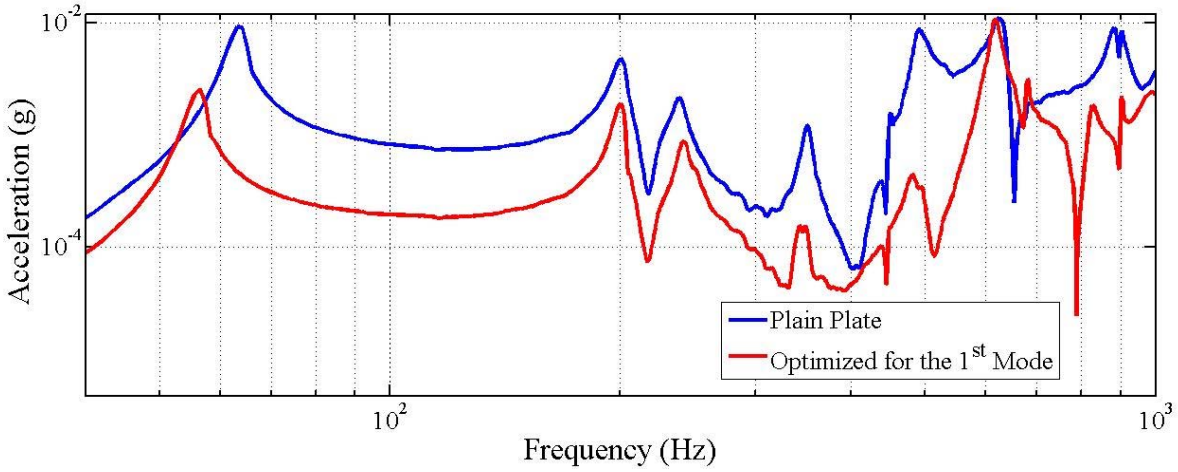

Figure 4.15 : Plate acceleration for plain and 1st mode optimized cases

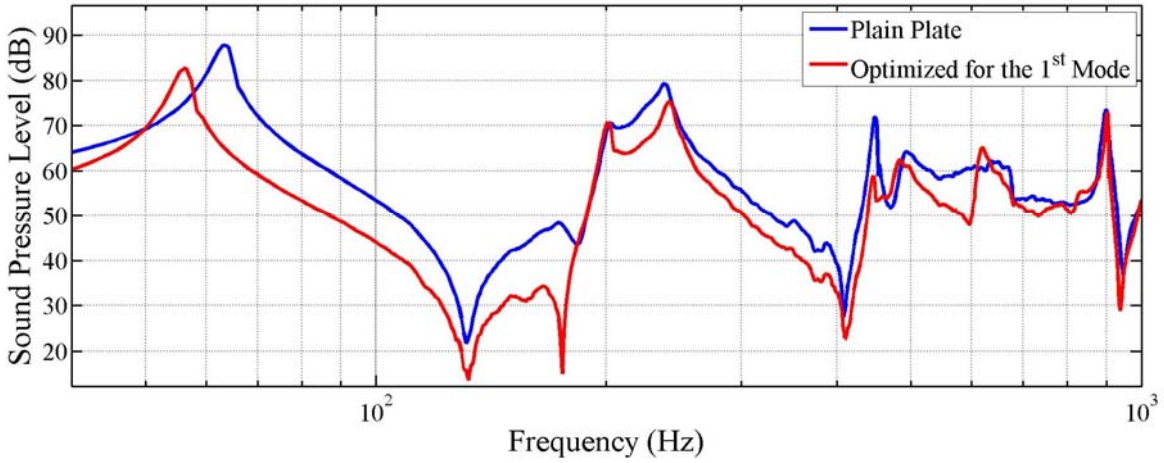

Figure 4.16 : Sound Pressure level for plain and 1st mode optimized cases

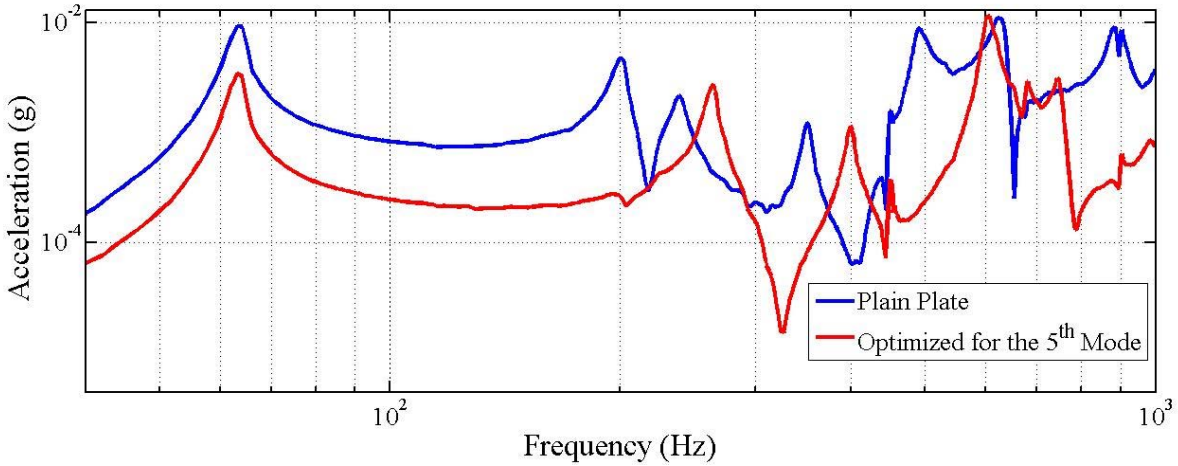

Figure 4.17 : Plate acceleration for plain and 5th mode optimized cases

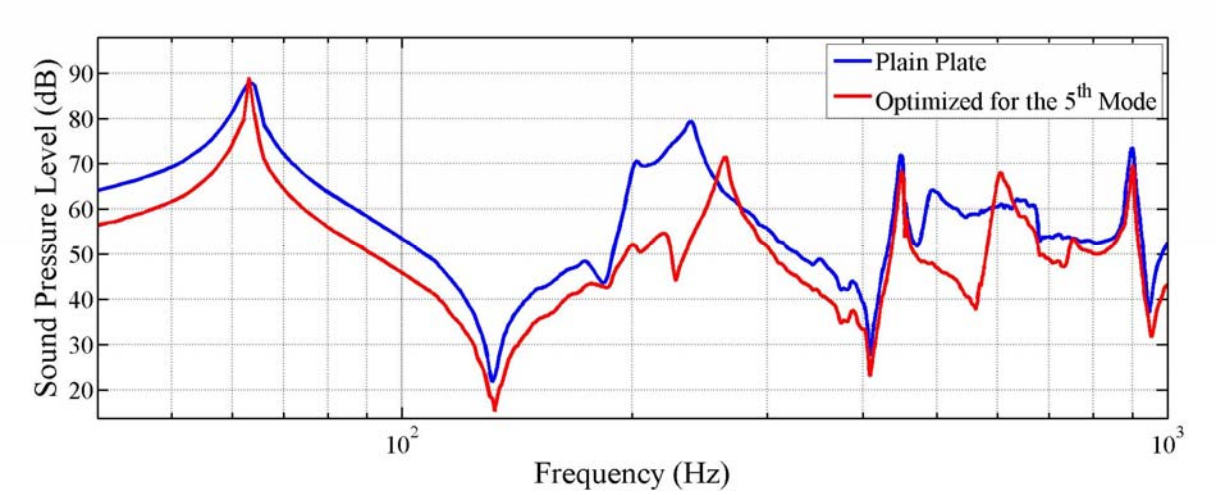

Figure 4.18 : Sound Pressure level for plain and 5th mode optimized cases

The displacement fields for the FullCure720 plates excited at different frequencies using a vibrometer are shown in Figure 4.19 through Figure 4.21.

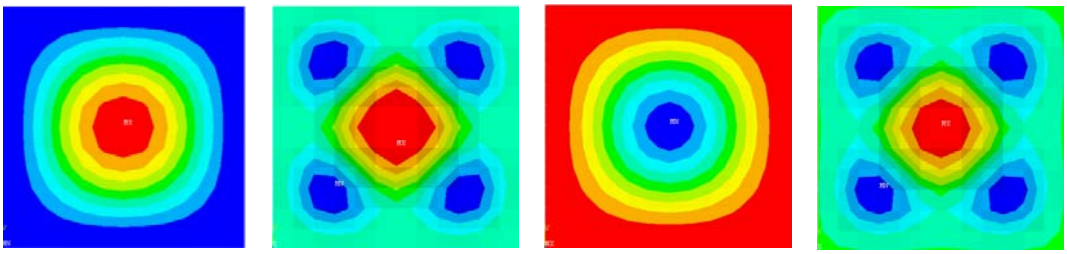

f =63Hz *f* =244Hz *f* =54Hz *f* =272Hz

(a)

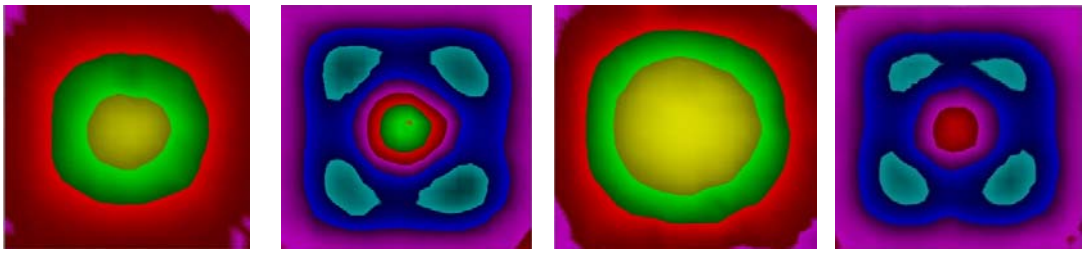

f =63Hz *f* =244Hz *f* =54Hz *f* =272Hz

(b)

Figure 4.19: Displacement field for the plain plate excited at different frequencies for the plain and optimized plates. (a) Analytical (b) Experimental.

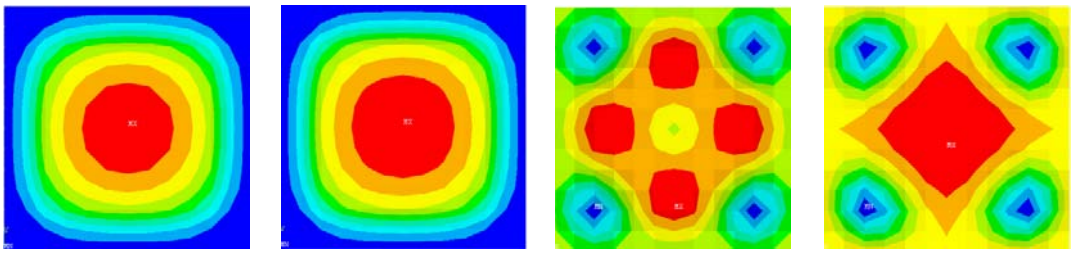

f =63Hz *f* =54Hz *f* =244Hz *f* =272Hz

(a)

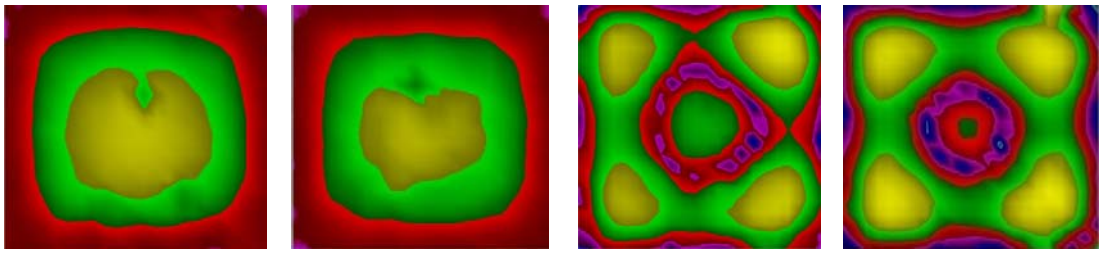

f =63Hz *f* =54Hz *f* =244Hz *f* =272Hz

(b)

Figure 4.20: Displacement field for 1st mode optimized plate excited at different frequencies. (a) Analytical (b) Experimental.

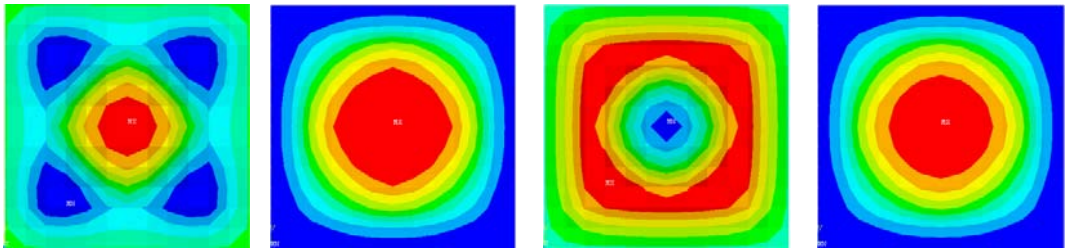

f =272Hz *f* =63Hz *f* =244Hz *f* =54Hz

(a)

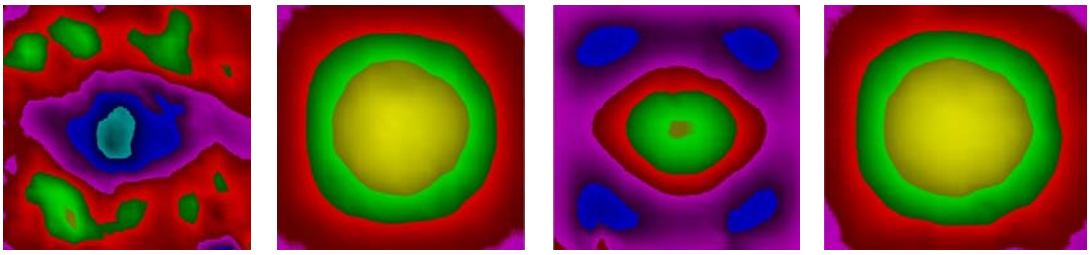

f =272Hz *f* =63Hz *f* =244Hz *f* =54Hz

(b)

Figure 4.21: Displacement field for 5th mode optimized plate excited at different frequencies. (a) Analytical (b) Experimental.

4.3 Summary

This chapter has presented an experimental validation of the predictions of the developed theoretical model when integrated with the topology optimization algorithm. Prototypes of plates with optimized topologies are manufactured at tested to validate the developed theoretical model. The performance characteristics of plates optimized for different frequency ranges are determined and compared with the theoretical predictions of the developed mathematical model. A close agreement is observed between theory and experiments.

CHAPTER 5

ANSYS VERIFICATIONS

5.1 Model development

ANSYS offers its users a wide range on analytical options in acoustic analysis. The solver supports simple solutions such as modal analysis and harmonic analysis, and more coupled structural-acoustics such that the interaction of the fluid (air and water in this case) and the structure can be build into the assessment.

The model analysis presented in this chapter aims at determining the response of the coupled fluid-structure system in order to draw a comparison with the results obtained from the theoretical model using MATLAB.

The structural elements in the model will require Young's Modulus (defined in ANSYS by EX, EY and EZ), Poisson's Ratio (defined in ANSYS by PRXY, PRYZ and PRXZ) and Density (defined in ANSYS by DENS) to be input as material properties. The thickness of each structural element is being defined through the material real constants by specifying the element thickness at each node. The fluid elements of the analysis will require that Speed of Sound (defined in ANSYS by SONC), Density and viscosity (defined in ANSYS by VISC) to be input.

Three types of elements were used to model the complete fluid-structure interaction problem in ANSYS. SHELL181element type was used for the structural elements (i.e. plate elements) while FLUID30 element type was used for the fluid domain elements. To distinguish between interfacing and non-interfacing fluid elements, another FLUID30 element type was used to represent the fluid elements on the interfacing layer. These three types of elements as well as the complete ANSYS model are shown in Figure 5.1.

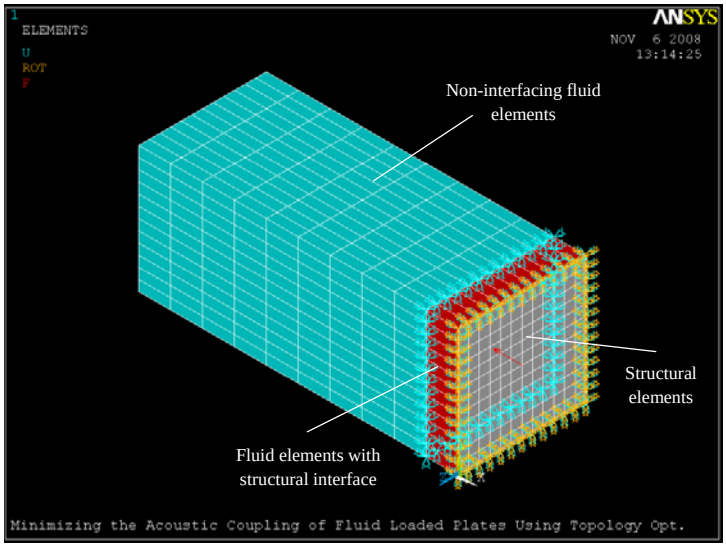

Figure 5.1: Complete ANSYS model with different types of elements used to simulate the dynamics of the structural and fluid domains

The developed model in ANSYS has been used to predict the response of the midpoint of the plate as it has been done using MATLAB. Also, the sound pressure level was measured at a point corresponding to the midpoint of the plate and 3" away inside the cavity. These two measurements were used to verify the accuracy of the theoretical model.

The construction and analysis of the model is completed via a macro, written in the proper command format for ANSYS. The resulting macros are relatively simple text files that are easy to read and understand.

5.2 ANSYS verification for the Air-Aluminum cavity mode

A model that simulates the Air-Aluminum cavity was developed in ANSYS using actual dimensions of the real model and the proper element types. The results for the plain, 1st and 5th

structural mode optimized cavities compared to MATLAB analytical model are shown in Figure 5.2 through Figure 5.7.

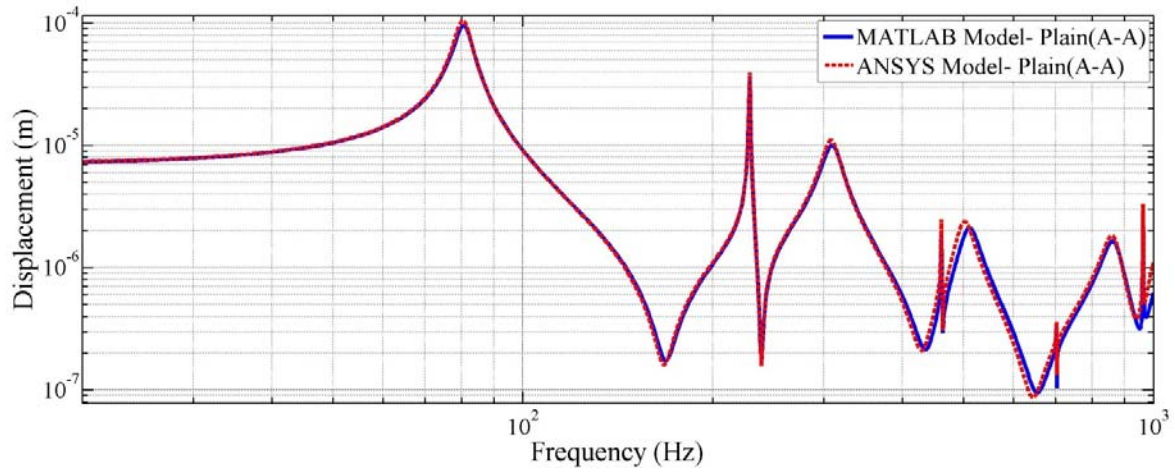

Figure 5.2: MATLAB and ANSYS models' displacement comparison for plain aluminum plates (Air-Aluminum cavity)

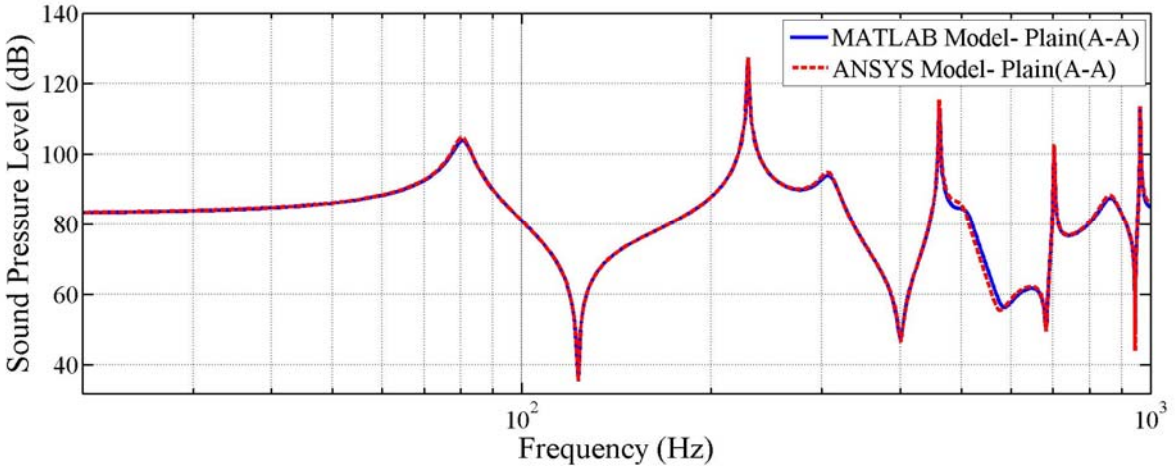

Figure 5.3: MATLAB and ANSYS models' sound pressure level comparison for plain aluminum plates (Air-Aluminum cavity)

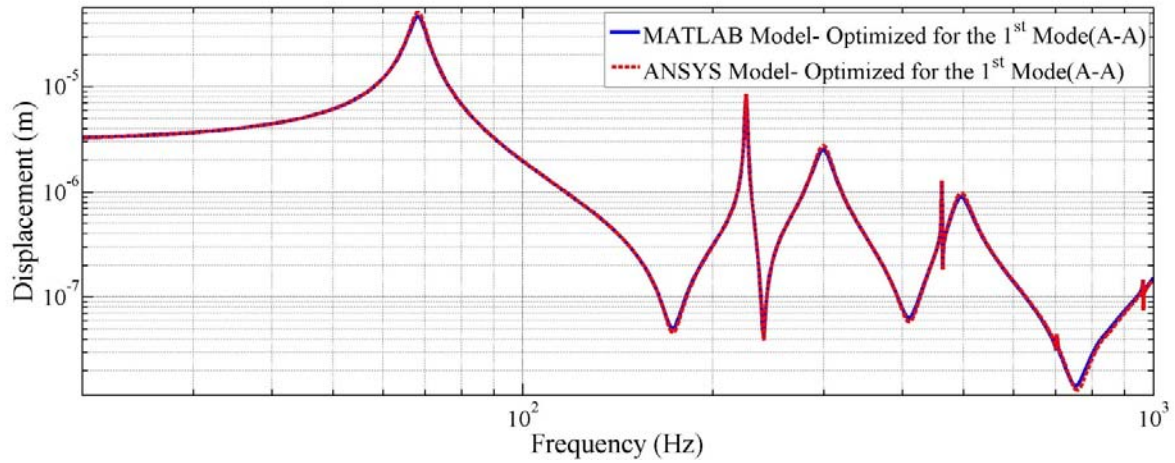

Figure 5.4: MATLAB and ANSYS models' displacement comparison for plain and 1st structural mode optimized aluminum plates (Air-Aluminum cavity)

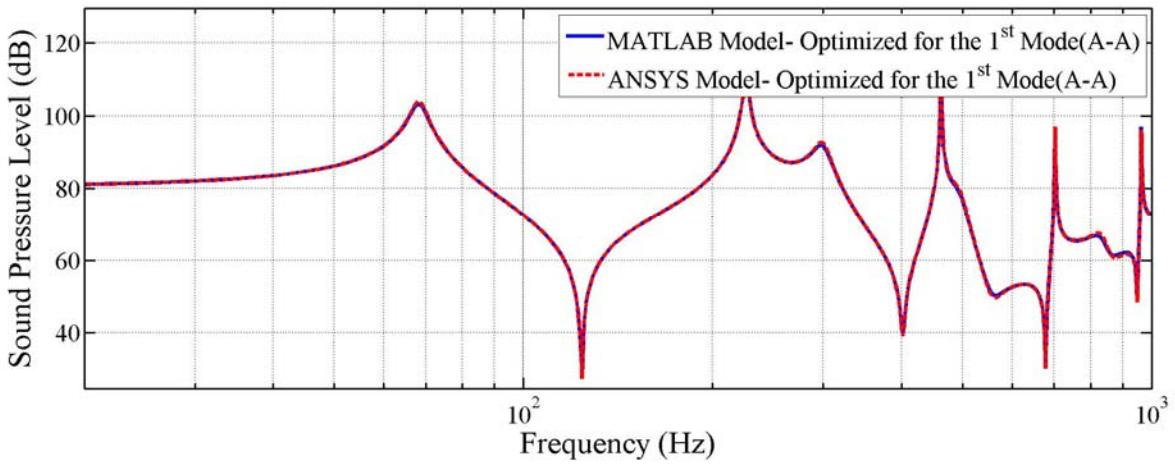

Figure 5.5: MATLAB and ANSYS models' sound pressure level comparison for plain and 1st structural mode optimized aluminum plates (Air-Aluminum cavity)

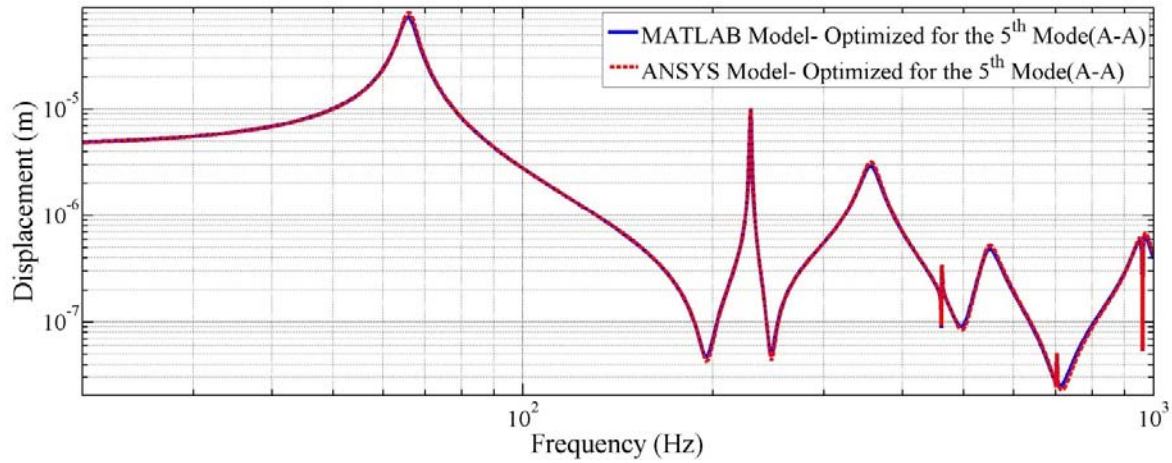

Figure 5.6: MATLAB and ANSYS models' displacement comparison for plain and 5th structural mode optimized aluminum plates (Air-Aluminum cavity)

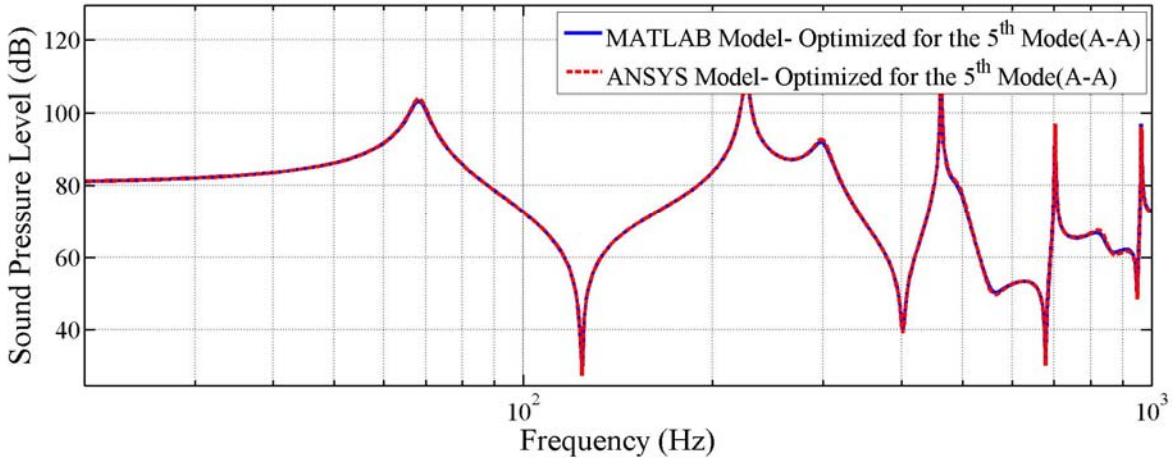

Figure 5.7: MATLAB and ANSYS models' sound pressure level comparison for plain and 5th structural mode optimized aluminum plates (Air-Aluminum cavity)

As it can be seen from the previous results, there is an excellent agreement between the system responses obtained using MATLAB and ANSYS models for the three different cases of the structural medium (i.e. the aluminum plate). This remarkable agreement emphasizes the

accuracy of the developed MATLAB model and its ability to accurately capture the dynamics of the fluid-structure coupled system.

5.3 ANSYS verification for the Water-Aluminum cavity model

Similarly, a model simulating the Water-Aluminum cavity was also developed in ANSYS using actual dimensions of the real model and the proper element types. The results for the plain, 1st and 5th structural mode optimized cavities compared to MATLAB analytical model are shown in Figure 5.8 through Figure 5.13.

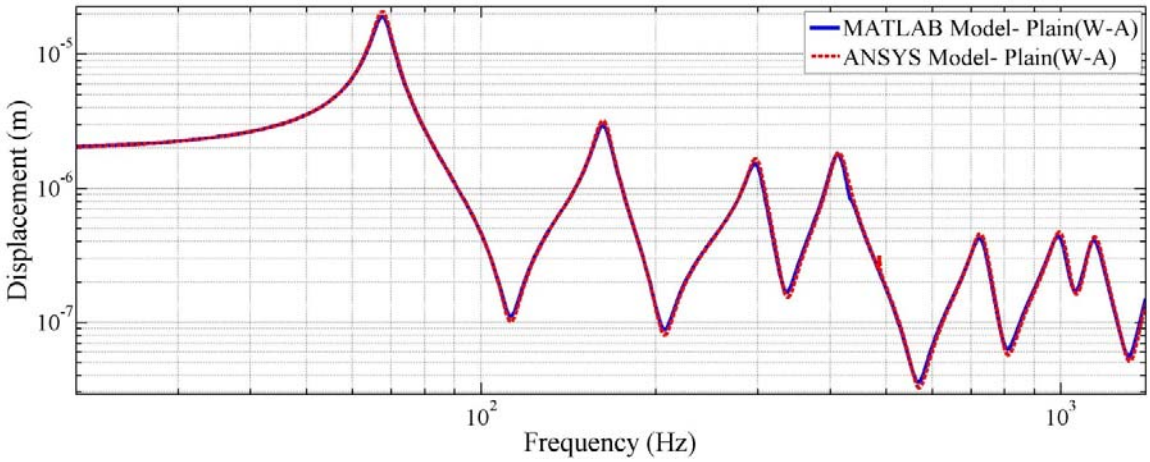

Figure 5.8: MATLAB and ANSYS models' displacement comparison for plain aluminum plates (Water-Aluminum cavity)

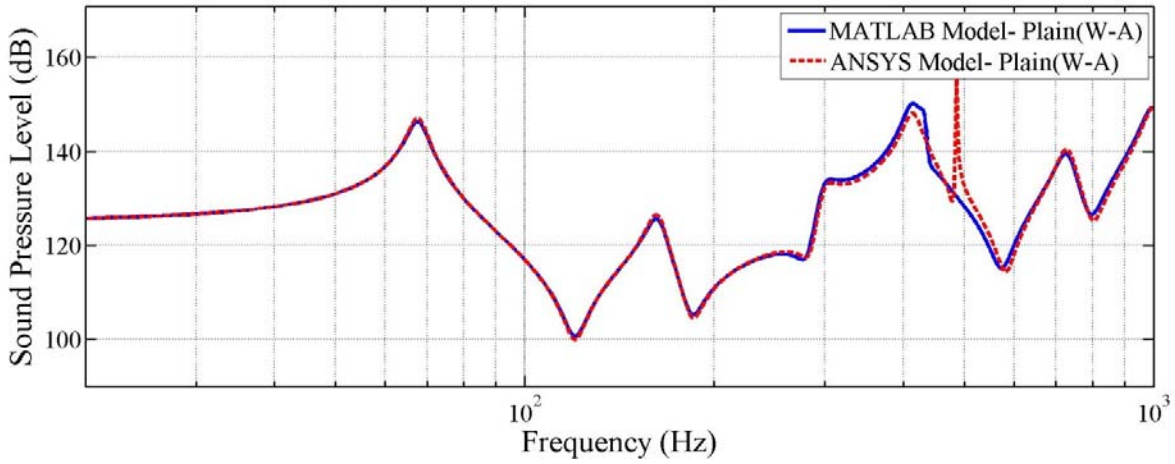

Figure 5.9: MATLAB and ANSYS models' sound pressure level comparison for plain aluminum plates (Water-Aluminum cavity)

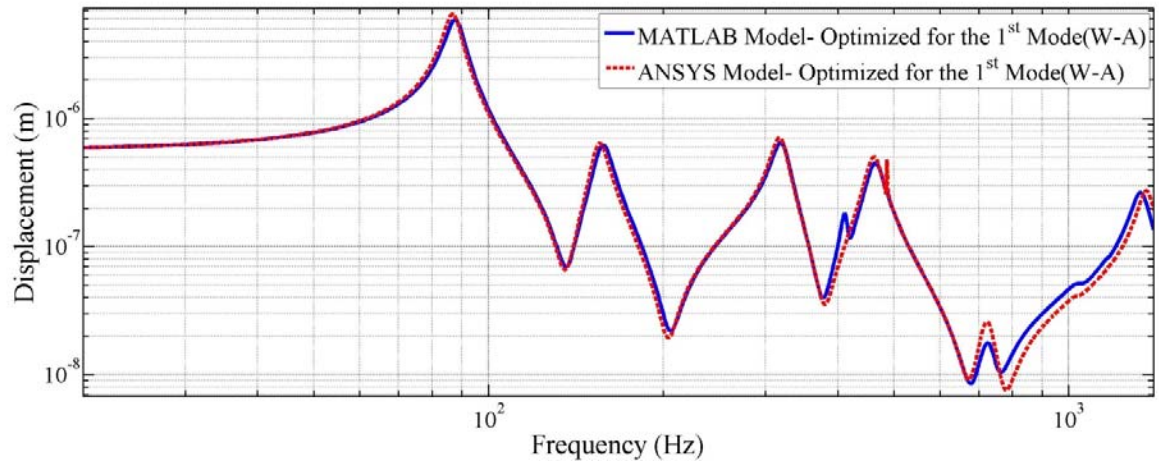

Figure 5.10: MATLAB and ANSYS models' displacement comparison for plain and 1st structural mode optimized aluminum plates (Water-Aluminum cavity)

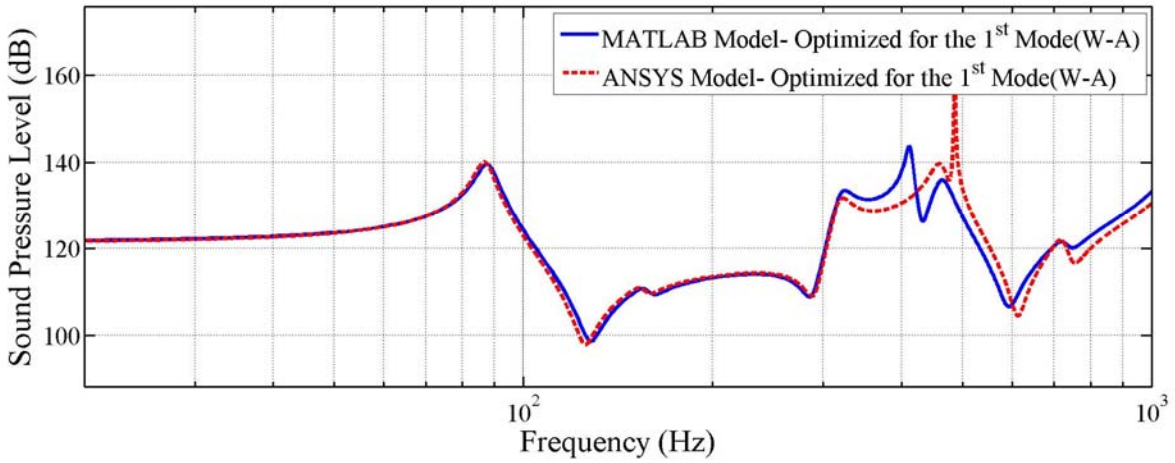

Figure 5.11: MATLAB and ANSYS models' sound pressure level comparison for plain and 1st structural mode optimized aluminum plates (Water-Aluminum cavity)

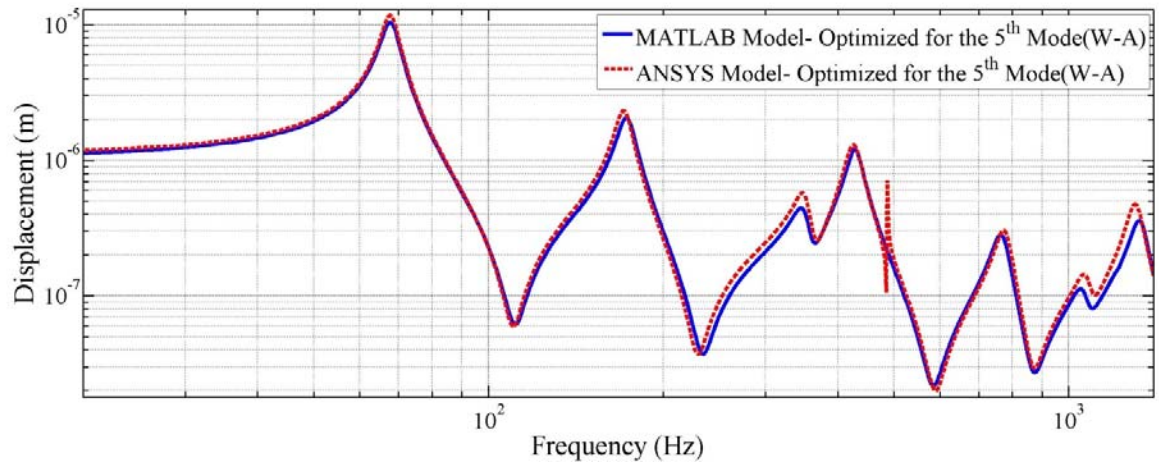

Figure 5.12: MATLAB and ANSYS models' displacement comparison for plain and 5th structural mode optimized aluminum plates (Water-Aluminum cavity)

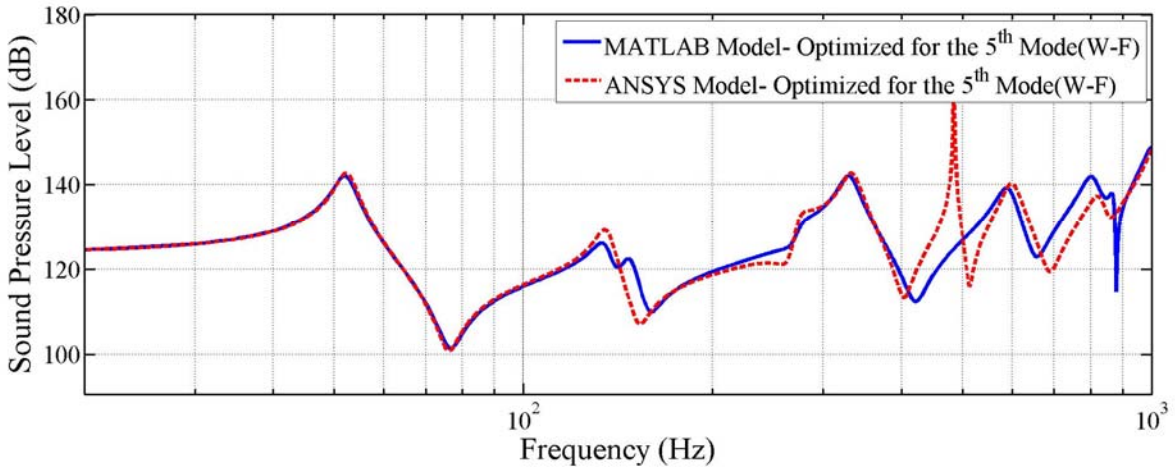

Figure 5.13: MATLAB and ANSYS models' sound pressure level comparison for plain and 5th structural mode optimized aluminum plates (Water-Aluminum cavity)

5.4 ANSYS verification for the Air-Fullcure720 cavity model

Similarly, a model simulating the Air-Fullcure720 cavity was also developed in ANSYS using actual dimensions of the real model and the proper element types. The results for the plain, 1st and 5th structural mode optimized cavities compared to MATLAB analytical model are shown in Figure 5.14 through Figure 5.19.

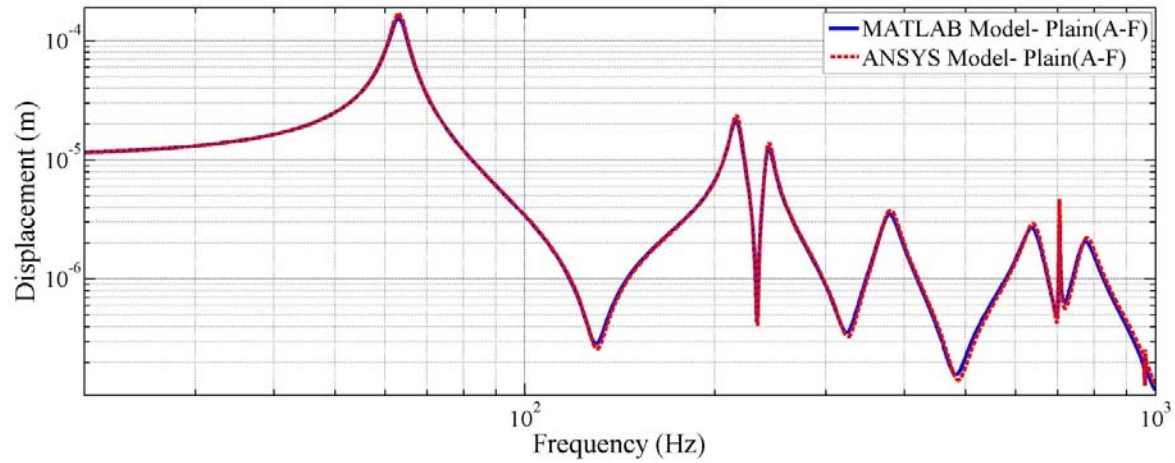

Figure 5.14: MATLAB and ANSYS models' displacement comparison for plain Fullcure720 plates (Air-Fullcure720 cavity)

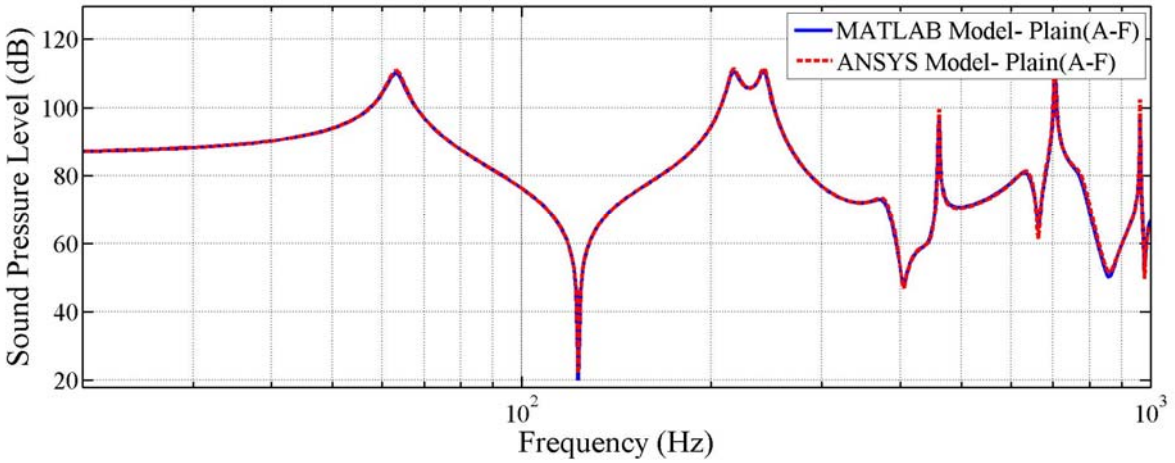

Figure 5.15: MATLAB and ANSYS models' sound pressure level comparison for plain Fullcure720 plates (Air-Fullcure720 cavity)

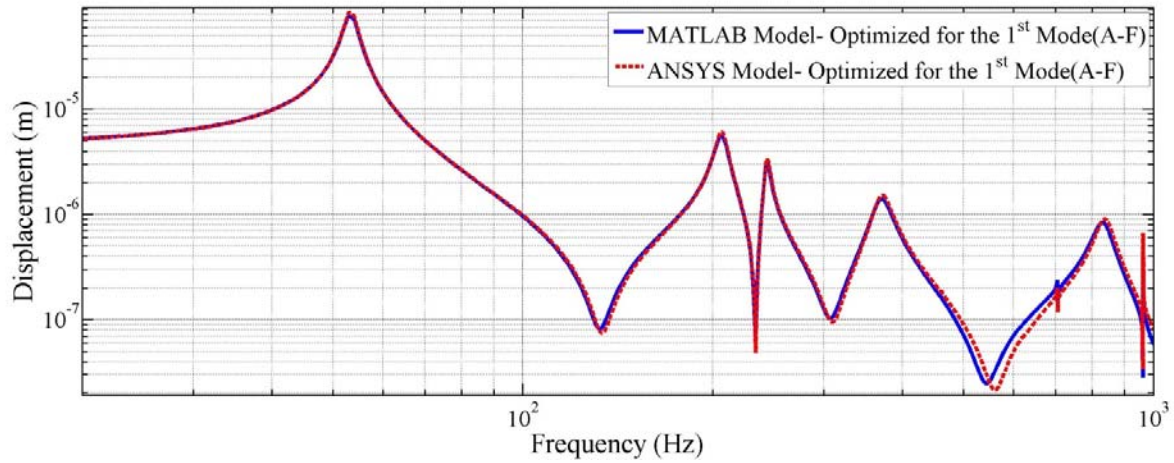

Figure 5.16: MATLAB and ANSYS models' displacement comparison for plain and 1st structural mode optimized Fullcure720 plates (Air-Fullcure720 cavity)

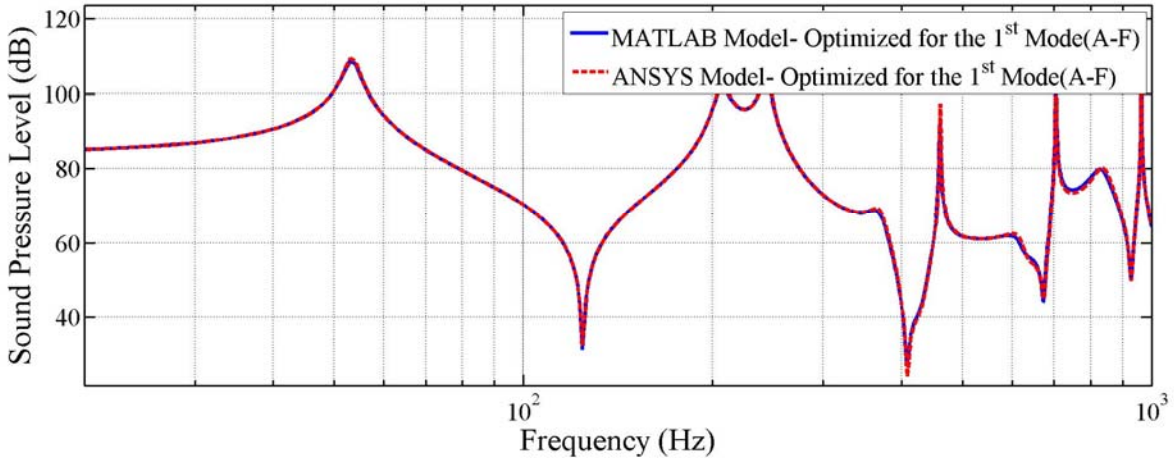

Figure 5.17: MATLAB and ANSYS models' sound pressure level comparison for plain and 1st structural mode optimized Fullcure720 plates (Air-Fullcure720 cavity)

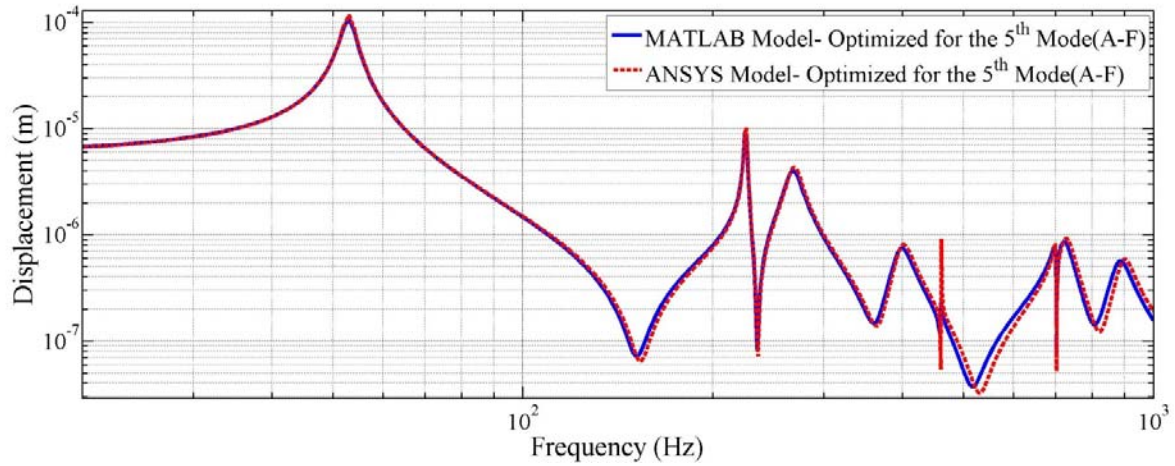

Figure 5.18: MATLAB and ANSYS models' displacement comparison for plain and 5th structural mode optimized Fullcure720 plates (Air-Fullcure720 cavity)

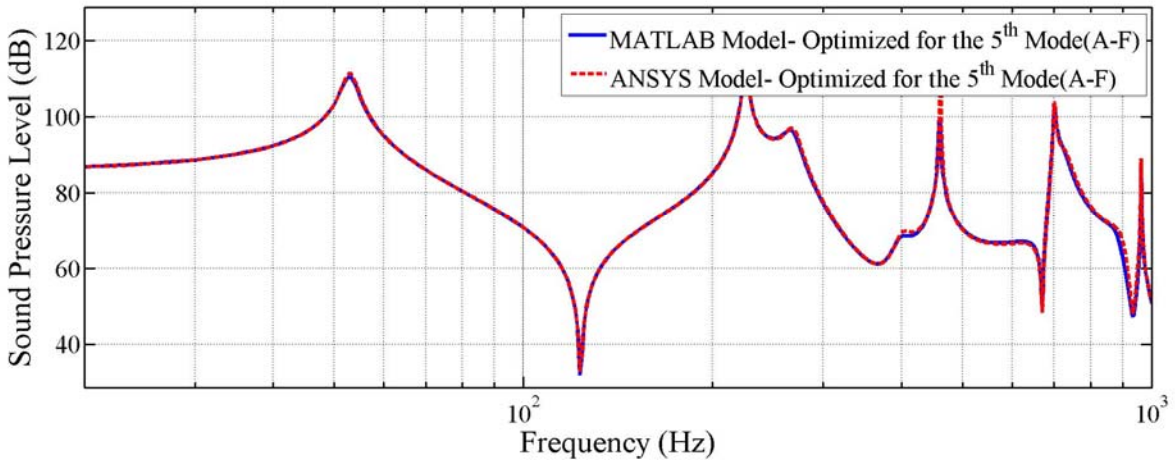

Figure 5.19: MATLAB and ANSYS models' sound pressure level comparison for plain and 5th structural mode optimized Fullcure720 plates (Air-Fullcure720 cavity)

Again, there is an excellent agreement between the system responses obtained using MATLAB and ANSYS models for the three different cases of the structural medium (i.e. the Fullcure720 plate).

5.5 ANSYS verification for the Water-Fullcure720 cavity model

Finally, a model to simulating the Water-Fullcure720 cavity was also developed in ANSYS using actual dimensions of the real model and the proper element types. The results for the plain, 1st and 5th structural mode optimized cavities compared to MATLAB analytical model are shown in Figure 5.20 through Figure 5.25.

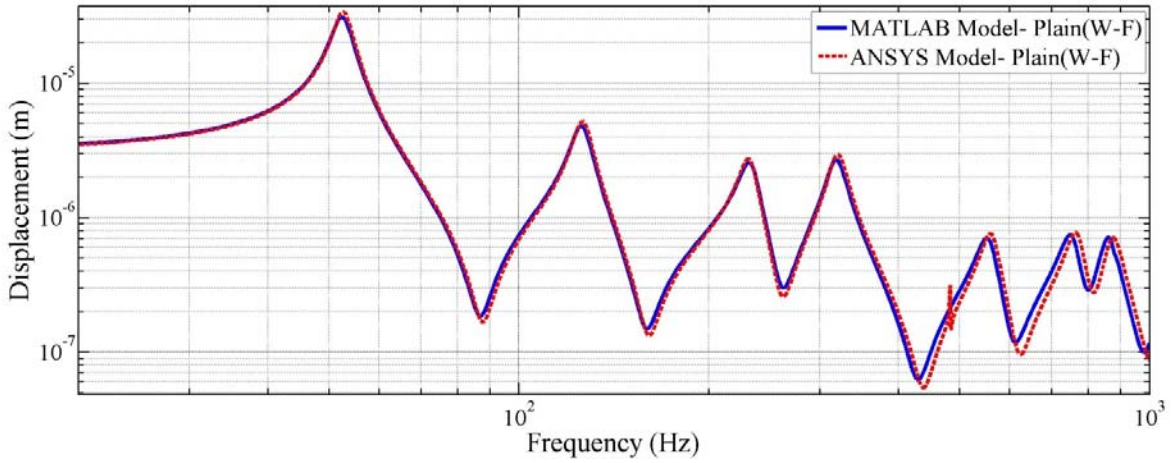

Figure 5.20: MATLAB and ANSYS models' displacement comparison for plain Fullcure720 plates (Water-Fullcure720 cavity)

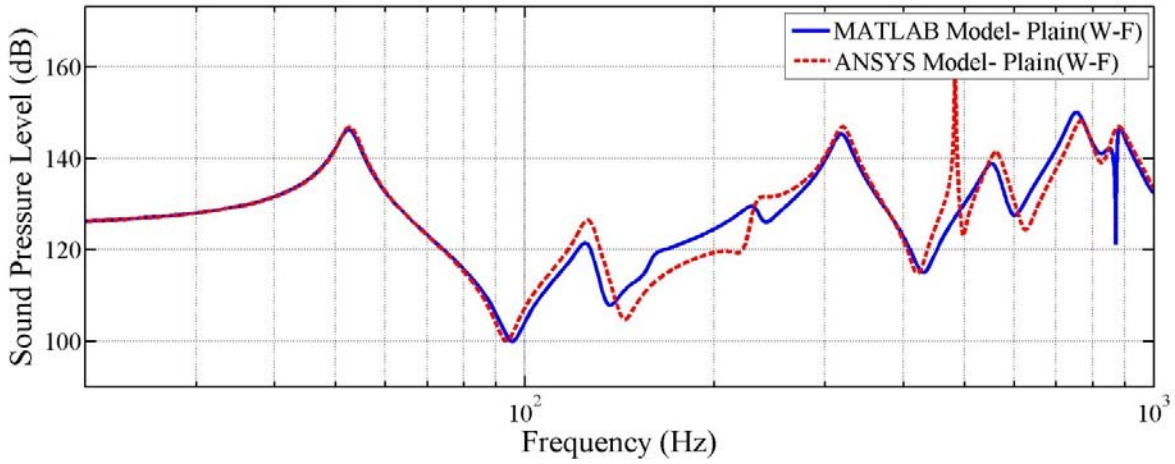

Figure 5.21: MATLAB and ANSYS models' sound pressure level comparison for plain Fullcure720 plates (Water-Fullcure720 cavity)

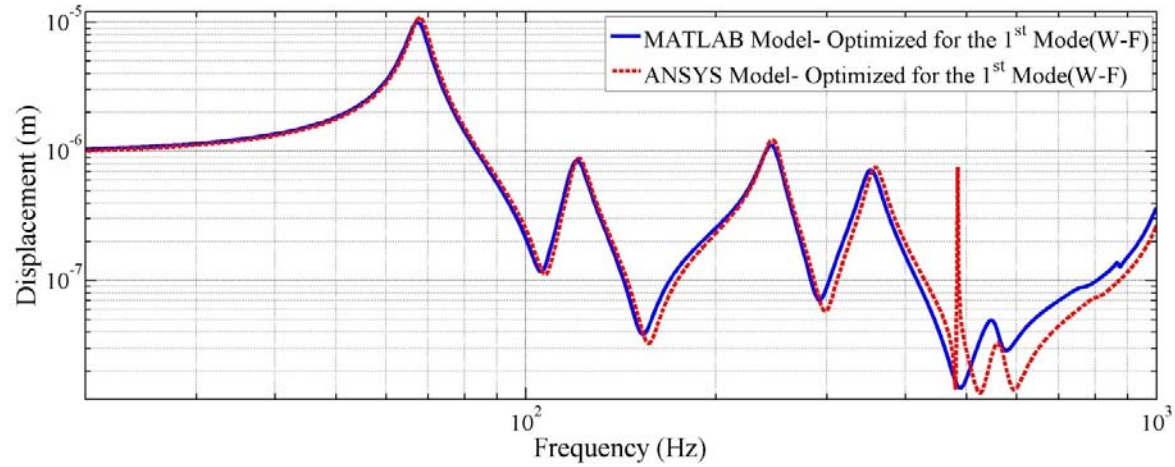

Figure 5.22: MATLAB and ANSYS models' displacement comparison for plain and 1st structural mode optimized Fullcure720 plates (Water-Fullcure720 cavity)

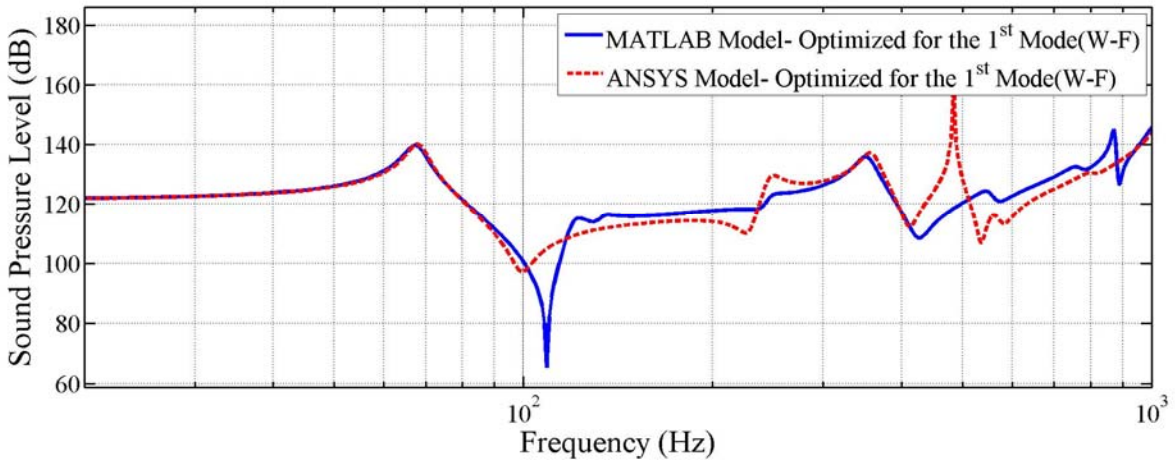

Figure 5.23: MATLAB and ANSYS models' sound pressure level comparison for plain and 1st structural mode optimized Fullcure720 plates (Water-Fullcure720 cavity)

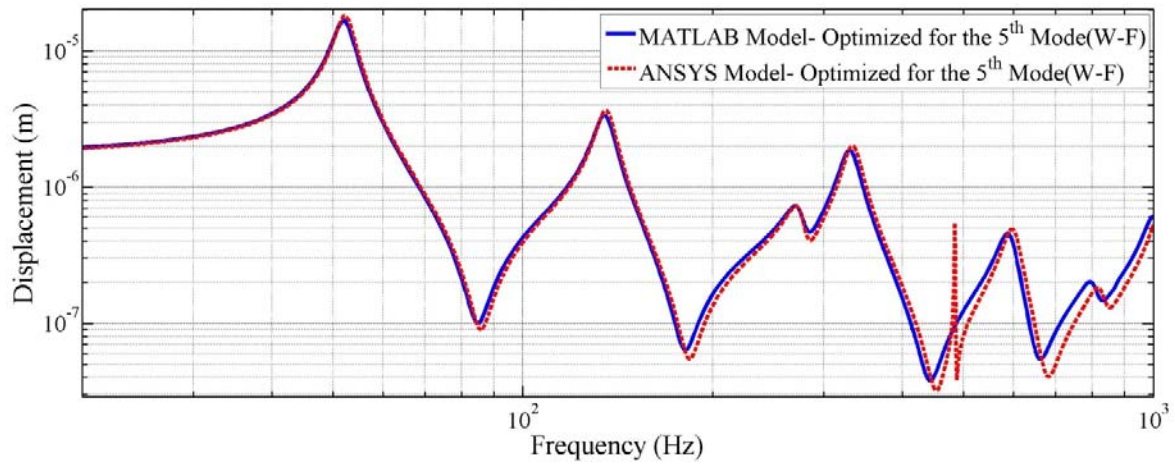

Figure 5.24: MATLAB and ANSYS models' displacement comparison for plain and 5th structural mode optimized Fullcure720 plates (Water-Fullcure720 cavity)

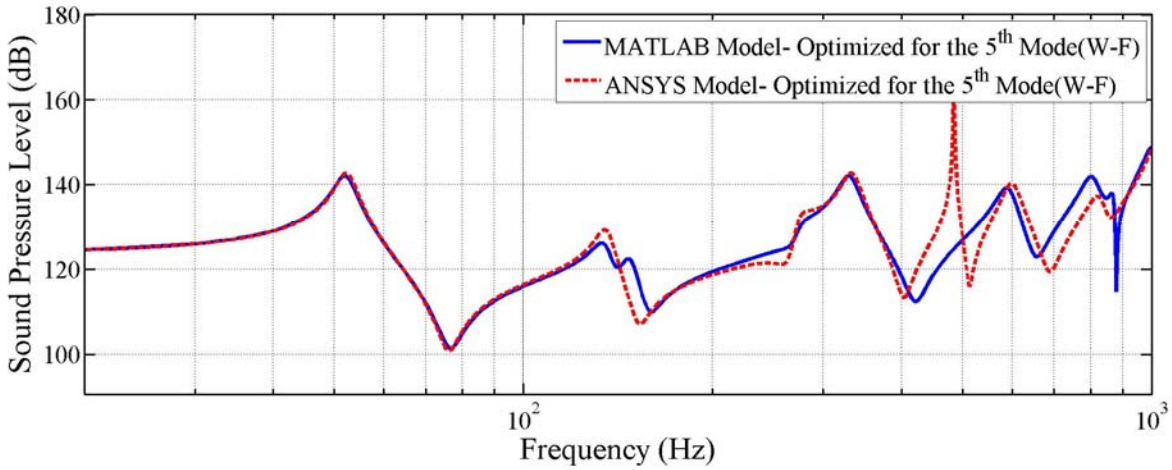

Figure 5.25: MATLAB and ANSYS models' sound pressure level comparison for plain and 5th structural mode optimized Fullcure720 plates (Water-Fullcure720 cavity)

5.6 Summary

This chapter has presented ANSYS validation of the predictions of the developed theoretical model when integrated with the topology optimization algorithm. Different models of Fluid-structure were developed and solved in ANSYS. An excellent match with the theoretical model using MATLAB was noted in the plates' displacements and sound pressure levels inside the cavity.

CHAPTER 6

CONCLUSIONS AND SUGGESTIONS FOR FUTURE WORK

6.1 Conclusions

This dissertation aimed at the development of a topology optimization approach for fluid-structure interaction between a flexible plate coupled with a rigid acoustic cavity. The objective of the optimization was to redistribute the material of the flexible plate in order to minimize the fluid-structure coupling. A finite element model was developed to simulate the fluid-structure interactions and was integrated with the topology optimization approach. The model was used to develop the sensitivity analysis necessary for the operation of the topology optimization algorithm. The excitation acting on the plate was locked at the first or second structural odd modes to ensure the effectiveness of the optimization in reducing the sound pressure at the modal frequencies. The analytical model showed considerable attenuation for the first structural odd mode as well as consecutive modes, when the optimization was targeting that mode specifically. On the other hand excellent attenuation was obtained for the second structural odd mode, when targeting the optimization scheme towards that specific mode.

Experimental verification was carried out by manufacturing three sets of topology optimized plates that approximate the results obtained from the analytical model. One set of the topology optimized plates was made of aluminum sections which are bonded together. The other two sets were manufactured using stereolithography techniques by exporting the topology optimized geometry files directly to the stereolithography machine. The three sets of plates were coupled, one a time, to an acoustic cavity. Plate vibration acceleration and sound pressure inside the acoustic cavity were measured and compared with the plain-plate case. Considerable

attenuation in both the plate vibration acceleration and sound pressure inside the acoustic cavity were recorded. A good match with the analytical model was observed. The displacement fields of the plate were also measured using a laser vibrometer, and good agreement was observed with the analytical case.

The predictions of the mathematical model were also validated against the predictions of models developed using ANSYS® software. This was carried out for all the three sets of plates and all the optimized configurations for the first two odd modes.

Different acoustic media were also considered. Water, for example, was considered as an alternative acoustic media due to the wide applications of submerged structures.

6.2 Future work

The presented topology optimization approach can be an invaluable tool in the design of a wide variety of critical structures which must operate quietly when subjected to fluid loading. Note that the utility of such a design tool is enhanced through the use of the first order shear deformation theory which makes the analysis equally applicable to thin and thick plate structures. Therefore, a natural extension of the present work is to theoretically predict and experimentally validate the performance of topology optimized thick plates coupled with acoustic cavities.

The work presented here can also be extended to shell structures because of their wide use in various applications such as aircraft fuselage and underwater vehicles. In these critical

applications, the optimization of the interaction of the shell structure and the neighboring fluid medium is essential to the quiet operation of these shells and to the minimization of their weight.

Although the experimental work presented in this dissertation was limited to air-filled acoustic cavities, work is needed to validate the predictions of the developed model when the cavity is filled was water.

More work is needed to generalize the objective function considered during the topology optimization process. In this work, only the coupling between the structure and fluid was minimized. Other objective functions that should be considered may include: minimizing the average sound pressure levels in the cavity, minimizing the sound intensity, and minimizing the structural vibration. These additional objective functions may be considered one at a time, or more appropriately the topology optimization problem may be cast as a multi-objective optimization problem.

Finally, in the present work, the topology optimization has not capitalized on the potential of introducing periodicity in the structural system in order to generate the favorable stop/pass band filtering characteristics that can impede the wave propagation over the structure. Such characteristics can reduce not only the structural vibration but also the noise radiation in the acoustic cavity. Furthermore, using such periodicity in the context of topology optimization can reduce the dimensionality of the problem considerably and speed the implementation of the topology optimization for more complex structures.

APPINDEX A

MATLAB CODES

Main file:

```
function  sound_optimization(Lx_ov, Ly_ov, Lz_ov, nelx, nely, nelz)
volfrac=0.5;
nel=nelx*nely;
residual_frac=0.25;
n=nel;
m=1;
xval = ones(n,1)*volfrac;
xmin = ones(n,1)*residual_frac;
xmax = ones(n,1)*1;
xold1=xval;
xold2=xval;
low=0*ones(nel,1);
upp=1000*ones(nel,1);
a0=1;
c=1000*ones(m,1);
d=0*ones(m,1);
a=zeros(m,1);
iter=0;
maxite=12;
itte = 0;
asyinit = 0.5;
asyincr = 0.65;
asydecr = 0.5;
while itte < maxite
    iter = iter+1;
    itte = itte+1;
    t = clock;
    [freq_m]=Overall_Assembly_MMA_freq_search(Lx_ov, Ly_ov, Lz_ov,...
        nelx, nely, nelz, xval, itte);
    [f0val,df0dx,df0dx2,fval,dfdx,dfdx2,wc,P] = sound_objective_function...
        (Lx_ov, Ly_ov, Lz_ov, nelx, nely, nelz, freq_m, volfrac, m, xval);
    [xmma,ymma,zmma,lam,xsi,eta,mu,zet,s,low,upp] = ...
        mmasub(m,n,iter,xval,xmin,xmax,xold1,xold2,f0val,df0dx,df0dx2,...
        fval,dfdx,dfdx2,low,upp,a0,a,c,d,asyinit, asyincr, asydecr);
    xold2 = xold1;
    xold1 = xval;
    xval = xmma;
    outvector = [iter f0val fval' xval']';
    for ii=1:nely
        for jj=1:nelx
            xp(ii,jj)=xval((ii-1)*nelx+jj);
        end
```

```
end
xpp=zeros(size(xp));
for ii=1:nely
    xpp(nely-ii+1,:)=xp(ii,:);
end
target=full(P'*P)/length(P);
target_log=10*log10(target/1e-12);
if itte==1
    target_old=target_log;
    target_prev=target_log;
end
ddiiff=target_prev-target_log;
target_prev=target_log;
for ii=1:nely+1
    for jj=1:nelx+1
        pp(ii,jj)=wc((ii-1)*(nelx+1)+jj);
    end
end
h=[];
colormap gray;
figure(3);
colormap gray;
h = bar3(abs(xpp),1);
shading interp
for i = 1:length(h)
    zdata = ones(6*length(h),4);
    k = 1;
    for j = 0:6:(6*length(h)-6)
        zdata(j+1:j+6,:) = -abs(xpp(k,i));
        k = k+1;
    end
    set(h(i),'Cdata',zdata)
    set(h,'EdgeColor',[0.7 0.7 0.7])
end
grid
axis off
title(ss);
view([2 2 3]);
h=gcf;
s=sprintf('fig3d_%d',itte);
saveas(h,s);
colormap gray;
figure(4);
colormap gray;
subplot(1,2,1);
imagesc(-abs(xpp)); axis equal; axis tight; axis off;pause(1e-6);
subplot(1,2,2);
iter_p(iter)=target_log;
plot(1:iter,iter_p,'-rx','LineWidth',2,'MarkerEdgeColor','k',...
    'MarkerFaceColor','g','MarkerSize',8);
xlabel('Iteration')
ylabel ('Sound Power (dB)')
axis([0 30 100 130])
h=gcf;
s=sprintf('fig2d_%d',itte);
saveas(h,s);
figure(5)
```

```
surf(abs(pp),'FaceColor','interp','EdgeColor','none','FaceLighting','phong');
    axis([1 nelx 1 nely 0 0.0005])
    axis([1 nelx 1 nely 0 0.00005])
    axis off
    grid
    title(ss)
    h=gcf;
    s=sprintf('figS_%d',itte);
    saveas(h,s);
    etime(clock, t)
end


function [freq_m]=Overall_Assembly_MMA_freq_search(Lx_ov, Ly_ov, Lz_ov, nelx,
nely, nelz, xj, itte)
rho_air=1.2;
inch=25.4e-3;
nel=nelx*nely;
[K_p_front, M_p_front, Force_front, BC_front, K_p_array_front,
M_p_array_front, dK_dx_array_front, dM_dx_array_front,...
    dK_dxx_array_front, dM_dxx_array_front]=Plate_Assembly_MMA(Lx_ov, Ly_ov,
nelx, nely, inch/16, xj);
[K_p_back, M_p_back, Force_back, BC_back, K_p_array_back, M_p_array_back,
dK_dx_array_back, dM_dx_array_back,...
    dK_dxx_array_back, dM_dxx_array_back]=Plate_Assembly_MMA(Lx_ov, Ly_ov,
nelx, nely, 2.0*inch, xj);
[K_fluid, M_fluid]=Fluid_Assembly_MMA(Lx_ov, Ly_ov, Lz_ov, nelx, nely, nelz);
xlen=Lx_ov/nelx;
ylen=Ly_ov/nely;
zlen=Lz_ov/nelz;
x=[0 1 1 0 0 1 1 0]*xlen;
y=[0 0 1 1 0 0 1 1]*ylen;
z=[0 0 0 0 1 1 1 1]*zlen;
K_f_array=zeros(8,8,nel);
M_f_array=zeros(8,8,nel);
for ii=1:nel
    [K_f_array(:,:,ii),K_f_array(:,:,ii)]=cavity_matrices(x,y,z);
end
[c_front, C_array_front]=coupling_Assembly_MMA(Lx_ov, Ly_ov, nelx, nely, 1);
[c_back, C_array_back]=coupling_Assembly_MMA(Lx_ov, Ly_ov, nelx, nely, 2);
dof_front=length(K_p_front);
dof_back=length(K_p_back);
dof_struct=dof_front+dof_back;
dof_fluid=length(K_fluid);
dof_overall=dof_struct+dof_fluid;
dof_coup_press_front=(nelx+1)*(nely+1)*1;
dof_coup_press_back=(nelx+1)*(nely+1)*1;
K_overall=sparse(dof_overall,dof_overall);
M_overall=sparse(dof_overall,dof_overall);
K_struct=[K_p_front         zeros(dof_front);...
          zeros(dof_back)   K_p_back];
M_struct=[M_p_front         zeros(dof_front);...
          zeros(dof_back)   M_p_back];
K_overall(1:dof_struct,1:dof_struct)=K_overall(1:dof_struct,1:dof_struct)+K_s
truct;
```

```
M_overall(1:dof_struct,1:dof_struct)=M_overall(1:dof_struct,1:dof_struct)+M_s
truct;
K_overall(dof_struct+1:dof_overall,dof_struct+1:dof_overall)=...
    K_overall(dof_struct+1:dof_overall,dof_struct+1:dof_overall)+K_fluid;
M_overall(dof_struct+1:dof_overall,dof_struct+1:dof_overall)=...
    M_overall(dof_struct+1:dof_overall,dof_struct+1:dof_overall)+M_fluid;
start_=dof_struct+1;
end_=dof_struct+dof_coup_press_front;
M_overall(start_:end_,1:dof_front)=...
    M_overall(start_:end_,1:dof_front)+c_front;
start_=dof_overall-dof_coup_press_back+1;
end_=dof_overall;
M_overall(start_:end_,dof_front+1:dof_struct)=...
    M_overall(start_:end_,dof_front+1:dof_struct)+c_back;
c_front_k=-c_front'/rho_air;
c_back_k=-c_back'/rho_air;
start_=dof_struct+1;
end_=dof_struct+dof_coup_press_front;
K_overall(1:dof_front,start_:end_)=...
    K_overall(1:dof_front,start_:end_)+c_front_k;
start_=dof_overall-dof_coup_press_back+1;
end_=dof_overall;
K_overall(dof_front+1:dof_struct,start_:end_)=...
    K_overall(dof_front+1:dof_struct,start_:end_)+c_back_k;
% Applying the forces
Force=sparse(dof_overall,1);
Force(1:dof_front)=Force(1:dof_front)+Force_front;
% Applying Boundary conditions
alldofs     = 1:dof_overall;
BC_back=dof_front+BC_back;
BC=[BC_front BC_back];
freedofs    = setdiff(alldofs,BC);
%% Solution %%%%%%%%%%%%
dim=length(K_p_front)-length(BC_front);
Kbc1=sparse(dim,dim);
Mbc1=sparse(dim,dim);
K_p_front1=K_p_front;
M_p_front1=M_p_front;
K_p_front1(BC_front,:)=[];
K_p_front1(:,BC_front)=[];
M_p_front1(BC_front,:)=[];
M_p_front1(:,BC_front)=[];
Mbc1 =M_p_front1;
Kbc1 =K_p_front1;
opts.disp=0;
disp('inverse started')
AA=Mbc1\Kbc1;
disp('eigs started')
[v,wn]=eigs(AA,11,'SM',opts);
[wn_or,or]=sort(real(diag(wn)));
%lamda_p(1)=(wn_or(1).^0.5)/2/pi;
lamda_p(1)=(wn_or(5).^0.5)/2/pi;
freq_m=lamda_p;
search_pattern_no_FRF;
[lamda_p; freq_m]
disp('search ended')
```

```
function [K_elem, M_elem]=cavity_matrices(x,y,z)
c_air=343;
pa(1)=-1/sqrt(3);
pa(2)=1/sqrt(3);
pb(1)=-1/sqrt(3);
pb(2)=1/sqrt(3);
pc(1)=-1/sqrt(3);
pc(2)=1/sqrt(3);
K_elem=zeros(8,8);
M_elem=zeros(8,8);
for ii=1:2
    for jj=1:2
        for kk=1:2
            a=pa(kk);
            b=pb(jj);
            c=pc(ii);
            cc=1;
            alpha=1/8;
            N1=alpha*(1-a)*(1-b)*(1-c);
            N1a=-alpha*(1-b)*(1-c);
            N1b=-alpha*(1-a)*(1-c);
            N1c=-alpha*(1-a)*(1-b);
            N2=alpha*(1+a)*(1-b)*(1-c);
            N2a=alpha*(1-b)*(1-c);
            N2b=-alpha*(1+a)*(1-c);
            N2c=-alpha*(1+a)*(1-b);
            N3=alpha*(1+a)*(1+b)*(1-c);
            N3a=alpha*(1+b)*(1-c);
            N3b=alpha*(1+a)*(1-c);
            N3c=-alpha*(1+a)*(1+b);
            N4=alpha*(1-a)*(1+b)*(1-c);
            N4a=-alpha*(1+b)*(1-c);
            N4b=alpha*(1-a)*(1-c);
            N4c=-alpha*(1-a)*(1+b);
            N5=alpha*(1-a)*(1-b)*(1+c);
            N5a=-alpha*(1-b)*(1+c);
            N5b=-alpha*(1-a)*(1+c);
            N5c=alpha*(1-a)*(1-b);
            N6=alpha*(1+a)*(1-b)*(1+c);
            N6a=alpha*(1-b)*(1+c);
            N6b=-alpha*(1+a)*(1+c);
            N6c=alpha*(1+a)*(1-b);
            N7=alpha*(1+a)*(1+b)*(1+c);
            N7a=alpha*(1+b)*(1+c);
            N7b=alpha*(1+a)*(1+c);
            N7c=alpha*(1+a)*(1+b);
            N8=alpha*(1-a)*(1+b)*(1+c);
```

```
            N8a=-alpha*(1+b)*(1+c);
            N8b=alpha*(1-a)*(1+c);
            N8c=alpha*(1-a)*(1+b);

xa=N1a*x(1)+N2a*x(2)+N3a*x(3)+N4a*x(4)+N5a*x(5)+N6a*x(6)+N7a*x(7)+N8a*x(8);

xb=N1b*x(1)+N2b*x(2)+N3b*x(3)+N4b*x(4)+N5b*x(5)+N6b*x(6)+N7b*x(7)+N8b*x(8);

xc=N1c*x(1)+N2c*x(2)+N3c*x(3)+N4c*x(4)+N5c*x(5)+N6c*x(6)+N7c*x(7)+N8c*x(8);

ya=N1a*y(1)+N2a*y(2)+N3a*y(3)+N4a*y(4)+N5a*y(5)+N6a*y(6)+N7a*y(7)+N8a*y(8);

yb=N1b*y(1)+N2b*y(2)+N3b*y(3)+N4b*y(4)+N5b*y(5)+N6b*y(6)+N7b*y(7)+N8b*y(8);

yc=N1c*y(1)+N2c*y(2)+N3c*y(3)+N4c*y(4)+N5c*y(5)+N6c*y(6)+N7c*y(7)+N8c*y(8);

za=N1a*z(1)+N2a*z(2)+N3a*z(3)+N4a*z(4)+N5a*z(5)+N6a*z(6)+N7a*z(7)+N8a*z(8);

zb=N1b*z(1)+N2b*z(2)+N3b*z(3)+N4b*z(4)+N5b*z(5)+N6b*z(6)+N7b*z(7)+N8b*z(8);

zc=N1c*z(1)+N2c*z(2)+N3c*z(3)+N4c*z(4)+N5c*z(5)+N6c*z(6)+N7c*z(7)+N8c*z(8);
            Jac=[xa ya za; xb yb zb; xc yc zc];
            Jaci=inv(Jac);
            detJac=det(Jac);
            p=[N1 N2 N3 N4 N5 N6 N7 N8];
            p_x=Jaci(1,:)*[N1a N2a N3a N4a N5a N6a N7a N8a;...
                           N1b N2b N3b N4b N5b N6b N7b N8b;...
                           N1c N2c N3c N4c N5c N6c N7c N8c];
            p_y=Jaci(2,:)*[N1a N2a N3a N4a N5a N6a N7a N8a;...
                           N1b N2b N3b N4b N5b N6b N7b N8b;...
                           N1c N2c N3c N4c N5c N6c N7c N8c];
            p_z=Jaci(3,:)*[N1a N2a N3a N4a N5a N6a N7a N8a;...
                           N1b N2b N3b N4b N5b N6b N7b N8b;...
                           N1c N2c N3c N4c N5c N6c N7c N8c];
            grad_x=p_x;
            grad_y=p_y;
            grad_z=p_z;

K_elem=K_elem+(grad_x'*grad_x+grad_y'*grad_y+grad_z'*grad_z)*detJac*cc;
            M_elem=M_elem+(1/c_air^2)*(p'*p)*detJac*cc;
        end
    end
end
```

```
function [f0val,df0dx,df0dx2,fval,dfdx,dfdx2,wc,P] =
sound_objective_function(Lx_ov, Ly_ov, Lz_ov, nelx, nely, nelz, freq,
volfrac, m, xj)
nel=nelx*nely;
```

```
[objec, dobjec_dx, wc, P]=Overall_Assembly_MMA(Lx_ov, Ly_ov, Lz_ov, nelx,
nely, nelz, freq, xj);
f0val=objec;
df0dx=dobjec_dx';
df0dx2=0*df0dx;
fval(1,1)=sum(xj)-volfrac*nel;
dfdx(1,:)=ones(1,nel);
dfdx2(1,:)=0*dfdx(1,:);



function [objec, dobjec_dx, wc, P]=Overall_Assembly_MMA(Lx_ov, Ly_ov, Lz_ov,
nelx, nely, nelz, freq, xj)
rho_air=1.2;
inch=25.4e-3;
nel=nelx*nely;
omega=2*pi*freq;
[K_p_front, M_p_front, Force_front, BC_front, K_p_array_front,
M_p_array_front, dK_dx_array_front, dM_dx_array_front,...
    dK_dxx_array_front, dM_dxx_array_front]=Plate_Assembly_MMA(Lx_ov, Ly_ov,
nelx, nely, inch/16, xj);
[K_p_back, M_p_back, Force_back, BC_back, K_p_array_back, M_p_array_back,
dK_dx_array_back, dM_dx_array_back,...
    dK_dxx_array_back, dM_dxx_array_back]=Plate_Assembly_MMA(Lx_ov, Ly_ov,
nelx, nely, 2.0*inch, xj);
[K_fluid, M_fluid]=Fluid_Assembly_MMA(Lx_ov, Ly_ov, Lz_ov, nelx, nely, nelz);
xlen=Lx_ov/nelx;
ylen=Ly_ov/nely;
zlen=Lz_ov/nelz;
x=[0 1 1 0 0 1 1 0]*xlen;
y=[0 0 1 1 0 0 1 1]*ylen;
z=[0 0 0 0 1 1 1 1]*zlen;
K_f_array=zeros(8,8,nel);
M_f_array=zeros(8,8,nel);
for ii=1:nel
    [K_f_array(:,:,ii),K_f_array(:,:,ii)]=cavity_matrices(x,y,z);
end
[c_front, C_array_front]=coupling_Assembly_MMA(Lx_ov, Ly_ov, nelx, nely, 1);
[c_back, C_array_back]=coupling_Assembly_MMA(Lx_ov, Ly_ov, nelx, nely, 2);
dof_front=length(K_p_front);
dof_back=length(K_p_back);
dof_struct=dof_front+dof_back;
dof_fluid=length(K_fluid);
dof_overall=dof_struct+dof_fluid;
dof_coup_press_front=(nelx+1)*(nely+1)*1;
dof_coup_press_back=(nelx+1)*(nely+1)*1;
K_overall=sparse(dof_overall,dof_overall);
M_overall=sparse(dof_overall,dof_overall);
K_struct=[K_p_front         zeros(dof_front);...
          zeros(dof_back)   K_p_back];
M_struct=[M_p_front         zeros(dof_front);...
          zeros(dof_back)   M_p_back];
K_overall(1:dof_struct,1:dof_struct)=K_overall(1:dof_struct,1:dof_struct)+K_s
truct;
M_overall(1:dof_struct,1:dof_struct)=M_overall(1:dof_struct,1:dof_struct)+M_s
truct;
```

```
K_overall(dof_struct+1:dof_overall,dof_struct+1:dof_overall)=...
    K_overall(dof_struct+1:dof_overall,dof_struct+1:dof_overall)+K_fluid;
M_overall(dof_struct+1:dof_overall,dof_struct+1:dof_overall)=...
    M_overall(dof_struct+1:dof_overall,dof_struct+1:dof_overall)+M_fluid;
start_=dof_struct+1;
end_=dof_struct+dof_coup_press_front;
M_overall(start_:end_,1:dof_front)=...
    M_overall(start_:end_,1:dof_front)+c_front;
start_=dof_overall-dof_coup_press_back+1;
end_=dof_overall;
M_overall(start_:end_,dof_front+1:dof_struct)=...
    M_overall(start_:end_,dof_front+1:dof_struct)+c_back;
c_front_k=-c_front'/rho_air;
c_back_k=-c_back'/rho_air;
start_=dof_struct+1;
end_=dof_struct+dof_coup_press_front;
K_overall(1:dof_front,start_:end_)=...
    K_overall(1:dof_front,start_:end_)+c_front_k;
start_=dof_overall-dof_coup_press_back+1;
end_=dof_overall;
K_overall(dof_front+1:dof_struct,start_:end_)=...
    K_overall(dof_front+1:dof_struct,start_:end_)+c_back_k;
Force=sparse(dof_overall,1);
Force(1:dof_front)=Force(1:dof_front)+Force_front;
alldofs     = 1:dof_overall;
BC_back=dof_front+BC_back;
BC=[BC_front BC_back];
freedofs    = setdiff(alldofs,BC);
UPP=sparse(dof_overall,1);
for ii=1:length(omega)
   UP(freedofs,:) = (K_overall(freedofs,freedofs)-
omega(ii).^2*M_overall(freedofs,freedofs)) \ Force(freedofs,:);
   UP(BC,:)= 0;
   UPP=UPP+UP;
end
U=UPP(1:dof_front);
wc=U(1:3:length(U));
P=UPP(dof_struct+1:dof_overall,1);
p_coup=(nelx+1)*(nely+1);
pc=P(1:p_coup);
pc_L1=P(1:2*p_coup);
objec=full(wc'*pc);
for ii=1:nely
    for jj=1:nelx
        c1=0;
        c2=0;
        for kk=1:length(omega)
            n1=(ii-1)*(nelx+1)+jj;
            n2=n1+1;
            n3=(ii)*(nelx+1)+jj+1;
            n4=n3-1;
            DOF=3;
            edof1=[(n1-1)*DOF+1, (n1-1)*DOF+2, (n1-1)*DOF+3];
            edof2=[(n2-1)*DOF+1, (n2-1)*DOF+2, (n2-1)*DOF+3];
            edof3=[(n3-1)*DOF+1, (n3-1)*DOF+2, (n3-1)*DOF+3];
            edof4=[(n4-1)*DOF+1, (n4-1)*DOF+2, (n4-1)*DOF+3];
            DOF=1;
```

```
            pdof1=(n1-1)*DOF+1;
            pdof2=(n2-1)*DOF+1;
            pdof3=(n3-1)*DOF+1;
            pdof4=(n4-1)*DOF+1;
            pdof5=pdof1+(nelx+1)*(nely+1);
            pdof6=pdof2+(nelx+1)*(nely+1);
            pdof7=pdof3+(nelx+1)*(nely+1);
            pdof8=pdof4+(nelx+1)*(nely+1);
            edof=[edof1 edof2 edof3 edof4];
            pdof=[pdof1 pdof2 pdof3 pdof4 pdof5 pdof6 pdof7 pdof8];
            Ue=U(edof,1);
            pce=pc_L1(pdof,1);
            index=(ii-1)*(nelx)+jj;
            Kst_D = K_p_array_front(:,:,index)-
omega(kk).^2*M_p_array_front(:,:,index);
            Kfl_D = K_f_array(:,:,index)-omega(kk).^2*M_f_array(:,:,index);
            A1    = C_array_front(:,:,index);
            D     = omega(kk).^2*A1;
            A     = A1'/rho_air*inv(Kfl_D)*D;
            B     = Kst_D - A;
            C     = dK_dx_array_front(:,:,index)-
omega(kk).^2*dM_dx_array_front(:,:,index);
            ddelta_drho=-inv(B)*C*Ue;
            t1=ddelta_drho';
            c1=c1+t1(1:3:12)*pce(1:4);
            dp_drho=inv(Kfl_D)*D*ddelta_drho;
            t2=Ue';
            c2=c2+t2(1:3:12)*dp_drho(1:4);
        end
        if objec>0
            dobjec_dx(index) = (c1+c2);
        else
            dobjec_dx(index) = (c1+c2);
        end
    end
end



function [K_assembly, M_assembly, Force, BC, K_el_array, M_el_array,
dK_el_dx_array, dM_el_dx_array,...
    dK_el_dxx_array, dM_el_dxx_array]=Plate_Assembly_MMA(Lx_ov, Ly_ov, nelx,
nely, h0, xj)
xlen=Lx_ov/nelx;
ylen=Ly_ov/nely;
x=[0 1 1 0]*xlen;
y=[0 0 1 1]*ylen;
DOF=3;
Nnodesoverall=(nelx+1)*(nely+1);
nel=nelx*nely;
NDOFOverall=DOF*Nnodesoverall;
K_assembly=sparse(NDOFOverall,NDOFOverall);
M_assembly=sparse(NDOFOverall,NDOFOverall);
Force=zeros(NDOFOverall,1);
dK_el_dx_array=zeros(DOF*4,DOF*4,nel);
dK_el_dxx_array=zeros(DOF*4,DOF*4,nel);
```

```
K_el_array=zeros(DOF*4,DOF*4,nel);
dM_el_dx_array=zeros(DOF*4,DOF*4,nel);
dM_el_dxx_array=zeros(DOF*4,DOF*4,nel);
M_el_array=zeros(DOF*4,DOF*4,nel);
for ii=1:nely
    for jj=1:nelx
        index=(ii-1)*(nelx)+jj;
        xj_c = xj(index);
        [K_el, M_el, dK_el_dx, dM_el_dx, dK_el_dxx,
dM_el_dxx]=plate_matrices_3dof(x,y,h0,xj_c);
        dK_el_dx_array(:,:,index)=dK_el_dx;
        dK_el_dxx_array(:,:,index)=dK_el_dxx;
        K_el_array(:,:,index)=K_el;
        dM_el_dx_array(:,:,index)=dM_el_dx;
        dM_el_dxx_array(:,:,index)=dM_el_dxx;
        M_el_array(:,:,index)=M_el;
        globn(1)=(ii-1)*(nelx+1)+jj;
        globn(2)=globn(1)+1;
        globn(3)=ii*(nelx+1)+(jj+1);
        globn(4)=globn(3)-1;
        globndof1=(globn(1)-1)*DOF+1:(globn(1)-1)*DOF+DOF;
        globndof2=(globn(2)-1)*DOF+1:(globn(2)-1)*DOF+DOF;
        globndof3=(globn(3)-1)*DOF+1:(globn(3)-1)*DOF+DOF;
        globndof4=(globn(4)-1)*DOF+1:(globn(4)-1)*DOF+DOF;
        globndof=[globndof1 globndof2 globndof3 globndof4];
        K_assembly(globndof,globndof)=K_assembly(globndof,globndof)+K_el;
        M_assembly(globndof,globndof)=M_assembly(globndof,globndof)+M_el;
    end
end

for ii=nely/2+1:nely/2+1
    for jj=nelx/2+1:nelx/2+1
        location=(ii-1)*(nelx+1)+jj;
        Force_Node=(location-1)*DOF+1;
        Force(Force_Node,1)=0.1;
    end
end
BN1=1:nelx+1;
BN2=(nelx+1)*nely+1:(nelx+1)*(nely+1);
BN3=nelx+2:nelx+1:(nelx+1)*nely;
BN4=2*(nelx+1):nelx+1:(nelx+1)*nely;
BC1=[(BN1-1)*DOF+1, (BN1-1)*DOF+2, (BN1-1)*DOF+3];
BC2=[(BN2-1)*DOF+1, (BN2-1)*DOF+2, (BN2-1)*DOF+3];
BC3=[(BN3-1)*DOF+1, (BN3-1)*DOF+2, (BN3-1)*DOF+3];
BC4=[(BN4-1)*DOF+1, (BN4-1)*DOF+2, (BN4-1)*DOF+3];
BC=sort([BC1 BC2 BC3 BC4]);




function [K_elem, M_elem, dK_elem_dx, dM_elem_dx, dK_elem_dxx,
dM_elem_dxx]=plate_matrices_3dof(x,y,h0,xj)
mu=0.3;
rho=2700;
Em=71e9*(1+0.07i);
GG=1/2/(1+mu);
```

```
h=xj*h0;
pa(1)=-1/sqrt(3);
pa(2)=1/sqrt(3);
pb(1)=-1/sqrt(3);
pb(2)=1/sqrt(3);
K_elem_b=zeros(12,12);
dK_elem_b_dx=zeros(12,12);
dK_elem_b_dxx=zeros(12,12);
K_elem_s=zeros(12,12);
dK_elem_s_dx=zeros(12,12);
dK_elem_s_dxx=zeros(12,12);
M_elem=zeros(12,12);
dM_elem_dx=zeros(12,12);
dM_elem_dxx=zeros(12,12);
for ii=1:2
    for jj=1:2
        a=pa(ii);
        b=pb(jj);
        cc=1;
        alpha=1/4;
        N1=alpha*(1-a)*(1-b);
        N1a=-alpha*(1-b);
        N1b=-alpha*(1-a);
        N2=alpha*(1+a)*(1-b);
        N2a=alpha*(1-b);
        N2b=-alpha*(1+a);
        N3=alpha*(1+a)*(1+b);
        N3a=alpha*(1+b);
        N3b=alpha*(1+a);
        N4=alpha*(1-a)*(1+b);
        N4a=-alpha*(1+b);
        N4b=alpha*(1-a);
        xa=N1a*x(1)+N2a*x(2)+N3a*x(3)+N4a*x(4);
        xb=N1b*x(1)+N2b*x(2)+N3b*x(3)+N4b*x(4);
        ya=N1a*y(1)+N2a*y(2)+N3a*y(3)+N4a*y(4);
        yb=N1b*y(1)+N2b*y(2)+N3b*y(3)+N4b*y(4);
        Jac=[xa ya; xb yb];
        Jaci=inv(Jac);
        detJac=det(Jac);
w=[N1 0 0 N2 0 0 N3 0 0 N4 0 0];
thx=[0 N1 0 0 N2 0 0 N3 0 0 N4 0];
thx_x=Jaci(1,:)*[0 N1a 0 0 N2a 0 0 N3a 0 0 N4a 0;...
                 0 N1b 0 0 N2b 0 0 N3b 0 0 N4b 0];
thx_y=Jaci(2,:)*[0 N1a 0 0 N2a 0 0 N3a 0 0 N4a 0;...
                 0 N1b 0 0 N2b 0 0 N3b 0 0 N4b 0];
thy=[0 0 N1 0 0 N2 0 0 N3 0 0 N4];
thy_x=Jaci(1,:)*[0 0 N1a 0 0 N2a 0 0 N3a 0 0 N4a;...
                 0 0 N1b 0 0 N2b 0 0 N3b 0 0 N4b];
thy_y=Jaci(2,:)*[0 0 N1a 0 0 N2a 0 0 N3a 0 0 N4a;...
                 0 0 N1b 0 0 N2b 0 0 N3b 0 0 N4b];
strain_bend  = [-thx_x ; -thy_y ; -(thx_y+thy_x)];

DD=Em*[h^3/12/(1-mu^2)     mu*h^3/12/(1-mu^2)  0           ;...
       mu*h^3/12/(1-mu^2)  h^3/12/(1-mu^2)     0           ;...
       0                   0                   GG*h^3/12];
DD_x=Em*[3*xj^2*h0^3/12/(1-mu^2)     mu*3*xj^2*h0^3/12/(1-mu^2)  0
;...
```

```
         mu*3*xj^2*h0^3/12/(1-mu^2)  3*xj^2*h0^3/12/(1-mu^2)     0
;...
         0                           0
GG*3*xj^2*h0^3/12];
DD_xx=Em*[6*xj*h0^3/12/(1-mu^2)     mu*6*xj*h0^3/12/(1-mu^2)  0
;...
          mu*6*xj*h0^3/12/(1-mu^2)  6*xj*h0^3/12/(1-mu^2)     0
;...
          0                         0
GG*6*xj*h0^3/12];
stress_bend = DD*strain_bend;
stress_bend_dx=DD_x*strain_bend;
stress_bend_dxx=DD_xx*strain_bend;
        K_elem_b=K_elem_b+(strain_bend'*stress_bend)*detJac*cc;
        dK_elem_b_dx=dK_elem_b_dx+(strain_bend'*stress_bend_dx)*detJac*cc;
        dK_elem_b_dxx=dK_elem_b_dxx+(strain_bend'*stress_bend_dxx)*detJac*cc;

        M_elem=M_elem+rho*(h*(w'*w)+h^3/12*(thx'*thx+thy'*thy))*detJac*cc;

dM_elem_dx=dM_elem_dx+rho*(h0*(w'*w)+3*xj^2*h0^3/12*(thx'*thx+thy'*thy))*detJ
ac*cc;

dM_elem_dxx=dM_elem_dxx+rho*(6*xj*h0^3/12*(thx'*thx+thy'*thy))*detJac*cc;
    end
end

clear pa;
clear pb;
clear ww;
for ii=1:1
    for jj=1:1
        a=0;
        b=0;
        cc=2;
        alpha=1/4;
        N1=alpha*(1-a)*(1-b);
        N1a=-alpha*(1-b);
        N1b=-alpha*(1-a);
        N2=alpha*(1+a)*(1-b);
        N2a=alpha*(1-b);
        N2b=-alpha*(1+a);
        N3=alpha*(1+a)*(1+b);
        N3a=alpha*(1+b);
        N3b=alpha*(1+a);
        N4=alpha*(1-a)*(1+b);
        N4a=-alpha*(1+b);
        N4b=alpha*(1-a);
        xa=N1a*x(1)+N2a*x(2)+N3a*x(3)+N4a*x(4);
        xb=N1b*x(1)+N2b*x(2)+N3b*x(3)+N4b*x(4);
        ya=N1a*y(1)+N2a*y(2)+N3a*y(3)+N4a*y(4);
        yb=N1b*y(1)+N2b*y(2)+N3b*y(3)+N4b*y(4);
        Jac=[xa ya; xb yb];
        Jaci=inv(Jac);
        detJac=det(Jac);
        w_x=Jaci(1,:)*[N1a 0 0 N2a 0 0 N3a 0 0 N4a 0 0;...
            N1b 0 0 N2b 0 0 N3b 0 0 N4b 0 0];
```

```
        w_y=Jaci(2,:)*[N1a 0 0 N2a 0 0 N3a 0 0 N4a 0 0;...
            N1b 0 0 N2b 0 0 N3b 0 0 N4b 0 0];
        thx=[0 N1 0 0 N2 0 0 N3 0 0 N4 0];
        thy=[0 0 N1 0 0 N2 0 0 N3 0 0 N4];
        strain_shear  = [-(thx-w_x) ; -(thy-w_y)];
        DD=Em*[h/2.4/(1+mu)    0;...
            0               h/2.4/(1+mu)];
        DD_x=Em*[h0/2.4/(1+mu)      0;...
                 0                  h0/2.4/(1+mu)];
        DD_xx=0*Em*[h0/2.4/(1+mu)      0;...
                    0                  h0/2.4/(1+mu)];
        stress_shear = DD*strain_shear;
        stress_shear_x = DD_x*strain_shear;
        stress_shear_xx = DD_xx*strain_shear;
        K_elem_s=K_elem_s+(strain_shear'*stress_shear)*detJac*cc;
        dK_elem_s_dx=dK_elem_s_dx+(strain_shear'*stress_shear_x)*detJac*cc;

dK_elem_s_dxx=dK_elem_s_dxx+(strain_shear'*stress_shear_xx)*detJac*cc;
    end
end
K_elem=K_elem_b+K_elem_s;
dK_elem_dx=dK_elem_b_dx+dK_elem_s_dx;
dK_elem_dxx=dK_elem_b_dxx+dK_elem_s_dxx;




function [K_fluid, M_fluid]=Fluid_Assembly_MMA(Lx_ov, Ly_ov, Lz_ov, nelx,
nely, nelz)
xlen=Lx_ov/nelx;
ylen=Ly_ov/nely;
zlen=Lz_ov/nelz;
x=[0 1 1 0 0 1 1 0]*xlen;
y=[0 0 1 1 0 0 1 1]*ylen;
z=[0 0 0 0 1 1 1 1]*zlen;
DOF=1;
Nnodesoverall=(nelx+1)*(nely+1)*(nelz+1);
NDOFOverall=DOF*Nnodesoverall;
K_fluid=sparse(NDOFOverall,NDOFOverall);
M_fluid=sparse(NDOFOverall,NDOFOverall);
[K_el, M_el]=cavity_matrices(x,y,z);
for kk=1:nelz
    for ii=1:nely
        for jj=1:nelx
            globn(1)=(ii-1)*(nelx+1)+jj+(kk-1)*(nelx+1)*(nely+1);
            globn(2)=globn(1)+1;
            globn(3)=ii*(nelx+1)+(jj+1)+(kk-1)*(nelx+1)*(nely+1);
            globn(4)=globn(3)-1;
            globn(5)=(ii-1)*(nelx+1)+jj+kk*(nelx+1)*(nely+1);
            globn(6)=globn(5)+1;
            globn(7)=ii*(nelx+1)+(jj+1)+kk*(nelx+1)*(nely+1);
            globn(8)=globn(7)-1;
            globndof1=(globn(1)-1)*DOF+1:(globn(1)-1)*DOF+DOF;
            globndof2=(globn(2)-1)*DOF+1:(globn(2)-1)*DOF+DOF;
            globndof3=(globn(3)-1)*DOF+1:(globn(3)-1)*DOF+DOF;
            globndof4=(globn(4)-1)*DOF+1:(globn(4)-1)*DOF+DOF;
```

```
            globndof5=(globn(5)-1)*DOF+1:(globn(5)-1)*DOF+DOF;
            globndof6=(globn(6)-1)*DOF+1:(globn(6)-1)*DOF+DOF;
            globndof7=(globn(7)-1)*DOF+1:(globn(7)-1)*DOF+DOF;
            globndof8=(globn(8)-1)*DOF+1:(globn(8)-1)*DOF+DOF;
            globndof=[globndof1 globndof2 globndof3 globndof4 globndof5
globndof6 globndof7 globndof8];
            K_fluid(globndof,globndof)=K_fluid(globndof,globndof)+K_el;
            M_fluid(globndof,globndof)=M_fluid(globndof,globndof)+M_el;
        end
    end
end



function [C_assembly, C_el_array]=coupling_Assembly_MMA(Lx_ov, Ly_ov, nelx,
nely, location)
xlen=Lx_ov/nelx;
ylen=Ly_ov/nely;
x=[0 1 1 0]*xlen;
y=[0 0 1 1]*ylen;
nel=nelx*nely;
DOF=3;
Nnodesoverall=(nelx+1)*(nely+1);
NDOFOverall_delta=DOF*Nnodesoverall;
NDOFOverall_press=1*Nnodesoverall;
C_assembly=sparse(NDOFOverall_press,NDOFOverall_delta);
C_el_array=zeros(1*8,3*4,nel);
for ii=1:nely
    for jj=1:nelx
        index=(ii-1)*(nelx)+jj;
        [c_matrix]=coupling_matrix_final(x,y,location);
        C_el_array(:,:,index)=c_matrix;
        if location == 1
            c_matrix(5:8,:)=[];
        else
            c_matrix(1:4,:)=[];
        end
        globn(1)=(ii-1)*(nelx+1)+jj;
        globn(2)=globn(1)+1;
        globn(3)=ii*(nelx+1)+(jj+1);
        globn(4)=globn(3)-1;
        DOF=3;
        globndof1=(globn(1)-1)*DOF+1:(globn(1)-1)*DOF+DOF;
        globndof2=(globn(2)-1)*DOF+1:(globn(2)-1)*DOF+DOF;
        globndof3=(globn(3)-1)*DOF+1:(globn(3)-1)*DOF+DOF;
        globndof4=(globn(4)-1)*DOF+1:(globn(4)-1)*DOF+DOF;
        globndof_delta=[globndof1 globndof2 globndof3 globndof4];
        DOF=1;
        globndof1=(globn(1)-1)*DOF+1:(globn(1)-1)*DOF+DOF;
        globndof2=(globn(2)-1)*DOF+1:(globn(2)-1)*DOF+DOF;
        globndof3=(globn(3)-1)*DOF+1:(globn(3)-1)*DOF+DOF;
        globndof4=(globn(4)-1)*DOF+1:(globn(4)-1)*DOF+DOF;
        globndof_press=[globndof1 globndof2 globndof3 globndof4];

C_assembly(globndof_press,globndof_delta)=C_assembly(globndof_press,globndof_
delta)+c_matrix;
```

```
    end
end
```

APPINDEX B

ANSYS MACRO

```
FINISH
/CLEAR
/NOPR
/FILNAME,PLAIN_AIR_ALUMINUM
/TITLE,MINIMIZING ACOUSTIC COUPLIG OF FLUID LOADED PLATES USING TOPOLOGY OPT.
/CONFIG,NRES,10000
/PREP7
INCH=25.4E-3
!DEFINE KEYPOINTS, LINES AND AREAS FOR THE COMPLETE MODEL
! FRONT FACE
K,1,0,0,0
K,2,0,0,-12*INCH
K,3,0,12*INCH,-12*INCH
K,4,0,12*INCH,0
! BACK FACE
K,5,-30*INCH,0,0
K,6,-30*INCH,0,-12*INCH
K,7,-30*INCH,12*INCH,-12*INCH
K,8,-30*INCH,12*INCH,0
! LINES FOR FRONT AREA
L,1,2,12
L,2,3,12
```

```
L,3,4,12
L,4,1,12
! LINES FOR BACK AREA
L,5,6,12
L,6,7,12
L,7,8,12
L,8,5,12
! LINES FOR TOP AREA LINES
L,8,4,10
L,3,7,10
! LINES FOR BOTTOM AREA LINES
L,5,1,10
L,2,6,10
! DEFINE FRONT AREA
AL,1,2,3,4              ! AREA # 1 ====> PLATE'S AREA
! DEFINE BACK AREA
AL,5,6,7,8
! DEFINE TOP AREA
AL,3,10,7,9
! DEFINE BOTTOM AREA
AL,1,12,5,11
! DEFINE RIGHT AREA
AL,12,6,10,2
! DEFINE LEFT AREA
AL,4,9,8,11
!DEFINE FLUID VOLUME
```

```
VA,1,2,3,4,5,6
!DEFINE MATERIALS
!MATERIAL FOR THE FLUID MEDIUM: AIR
MAT,1
MP,DENS,1,1.2        ! MATERIAL DENSITY
MP,SONC,1,343        ! SONIC VILOCITY
! MATERIAL FOR THE PLATE: ALUMINUM
MAT,2
MP,DENS,2,2700       ! MATERIAL DENSITY
MP,DMPR,2,0.032      ! MATERIAL DAMPING
MP,EX,2,71E9         ! MODULUS OF ELASTICITY ALOMG X DIRECTION
MP,EY,2,71E9         ! MODULUS OF ELASTICITY ALOMG Y DIRECTION
MP,EZ,2,71E9         ! MODULUS OF ELASTICITY ALOMG Z DIRECTION
MP,PRXY,2,0.3        ! Major Poisson's ratios MAJOR POISSON'S RATIO IN XY PLANE
MP,PRYZ,2,0.3        ! Major Poisson's ratios MAJOR POISSON'S RATIO IN YZ PLANE
MP,PRXZ,2,0.3        ! Major Poisson's ratios MAJOR POISSON'S RATIO IN XZ PLANE
MP,GXY,2,27.3E9      ! SHEAR MODULUS OF RIGIDITY IN XY PLANE
MP,GYZ,2,27.3E9      ! SHEAR MODULUS OF RIGIDITY IN YZ PLANE
MP,GXZ,2,27.3E9      ! SHEAR MODULUS OF RIGIDITY IN XZ PLANE
! REAL CONSTANTS FOR MATERIAL 2
R,2,2.5*1/32*INCH,2.5*1/32*INCH,2.5*1/32*INCH,2.5*1/32*INCH
! DEFINE ELEMENT TYPES
ET,1,FLUID30,,1      ! NON-INTERFACING FLUID ELEMENTS
ET,2,FLUID30         ! FLUID ELEMENTS INTERFACING WITH STRUCTURE
ET,3,SHELL181        ! PLATE AND CAVITY ELEMENTS
KEYOPT,3,3,2
```

```
KEYOPT,3,8,2
! DEFINE ELEMENT TYPE AND MATERIAL TO MESH THE PLATE
! NESH THE PLATE USING RAEL CONSTANTS=1
ASEL,S,AREA,,1       ! SELECT AREA # 1
AATT,2,2,3           ! ASSIGN MATERIAL #2, REAL #2 AND ELEMENT TYPE #3 TO AREA #1
AMESH,1              ! MESH AREA #1
! DEFINE ELEMENT TYPE AND MATERIAL TO MESH THE FLUID MEDIUM (NON-INTERFACING)
VSEL,S,VOLU,,1     ! SELECT VOLUME #1
VATT,1,1,1         ! ASSIGN MATERIAL #1, REAL #1 AND ELEMENT TYPE #1 TO VOLUME #1
VMESH,1            ! MESH AREAS #2 TO 5
! DEFINE ELEMENT TYPE AND MATERIAL TO MESH THE FLUID MEDIUM (INTERFACING)
NSEL,S,LOC,X,0
ESLN,S
ESEL,R,TYPE,,1
EMODIF,ALL,TYPE,2
! DEFINE BOUNDARY CONDITIONS FOR PLATE AND FLUID
LSEL,S,LINE,,1,4
NSLL,S,1
D,ALL,UX,0,,,UY,UZ,ROTX,ROTY,ROTZ
! DEFINE BOUNDARY CONDITIONS FOR FLUID
NSEL,S,LOC,Y,12*INCH
NSEL,A,LOC,Y,0
NSEL,A,LOC,Z,-12*INCH
NSEL,A,LOC,Z,0
NSEL,R,LOC,X,0,-3*INCH
D,ALL,UX,0,,,UY,UZ
```

```
! DEFINE SURFACE LOADS
SFA,1,,FSI
ALLSEL
/SOLU
! DEFINE LOADS
F,109,FX,-0.05
!ANALYSIS TYPE AND OPTIONS
ANTYPE,HARMIC,NEW
HROPT,FULL
HARFRQ,,1000
NSUBST,1000
KBC,1
```

REFRENCES

[1] **Krog, L.; Olhoff, N.**, "Topology and reinforcement layout optimization of disk, plate, and shell structures", *Topology Optimization in Structural Mechanics (ed. G. Rozvany)*, Vol. 24, pp 237-322, 1997.

[2] **Bendsoe, M.**, *Optimization of structural topology, shape and material*, Springer, Berlin, 1997.

[3] **Bendsoe, M.; Sigmund, O.**, *Topology Optimization, Theory, Methods and Applications*, Springer, New York, 2003.

[4] **Bendsoe, M.; Kikuchi, N.**, "Generating optimal topologies in structural design using a homogenization method", *Computer Methods in Applied Mechanics and Engineering*, Vol. 71, No. 2, pp197-224, 1988.

[5] **Bendsoe, M.**, "Optimal shape design as a material distribution problem", *Structural Optimization*, Vol. 1, pp193–200, 1989.

[6] **Bendsoe, M.; Diaz, A.**, "Optimization of material properties for improved frequency response", *Structural Optimization*, Vol.7, pp138-140, 1994.

[7] **Krog, L.; Olhoff, N.**, "Optimum topology and reinforcement design of disk and plate structures with multiple stiffness and eigenfrequency objectives", *Computers and Structures*, Vol.72, pp 535-563, 1999.

[8] **Wang, M., Wang, S., Lim, K.**, "A density filtering approach for topology optimization", *7th World Congress on Structural and Multidisciplinary Optimization*, 2007.

[9] **Pederson, N.**, "Maximization of Eigenfrequencies using Topology Optimization", *Structural and Multidisciplinary Optimization*, Vol.20, pp 2-11, 2000.

[10] **Olhoff, N.; Du, J.**, "Topology optimization of structures against vibration and noise", *12th International Congress on Sound and Vibration, ICSV12*. Lisbon, Portugal, Vol.20, 2005.

[11] **Jensen, J.; Pedersen, N.**, "On maximal eigenfrequency separation in two-material structures: the 1D and 2D scalar cases", *Journal of Sound and Vibration*, Vol.289, pp 967-986, 2006.

[12] **Crocker, M.**, *Handbook of Acoustics*, John Wiley and Sons, New York, 1998.

[13] **Rossing, T.; Dunn, F.; Hartmann, W.; Campbell, D.; Fletcher, N.**, *Springer Handbook of Acoustics*, Springer Science and Business Media, New York, 2007.

[14] **Jog, C.**, "Topology design of structures subjected to periodic loading", *Journal of Sound and Vibration*, Vol.253, No. 3, pp 687-709, 2002.

[15] **Yoon, G.; Jensen, J.; Sigmund, O.**, "Topology optimization of acoustic–structure interaction problems using a mixed finite element formulation", *International Journal for Mechanical Methods in Engineering*, Vol.70, pp1049-1075, 2007.

[16] **Du, J.; Olhoff, N.**, "Minimization of sound radiation from vibrating bi-material structures using topology optimization", *Structural and Multidisciplinary Optimization*, pp305-321, 2007.

[17] **Wang, S.; Lee, J.**, "Acoustic design sensitivity analysis and optimization for reduced exterior noise", *AIAA Journal*, Vol.39, No.4, pp 574 -580, 2001.

[18] **Lee, J.; Wang, S.; Dikec, A.**, "Topology optimization for the radiation and scattering of sound from thin-body using genetic algorithms", *Journal of Sound and Vibration*, Vol.276, pp 899–918, 2004.

[19] **Wu, T.; Wan, G.**, "Numerical modeling of acoustic radiation and scattering from thin bodies using a Cauchy principal integral equation", *Journal of the Acoustical Society of America*, Vol.92**,** pp 2900–2906, 1992.

[20] **Sigmund, O.**, "A 99 line topology optimization code written in matlab", *Structural and Multidisciplinary Optimization*, Vol.21, pp 120-127, 2001.

[21] **Bendsoe, M.; Sigmund, O.**, Material interpolations in topology optimization.Arch. Appl. Mech., (69):635–654, 1999.

[22] **Wang, M., Wang, S., Lim, K.**, "A density filtering approach for topology optimization", *7th World Congress on Structural and Multidisciplinary Optimization*, 2007.

[23] **Petersson,J., Sigmund, O.**, "Slope constrained topology optimization", *International Journal for Numerical Methods in Engineering*, Vol.41, pp.1417-1434, 1998.

[24] **Zhou, M., Shyy, Y., Thomas, H.**, "Checkerboard and minimum member size control in topology optimization", *Structural and Multidisciplinary Optimization*, Vol.21, pp.152-158, 2001.

[25] **Cardoso, E.; Fonseca, J.**, "Complexity control in the topology optimization of continuum structures", *Journal of the Brazilian Society of Mechanical Sciences and Engineering*, Vol.25, n.3, pp.293-301, 2003.

[26] **Jang, G. W.; Jeong, J. H.; Kim, Y. Y.; Sheen, D.; Park, C.; Kim, M. N.**, "Checkerboard-free topology optimization using non-conforming finite elements", *International Journal for Numerical Methods in Engineering*, Vol.57, pp 1717-1735, 2003.

[27] **Svanberg, K.**, "The method of moving asymptotes – a new method for structural optimization", *Journal of Numerical Methods in Engineering*, Vol. 24, pp 359-373, 1987.

[28] **James, K.**, *Optimal Structural Topology Design for Multiple Load Case with Stress Constraints*, PhD Dissertation, Institute for Aerospace Studies, University of Toronto, 2006.

[29] **Zillober, Ch.**, "A globally convergent version of the method of moving asymptotes", *Structural Optimization*, Vol. 6, pp 166-174, 1993.

[30] **Bletzinger, K.U.**, "Extended method of moving asymptotes based on second order information", *Structural Optimization*, Vol. 5, pp 175-183, 1993.

[31] **Ni, Q.**, "A globally convergent method of moving asymptotes with trust region technique", *Optimization Methods and Software*, Vol. 18, n.2,pp 283-297, 2003.

[32] **Fleury, C.**, "First and second order convex approximation strategies in structural optimization", *Structural Optimization*, Vol. 1, pp 3-10, 1989.